University of London

University College London

Phases and Phase Transitions in Charged Colloidal Suspensions

Michael Knott

A thesis submitted for the degree of
Doctor of Philosophy

2001

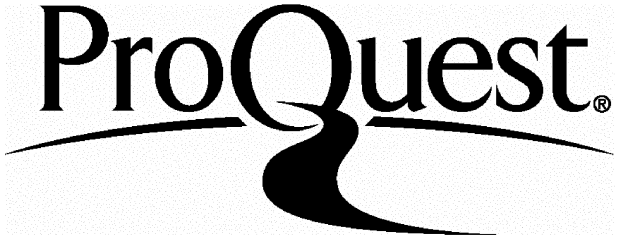

Abstract

We study the stability and phase behaviour of charged colloidal suspensions theoretically, starting from fundamental thermodynamics and electrostatics. The linearised Poisson-Boltzmann equation is solved, subject to justifiable approximations, for a suspension containing a large number of identical spherical macroions under conditions of constant surface charge. The electrostatic term in the Helmholtz free energy is cohesive, and this is opposed by a repulsive counterion ideal gas term. We argue that the stability and phase behaviour of a charged colloidal suspension result from competition between these two terms in the free energy, and that the DLVO theory is inappropriate for the description of these phenomena.

In a system containing no added salt, a van der Waals loop can appear in the pV diagram, indicating phase coexistence between phases with different macroion densities. This occurs when the ratio of the macroion charge to the macroion radius is greater than a critical value. Theoretical phase diagrams for systems containing salt show phase separation when the macroion charge is high and the salt concentration is low, in agreement with experimental results. Calculation of the partition of salt between coexisting phases having different macroion densities reveals a 'reverse Donnan effect': at sufficiently high values of the macroion charge and mean salt concentration, the salt is densest in the macroion-rich region. We show that phase coexistence persists when the macroion charge is allowed to vary, using a simple model for the ion dissociation at the surfaces of the macroions.

The square gradient approximation is used to calculate the surface tension between two colloidal phases of differing density, and the results are compared with evidence from various colloidal systems. The nucleation rate of a colloidal liquid cluster from a metastable colloidal gas is estimated using a version of classical nucleation theory. We explain the recently described 'Swiss Cheese effect' in terms of nucleation phenomena, and argue that it shows evidence both of homogeneous and of heterogeneous nucleation. Metastability is likely to be very important in colloidal systems, and therefore the consideration of nucleation rates is essential to the study of phase behaviour in such systems.

Contents

Acknowledgements

This work was carried out under the inspiring supervision of Dr Ian Ford. I would also like to thank all the other people who helped in various ways, especially Dr John Harding, Dr Lev Kantorovich, Andy Kerridge, Andreas Markmann, Dr Vladimir Mikheev, Dr Markus Rudek, Dr Martin Smalley, Prof. Ikuo Sogami, Dr Peter Sushko, Dr Hanna Vehkamäki and Dr Vladimir Ždímal.

The work was supported financially by a studentship from the U. K. Engineering and Physical Sciences Research Council.

Introduction

This thesis is concerned with suspensions of charged colloids. Colloidal systems are usually defined as systems which have inhomogeneity on a length scale of between approximately 10^{-9} and 10^{-6} m, consisting of matter of one phase dispersed in another, and whose components will therefore have a large surface area relative to their volume. Colloid science has both biological and industrial importance: for example, protein solutions, blood, inks, clays (as used in the manufacture of ceramics) and much food can be modelled as colloidal systems [1].

The suspensions in which we are interested here contain particles of colloidal dimensions (which might, for example, be composed of polystyrene latex) in a polar solvent such as water. We regard the colloidal particles as approximately spherical. Surface groups on the particles will tend to dissociate, resulting in a system composed of colloidal spheres (also known as macroions or polyions) carrying multiple charge, and oppositely charged ions (microions or simple ions) known as counterions. Additional microions will be present in the suspension, in the form of added salt. Overall, the system will be charge neutral, so the number of coions (simple ions having the same charge sign as the macroions) will be equal to the number of counterions contributed by the added salt. The presence of the microions is believed to stabilise the suspension against the formation of an aggregate.

Experimental observations on suspensions under conditions of low added salt concentration have produced evidence of dense phases with solid- or liquidlike ordering coexisting with voids or rarefied (gaslike) phases [2]. This phenomenon is strongly reminiscent of the phase coexistence between liquid or solid and gas which is observed in molecular matter. Phase coexistence between a dense and a rarefied phase appears to conflict with the standard views on the stability of charged colloidal suspensions which are epitomised by the Deryagin-Landau-Verwey-Overbeek (DLVO) theory [3]. For this reason, the mechanism which leads to the phenomenon, and even its very existence, have remained controversial.

The first aim of this thesis is to determine theoretically the phase behaviour of the system, starting from fundamental electrostatics and thermodynamics. Only by

beginning from first principles can we hope to produce a satisfactory and consistent view of such a complex system, and to dispel some of the controversy. This will help us to answer the question of what mechanism underlies the stability and phase behaviour of charged colloidal suspensions. We consider homogeneous phase stability for a variety of macroion and salt densities, and point out various inadequacies of earlier theories. Our main conclusion is that the traditional view of a colloidal suspension stabilised against aggregation by a purely repulsive electrostatic interaction must be replaced by a view of colloidal stability as a competition between the repulsive effect of the counterion entropy and the cohesive effect of the electrostatic contribution to the free energy.

The second aim is to investigate, from a theoretical point of view, the interfaces between the observed phases. We have calculated interfacial free energies in a zero added salt system. This has apparently never been attempted before. The thermodynamic properties of interfaces are extremely important in the formation of new phases by nucleation, and we have estimated rates of nucleation of droplets of the stable phase from the metastable phase. This allows us to interpret the fascinating nature of such non-equilibrium processes, which has been emphasised recently by the so-called 'Swiss Cheese effect' observed by Yoshida *et al.* [4].

We begin with an outline of equilibrium thermodynamics in chapter 1, and then describe the current situation of knowledge about charged colloidal suspensions in chapter 2. Chapter 3 details a calculation of the free energy of the system, beginning from fundamental thermodynamics; the results are applied to phase coexistence in colloidal systems under conditions of zero added salt in chapter 4, and to the calculation of phase diagrams in systems with added salt in chapter 5. In chapter 6, we investigate the effect of allowing the macroion surface charge to vary, by introducing a simple model for the dissociation reaction at the surfaces of the macroions. The classical theory of homogeneous nucleation is introduced in chapter 7, and example calculations, using data from simple molecular systems, illustrate how information on the thermodynamics of a nucleating cluster can be obtained from measured rates of nucleation. In chapter 8, we outline a method for the calculation of interfacial free energies, and apply it to the calculation of the surface tension in a colloidal suspension; this enables nucleation rates to be estimated. We then discuss the 'Swiss Cheese effect' in the light of nucleation theory. The conclusions of the thesis are presented in chapter 9.

Throughout the thesis, the temperature will be assumed to be around room temperature (298 K).

Chapter 1

Equilibrium thermodynamics

1.1 Introduction

Charged colloidal suspensions contain a large number of particles of various types: macroions, counterions, and added salt. The tools necessary to describe such large systems are provided by thermodynamics. Therefore, in this first chapter we shall outline the principles of equilibrium thermodynamics which will be used later in the thesis. We start by introducing the subject on the basis of the first and second laws of thermodynamics, and then proceed to discuss thermodynamic potentials and their minimisation to find the equilibrium state. Later, we introduce the concept of chemical potential and the features of a single-component fluid system that indicate phase coexistence.

1.2 The first and second laws of thermodynamics

The thermodynamics on which the calculations in this volume are based follows from just two basic assumptions: (i) the concepts involved, such as energy, work, equilibrium and temperature, are meaningful and understood, and (ii) the first and second laws of thermodynamics are valid. The second assumption is justified by an appeal to the fact that the laws of thermodynamics are supported by years of experimental results in many different fields of research.

The first law of thermodynamics is a statement of the conservation of energy; it specifies the change dU in the internal energy U of any system during any process,

$$dU = dQ - dW + dU_{mat}. \tag{1.1}$$

dQ is the heat transferred to the system from its surroundings, while dW is the

work performed by the system on its surroundings; dU_{mat} represents the energy transferred to a system from its surroundings due to the transfer of matter [5].

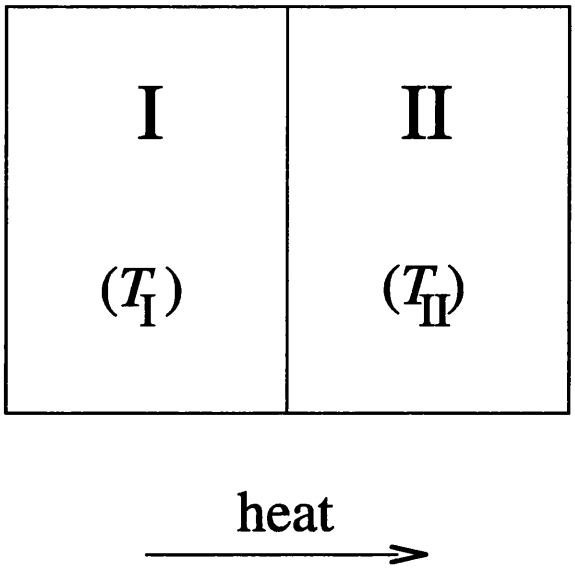

Figure 1.1: The flow of heat between two subsystems I and II of an isolated system. The temperatures are T_{I} and T_{II}, where $T_{\mathrm{I}} > T_{\mathrm{II}}$.

Perhaps the most intuitively obvious statement of the second law of thermodynamics is that heat flows spontaneously only from a hotter body to a colder one. Consider as an example the system illustrated in figure 1.1, containing two components I and II in thermal contact, at temperatures T_{I} and T_{II} such that $T_{\mathrm{I}} > T_{\mathrm{II}}$. Imagine that the system is isolated, and that no work is done on it, so that the only process which takes place is the flow of heat between the two components. During a given period of time, a quantity of heat dQ' will flow from component I to component II, leading to an increase in T_{II} and a decrease in T_{I}. The change dS in the entropy S of an arbitrary system (for example, of one of the components of our example system) due to an infinitesimal part of such a process (involving only the flow of heat), during which its temperature is T, is defined as

$$dS = \frac{dQ}{T}, \tag{1.2}$$

where dQ is the quantity of heat which flows into the arbitrary system. The total entropy change of our example system, $dS = dS_{\mathrm{I}} + dS_{\mathrm{II}}$, where dS_{I} and dS_{II} are the changes in the entropy of components I and II, respectively, is therefore given by

$$dS = \left(\frac{1}{T_{\mathrm{II}}} - \frac{1}{T_{\mathrm{I}}}\right) dQ'. \tag{1.3}$$

Since $T_{\mathrm{I}} > T_{\mathrm{II}}$, equation (1.3) implies that $dS > 0$, which leads us to another statement of the second law: that the entropy of an isolated system can never decrease:

$$dS \geq 0. \tag{1.4}$$

(The limit $dS \to 0$ corresponds to a reversible process, in which $T_{\mathrm{II}} \to T_{\mathrm{I}}$.) The rule that the entropy of an isolated system can never decrease also applies to systems in which processes other than the flow of heat take place.

We can write the entropy of a system which is not isolated as a sum of two terms [5],

$$dS = d_e S + d_i S, \tag{1.5}$$

where $d_e S$ is the entropy change of a system due to the exchange of heat and/or matter with its surroundings and $d_i S$ is the change due to internal processes (for example, a chemical reaction, or the flow of heat between two regions within the system). The term $d_e S$ can have any sign: a negative value of $d_e S$ in a system will always be balanced or outweighed by a positive value of $d_e S$ in its surroundings or by $d_i S$. In the example of figure 1.1, the change $-dQ'/T_{\mathrm{I}}$ in component I (now playing the role of 'the system') is outweighed by the change dQ'/T_{II} in component II ('the surroundings'); in this case, there are no internal processes either within I or within II, so $d_i S = 0$ in both components. If only heat, not matter, is exchanged,

$$d_e S = \frac{dQ}{T}. \tag{1.6}$$

$d_i S$, on the other hand, must always be positive if there are any internal processes, since there occurs no change in the entropy of the surroundings which could outweigh a decrease in the entropy of the system. It is clear that $d_i S$ must be zero in a reversible process.

In an isolated system $d_e S = 0$, and equations (1.4) and (1.5) then imply $d_i S \geq 0$: the equilibrium state is the state of maximum entropy. But only if we considered the entire universe could we imagine that we had a truly isolated system, and most systems of interest are not even approximately isolated. They may, for example be held at constant temperature by thermal contact with their surroundings. In such circumstances, the equilibrium state will correspond to the maximum value of the total entropy of the system and its surroundings. We need to calculate the behaviour of a non-isolated system without having to consider the rest of the universe, except to specify that the universe is large enough to act as a heat bath and hold the system at constant temperature (or to apply some other external constraint to the

system). The quantity that takes an extremal value within the system will be a thermodynamic potential such as the Helmholtz free energy.

1.3 The Helmholtz free energy

Consider a fluid system which is closed (that is, cannot exchange matter with its surroundings). Under these conditions, the first law of thermodynamics reduces to

$$dU = dQ - dW. \tag{1.7}$$

Assume further that the system is confined to a constant volume V and held at a constant temperature T by thermal contact with its surroundings, and that no external field is applied. The system may contain surfaces, different phases, or more than one species of particle. The Helmholtz free energy F is defined as

$$F = U - TS. \tag{1.8}$$

Therefore, the differential dF, representing the change in F due to an infinitesimal process, is

$$dF = dU - TdS - SdT; \tag{1.9}$$

recalling that the temperature is held constant ($dT = 0$) and inserting the first law of thermodynamics (1.7), equation (1.9) becomes

$$dF = dQ - dW - TdS. \tag{1.10}$$

If the only possible external work on a system is a pV term (this is the reason for the prohibition on external fields), we have $dW = pdV$, which is equal to zero since the volume is held constant ($dV = 0$). If we split the differential of the entropy into external and internal components, as in equation (1.5), dF now becomes

$$dF = dQ - Td_eS - Td_iS. \tag{1.11}$$

Equation (1.6) implies that, in a closed system, $dQ = Td_eS$, so we find

$$dF = -Td_iS. \tag{1.12}$$

We noted in the previous section that $d_i S \geq 0$ in any system, and so

$$dF \leq 0. \tag{1.13}$$

This shows that a system under these conditions will always evolve towards a state of lower Helmholtz free energy. An equilibrium state can be found by setting

$$dF = 0. \tag{1.14}$$

For a stable equilibrium state to exist, F must be a global minimum. If it is only a local minimum, the state is metastable: it is stable against small fluctuations but unstable against a larger fluctuation which can take the system over the 'barrier' into the global minimum of free energy or into another local minimum. Equation (1.14) will also be satisfied if the free energy is a local maximum: this corresponds to a state of unstable equilibrium, where the system is unstable against arbitrarily small fluctuations.

The closed nature of the system means only that no matter is exchanged with the surroundings; it does not imply that the number of particles in the system is held constant. Particles can be added or removed by means of internal chemical reactions without destroying the validity of equation (1.13). Similarly, the fact that no external field is applied does not mean that no fields can be present internally: for example, an electrostatic field may occur due to the arrangement of charged particles in the system.

Another feature of the Helmholtz free energy F is that the change of F in a closed system during some isothermal (constant temperature) reversible process is equal to the work done on the system during the process. To see this, we combine (1.7) and (1.9), remembering that $dT = 0$, to give

$$dW = dQ - dF - TdS. \tag{1.15}$$

In a closed system $dQ = Td_e S$, and so

$$dW = -dF - Td_i S, \tag{1.16}$$

leading to $dW = -dF$ for a reversible process.

Under different external constraints, different thermodynamic potentials must be minimised to find the equilibrium state, such as the internal energy U, enthalpy

H, Gibbs free energy G, or grand potential Ω. The Gibbs free energy is defined as

$$G = U - TS + pV, \tag{1.17}$$

where p is the pressure, and is used when the system is held at constant temperature and pressure, while the grand potential is given by

$$\Omega = U - TS - \sum_j \mu_j N_j. \tag{1.18}$$

where N_j is the number of particles of species j and μ_j is their chemical potential, which will be introduced in the next section. The grand potential Ω is used when the system is held at constant volume, temperature and chemical potential. In addition, the change in Ω in an system open to matter exchange at constant chemical potential during an isothermal reversible process is equal to the work done on the system during the process. The grand potential plays the role in an open system that is played in a closed system by the Helmholtz free energy.

1.4 The chemical potential

Recall from the previous section that, in a closed system with no external fields, $dQ = Td_eS$ and $dW = pdV$ during an infinitesimal process. Inserting these results into the first law, equation (1.7), gives

$$dU = Td_eS - pdV. \tag{1.19}$$

If there are no internal processes generating entropy, we can use $dS = d_eS$, and so equation (1.19) becomes

$$dU = TdS - pdV. \tag{1.20}$$

The chemical potential μ can be introduced as a means of extending equation (1.20) to a closed system in which there are internal processes, by adding extra terms to the differential of the internal energy,

$$dU = TdS - pdV + \sum_j \mu_j dN_j \tag{1.21}$$

$$= Td_eS + Td_iS - pdV + \sum_j \mu_j dN_j. \tag{1.22}$$

Here, N_j is the number of particles of species j, and μ_j is their chemical potential. Comparison of (1.22) with (1.19) reveals that

$$\sum_j \mu_j dN_j = -T d_i S. \tag{1.23}$$

Here we have considered a system which is closed to matter exchange, but equation (1.22) and the chemical potential apply also to open systems.

Since U must be linear in the extensive variables S, V and $\{N_j\}$, we can write

$$U(\lambda S, \lambda V, \{\lambda N_j\}) = \lambda U(S, V, \{N_j\}), \tag{1.24}$$

where λ is some constant. Differentiating (1.24) with respect to λ allows the derivation of the Euler relation,

$$U = TS - pV + \sum_j \mu_j N_j; \tag{1.25}$$

this relation, together with the definition of the Gibbs free energy given in equation (1.17), can be used to interpret the chemical potential, in a system with these particular constraints, as the Gibbs free energy per particle:

$$G = \sum_j \mu_j N_j. \tag{1.26}$$

Equation (1.25) can also be used together with (1.18) to find an expression for the grand potential:

$$\Omega = -pV. \tag{1.27}$$

Finally, taking the differential of (1.25) and substituting (1.21), we find the Gibbs-Duhem relation,

$$-SdT - Vdp + \sum_j N_j d\mu_j = 0. \tag{1.28}$$

1.5 Thermodynamic integration

Now consider dF as defined in equation (1.9). If we split dS into external and internal contributions, this is written

$$dF = dU - T d_e S - T d_i S - SdT. \tag{1.29}$$

Inserting equations (1.19) and (1.23) gives

$$dF = -SdT - pdV + \sum_j \mu_j dN_j. \tag{1.30}$$

Since the Helmholtz free energy is a state function, the difference between its values in two different states will be the same, irrespective of the thermodynamic path by which we travel between them, so to calculate F we can start from an arbitrary reference state and integrate over any path in state space. This process is known as thermodynamic integration [6]. The simplest path is to integrate over T, V and $\{N_j\}$ in turn, so that each stage involves only a single integration variable. The result will be the Helmholtz free energy relative to the reference state. If we wish to compare F for two states in order to find the equilibrium state of a system, the reference state must, of course, be the same for each calculation.

Equation (1.30) also makes it clear that

$$p = -\frac{\partial F}{\partial V} \tag{1.31}$$

and

$$\mu_j = \frac{\partial F}{\partial N_j}. \tag{1.32}$$

These two relations, together with the condition that F should be a minimum, imply that both the pressure and the chemical potential must be constant across a system if it is in a state of equilibrium. To illustrate this, consider a system divided into two phases α and β by a partition which is free to move and across which particles can be freely exchanged. The free energy change dF_V of transferring volume dV from phase α to phase β (that is, of moving the partition) is given by

$$\begin{aligned} dF_V &= -\frac{\partial F^\alpha}{\partial V^\alpha} dV + \frac{\partial F^\beta}{\partial V^\beta} dV \\ &= \left(p^\alpha - p^\beta\right) dV. \end{aligned} \tag{1.33}$$

If the two phases have different pressures, the system can always reduce its free energy by transferring volume from the phase with lower pressure to the phase with higher pressure. Similarly for the chemical potential: the free energy change dF_N of transferring dN_j particles from phase α to phase β is

$$dF_N = -\frac{\partial F^\alpha}{\partial N_j^\alpha} dN_j + \frac{\partial F^\beta}{\partial N_j^\beta} dN_j$$

$$= \left(-\mu_j^\alpha + \mu_j^\beta\right) dN_j. \tag{1.34}$$

If the two phases have different chemical potentials, the system can reduce its free energy by transferring matter from the phase with higher chemical potential to the phase with lower chemical potential. Only if the pressure and chemical potential are the same in each phase can the free energy be a minimum.

1.6 The ideal gas

The ideal gas is the theoretical noninteracting limit of a real gas; the equation of state is

$$pV = Nk_BT, \tag{1.35}$$

where N is the number of particles and k_B is Boltzmann's constant. The free energy F_{id} of an ideal gas containing N_j of each species j can be calculated using statistical mechanical methods to be

$$F_{id} = k_BT \sum_j N_j \left(\ln \frac{N_j}{V}\Lambda_j^3 - 1\right), \tag{1.36}$$

where

$$\Lambda_j = \left(\frac{h^2}{2\pi m_j k_B T}\right)^{1/2} \tag{1.37}$$

is the thermal wavelength of species j. Here, m_j is the mass of a particle, and h is Planck's constant. F_{id} can also be written as

$$F_{id} = \sum_j N_j \left[\frac{3}{2}k_BT + k_BT\left(\ln \frac{N_j}{V}\Lambda_j^3 - \frac{5}{2}\right)\right]. \tag{1.38}$$

The first term inside the square brackets represents the energy; the second is the Sackur-Tetrode entropy, multiplied by $-T$. This makes the link with the definition of the Helmholtz free energy in (1.8).

Equation (1.36) can be extended to an inhomogeneous ideal gas with density distributions $n_j(\mathbf{r})$. We represent the system as a collection of small regions, in each of which the density is approximately homogeneous. The total ideal gas free energy of the system is then given by a sum of terms of the form (1.36), and as the size of a region tends to zero the sum becomes an integral:

$$F_{id} = k_BT \sum_j \int d^3\mathbf{r} n_j(\mathbf{r}) \left[\ln n_j(\mathbf{r})\Lambda_j^3 - 1\right]. \tag{1.39}$$

However, such a system requires a field to hold the particles in their inhomogeneous distribution; the ideal gas free energy, is then only one component of the total free energy of the system. Equation (1.32) allows us to calculate the chemical potentials μ_j, again ignoring the contribution of the field,

$$\mu_j = k_B T \ln n_j(\mathbf{r}) \Lambda_j^3. \tag{1.40}$$

The activity $a_j = \exp(\mu_j / kT)$ is equal to $\Lambda_j^3 n_j(\mathbf{r})$.

1.7 Chemical potential in the presence of fields

The concept of chemical potential, as explored earlier in this chapter, can be used to take account of the effect of a field, for example an electrostatic field acting on charged particles in the system. However, in these circumstances the ideal gas chemical potential as defined in equation (1.40) clearly will not be constant across the system as required by (1.32); it is necessary to extend the definition by adding terms which take account of the field. There will be a density gradient, the result of a competition between energetic effects, which push the system towards inhomogeneity in the presence of a field, and entropic effects, which oppose this inhomogeneity. If the equilibrium state is to be calculated by minimising the Helmholtz free energy, only fields resulting from the internal arrangement of the system can be present, but in general the chemical potential can also incorporate external fields.

To extend the chemical potential to take account of a field, we add a term representing the energy $H_j(\mathbf{r})$ of a particle due to the field,

$$\tilde{\mu}_j(\mathbf{r}) = \mu_j(\mathbf{r}) + H_j(\mathbf{r}), \tag{1.41}$$

where $\mu_j(\mathbf{r})$ is the chemical potential of a hypothetical system, with the same particle density, in the absence of the field. Equation (1.41) is a natural extension of the concept of chemical potential, since (1.25) permits an interpretation of the chemical potential as a contribution to the energy. When the extra contribution has been added, $\tilde{\mu}_j(\mathbf{r}) = \partial \rho_F(\mathbf{r}) / \partial n_j(\mathbf{r})$, where $\rho_F(\mathbf{r})$ is the free energy density, and so $\tilde{\mu}_j$ is constant across the system. We can use $\tilde{\mu}_j$ whenever the chemical potential appears in the equations of thermodynamics. If the particles, in the absence of the field, behave as an ideal gas, equations (1.40) and (1.41) together lead to

$$n_j(\mathbf{r}) = n_{j0} e^{-H_j(\mathbf{r})/k_B T}, \tag{1.42}$$

where $n_{j0} = \exp\left(\tilde{\mu}_j / k_B T\right) / \Lambda_j^3$. This is the Boltzmann distribution.

For ions of charge $z_j e$ in an electrostatic field $\psi(\mathbf{r})$, we have $H_j(\mathbf{r}) = z_j e \psi(\mathbf{r})$, and $\tilde{\mu}$ is often then called the electrochemical potential. Putting this $H_j(\mathbf{r})$ into (1.42) and substituting the resulting $\tilde{\mu}$ for μ in equation (1.30) for the differential of F, we find

$$dF = -SdT - pdV + \sum_j \left(\mu_j(\mathbf{r}) + z_j e \psi(\mathbf{r})\right) dN_j. \tag{1.43}$$

The term involving the electrochemical potential term can be separated into ideal gas and electrostatic contributions. Since these contributions individually are not constant across the system, they must be written in terms of local particle densities rather than total particle numbers, and dF becomes

$$dF = -SdT - pdV + \sum_j \int d^3\mathbf{r} \left[\mu_j(\mathbf{r}) dn_j(\mathbf{r})\right] + \sum_j \int d^3\mathbf{r} \left[z_j e \psi(\mathbf{r}) dn_j(\mathbf{r})\right]. \tag{1.44}$$

1.8 Phase coexistence in a single-component fluid system

Separation into a dense and a rarefied phase in a single-component fluid can occur if the graph of the free energy f per particle as a function of the volume v per particle contains a region where there is an upward bulge (where $\partial^2 f / \partial v^2$ becomes negative) [7]. This allows a common tangent to be drawn across the bulge, as illustrated in figure 1.2. A hypothetical homogeneous state at some point B on the bulge can reduce its free energy by separating into a mixture of states A and C; this mixture can be visualised as a point on the tangent. At equilibrium, the proportion π_X of the particles that will be found in state X, where X represents A, B or C, is given by

$$\pi_X = \frac{|v_X - v_B|}{v_C - v_A}, \tag{1.45}$$

where v_X is the volume per particle in state X.

The common tangent construction stems from the requirement that the pressure and chemical potential be equal in the two coexisting phases A and C; that is, $p_A = p_C$ and $\mu_A = \mu_C$. The pressure is given by $p = -\partial F / \partial V = -\partial f / \partial v$, so equality of the pressures implies that the tangent to the $f(v)$ curve must have the same gradient at C as at A. Equation (1.17) allows us to express the chemical potential as $\mu = f + pv$, since in this system it is equal to the Gibbs free energy per

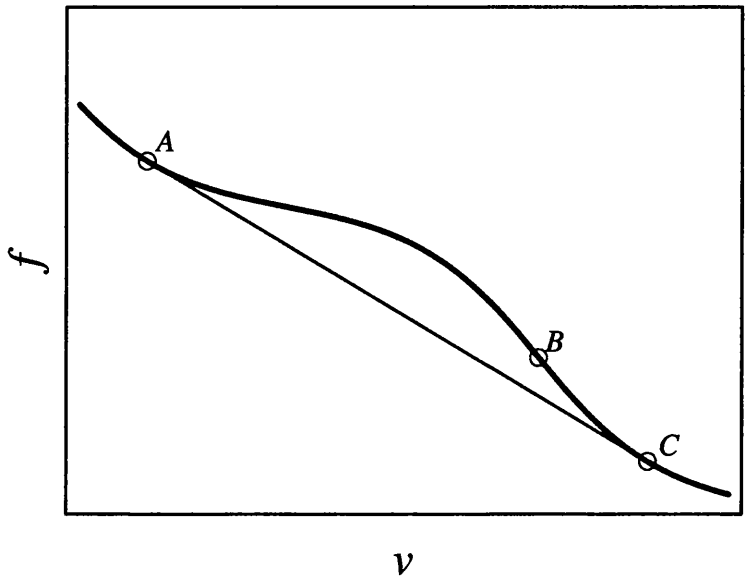

Figure 1.2: Example of an upward bulge in the graph of the free energy per particle as a function of volume per particle, which leads to phase coexistence.

particle, so $\mu_A = \mu_C$ implies

$$f_A - v_A \left(\frac{\partial f}{\partial v}\right)_A = f_C - v_C \left(\frac{\partial f}{\partial v}\right)_C , \tag{1.46}$$

where f_X is the free energy per particle in state X. Equation (1.46) means that the tangents to the $f(v)$ curve at A and C must have the same intercept on the f-axis. The two conditions together imply a common tangent.

It is illuminating to plot a pV diagram; that is, a plot of $p = -\partial f/\partial v$ against v. The presence of the upward bulge in the $f(v)$ curve leads to a so-called van der Waals loop in the pV diagram, as shown in figure 1.3. (The van der Waals equation of state for a nonideal gas produces this type of phenomenon, which can be interpreted as the result of competition between an attractive and a repulsive contribution to the free energy.) Homogeneous states on the curve between A and C will separate into a mixture represented by some point on the line AC, which is drawn according to Maxwell's equal area construction: it is horizontal and its pressure p_0 is such that the areas enclosed by AC and the analytical pressure $p(v)$ above and below AC (the areas denoted I and II in figure 1.3) are equal.

The horizontal nature of AC is clearly a consequence of the condition $p_A = p_B$.

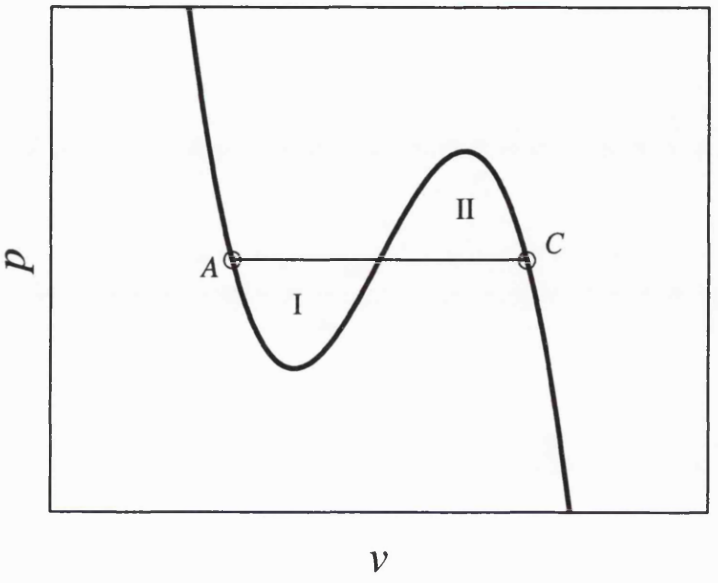

Figure 1.3: Example of a pV diagram illustrating phase coexistence.

Equality of the chemical potentials leads to

$$\begin{aligned} & f_C - f_A + p_0 (v_C - v_A) = 0 \\ \Rightarrow & \int_{f_A}^{f_C} df + p_0 \int_{v_A}^{v_C} dv = 0 \\ \Rightarrow & \int_{v_A}^{v_C} \frac{\partial f}{\partial v} dv + p_0 \int_{v_A}^{v_C} dv = 0 \\ \Rightarrow & \int_{v_A}^{v_C} (p_0 - p)\, dv = 0, \end{aligned} \tag{1.47}$$

which is the condition for equal areas above and below AC.

Varying a third parameter may allow us to produce a series of pV curves. Figure 1.4 shows the result for a simple fluid, where the third parameter is the temperature T. The binodal (marked as b) is the locus of the coexisting states at different temperatures. The spinodal (marked as s) links the local maxima and minima of the $p(v)$ curves. At the critical temperature, $T = T_c$, the binodal and spinodal each have a maximum and are tangential to one another; above this temperature no phase separation will occur. States within the spinodal are unstable and will always phase separate, since arbitrarily small density fluctuations will reduce the

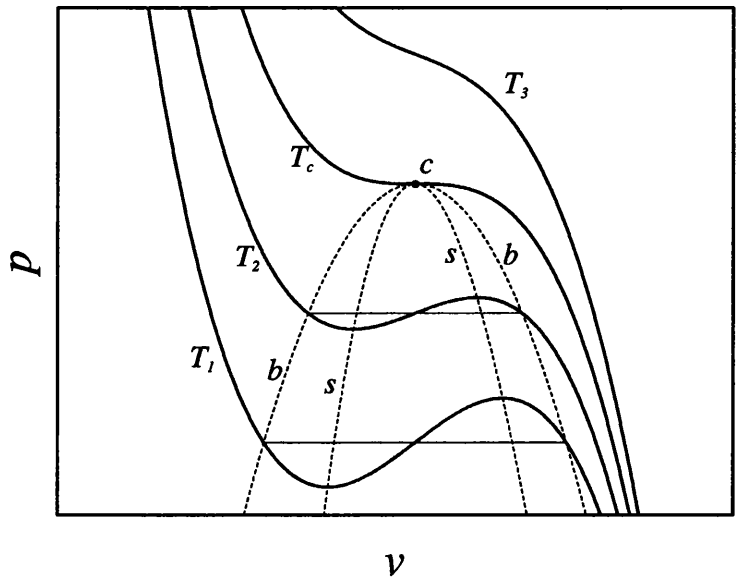

Figure 1.4: Example of a pV diagram for a simple fluid, showing phase coexistence.

free energy. States between the spinodal and binodal are metastable: a density fluctuation of finite size is required in order to reduce the free energy of the state, while smaller fluctuations will increase it. The result is that there is a free energy barrier against phase separation, which in the simple fluid system corresponds to the free energy cost of creating a surface between liquid and gaseous states. The barrier slows the phase separation, allowing the metastable state to persist for a finite time; some systems may not attain equilibrium on any observable timescale. Charged colloidal suspensions are an example of a metastable state, since the true equilibrium state would have the particles packed together as an aggregate, held by van der Waals forces, rather than in suspension. The suspension persists because of a free energy barrier.

The common tangent construction can also be used on a graph of free energy density ρ_F against particle density n, as illustrated in figure 1.5. Equality of the pressures implies

$$\left(\frac{\partial f}{\partial v}\right)_A = \left(\frac{\partial f}{\partial v}\right)_C$$

$$\Rightarrow \left(\frac{\partial f}{\partial n}\frac{\partial n}{\partial v}\right)_A = \left(\frac{\partial f}{\partial n}\frac{\partial n}{\partial v}\right)_C . \tag{1.48}$$

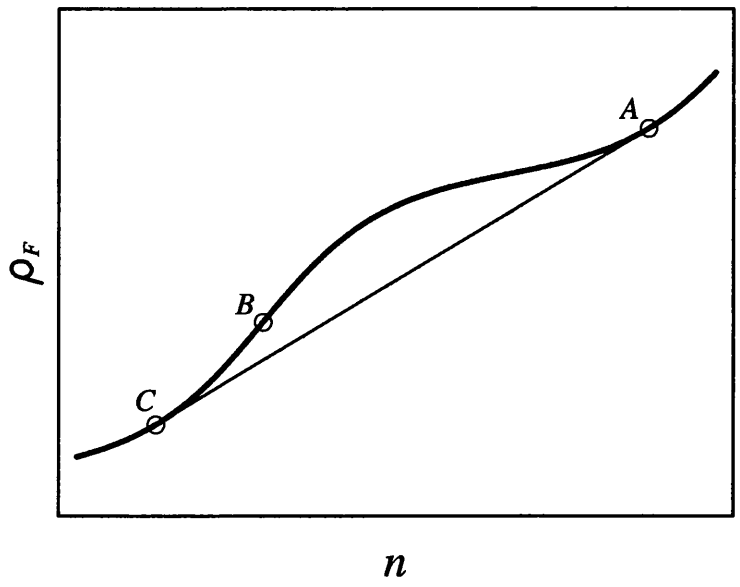

Figure 1.5: Example of an upward bulge in the graph of the free energy density against the particle density, leading to phase coexistence.

Since $n = 1/v$ and $f = \rho_F/n$, this leads to

$$\left(\rho_F - n\frac{\partial \rho_F}{\partial n}\right)_A = \left(\rho_F - n\frac{\partial \rho_F}{\partial n}\right)_C, \tag{1.49}$$

which means that the tangents to the $\rho_F(n)$ curve at A and C cross the ρ_F-axis at the same point. The condition for equality of the chemical potentials is

$$\begin{aligned} \left(f - v\frac{\partial f}{\partial v}\right)_A &= \left(f - v\frac{\partial f}{\partial v}\right)_C \\ \Rightarrow \left(f + n\frac{\partial f}{\partial n}\right)_A &= \left(f + n\frac{\partial f}{\partial n}\right)_C \\ \Rightarrow \left(\frac{\partial \rho_F}{\partial n}\right)_A &= \left(\frac{\partial \rho_F}{\partial n}\right)_C, \end{aligned} \tag{1.50}$$

so the tangents to the $\rho_F(n)$ curve at A and C must have the same gradient. Whereas in the $f(v)$ diagram the equality of pressures fixes the gradient and the equality of chemical potentials fixes the f-intercept, in the $\rho_F(n)$ diagram the gradient is fixed by equality of chemical potentials and the ρ_F-intercept by equality of pressures.

Chapter 2

What has gone before

2.1 Beginnings

Colloidal dispersions were first studied in the 1840s. The behaviour of solutions was well documented by then, but it was noticed that some substances (such as silver chloride and gold chloride, the latter famously studied by Faraday), formed solutions whose behaviour was different to that of ordinary solutions, notably in having a slower diffusion rate and in being unable to diffuse through a membrane [8]. Such substances were termed colloids by Graham, and it was hypothesised that the dispersed particles in a colloidal dispersion, although too small to be visible through a normal microscope, were much larger than those in an ordinary solution, and therefore much larger than the solvent molecules [9].

The invention at the turn of the twentieth century of ultramicroscopic techniques, which allow such small particles to be detected from their diffraction patterns, led to the confirmation of this hypothesis [9]. The term colloid is applied today to substances which are inhomogeneous on a length scale of approximately between 1 nm and 1 μm, consisting of matter of one phase (called the disperse phase), distributed in another phase (the dispersion medium). As well as the original solid-in-liquid colloids (known as sols or dispersions), this definition includes solid- and liquid-in-gas colloids (aerosols), liquid-in-liquid colloids (emulsions) and gas-in-liquid colloids (foams). There are also solid-, liquid- and gas-in-solid colloids, known respectively as solid dispersions, solid emulsions and solid foams [1]. This thesis concerns itself with solid-in-liquid colloids.

Two factors can lead to the particles of the disperse phase having colloidal dimensions. One possibility is that the material is dispersed as a polymolecular aggregate. This is the case with silver chloride and with gold chloride, and also with association colloids such as soap molecules in water, where the molecules in solution may

group together to form structures of colloidal size known as micelles (however, the term micelle was originally applied to any polymolecular aggregate which has an internal crystalline structure [9]). Alternatively, the molecules may themselves be macromolecules, large enough to fall into the colloidal range of length scales. This is the case with protein solutions.

2.2 Colloidal stability

Colloidal dispersions can be divided into two loose categories on the basis of their thermodynamic status. Lyophilic ('solvent-loving') colloids are formed spontaneously due to the interactions between the solute and the solvent; the dispersion is thus thermodynamically stable with respect to the undispersed phase. Macromolecules often fall into this category. Lyophobic ('solvent-hating') colloids, on the other hand, will not be dispersed spontaneously, but if dispersed by some means they can remain in a dispersed state for some time. The equilibrium state (state of lowest free energy) is the undispersed phase, but the dispersion is metastable because of a stabilisation mechanism which creates a thermodynamic barrier to aggregation. A physical or chemical process that removes or reduces this barrier will lead to aggregation due to, for example, the van der Waals forces between the molecules in the colloidal particles.

An alternative terminology, preferred by Kruyt [9], describes lyophilic colloids as reversible and lyophobic colloids as irreversible. The terms are not being used here in the sense in which they are used in thermodynamics, but refer in a direct way to the nature of the process of aggregation. For example, if a lyophobic colloid is caused to aggregate by some means, a return to the previous conditions will not redisperse the system: the aggregation is irreversible. Lyophilic colloids can only be aggregated by removing the solvent, and adding the solvent to the resulting state will lead to redispersion; hence the process is described as reversible.

Two of the mechanisms by which lyophobic colloids can be stabilised are steric and electrostatic stabilisation. Steric (or polymeric) stabilisation is caused by large chain molecules attached to the surfaces of the colloidal particles. Due to the lyophilic nature of these molecules, they repel one another, and two colloidal particles are prevented from approaching one another by the repulsions between their respective attached molecules. Electrostatic stabilisation occurs when surface groups on the colloidal particles dissociate from the surface, resulting in a system containing charged colloidal particles and oppositely charged simple ions. This provides stability against coagulation (as aggregation of the colloidal particles is termed in this

system). Both these stabilisation mechanisms result from surface phenomena, and this highlights one of the main features of colloidal systems: the effects of interfaces are significant.

The study of electrostatically stabilised colloids forms the subject of this thesis. The mechanism which leads to stability in these systems has been the subject of some controversy. The mechanism which leads to the dissolution of simple electrolytes is clear: although from an energetic point of view, the separation of positively and negatively charged ions in a solution is unfavourable, the entropic benefit of dispersing the ions outweighs this, and leads to a reduction in the free energy. As for the stabilisation of charged colloidal suspensions, a consensus was reached in the middle of the twentieth century which was based on the DLVO theory of colloidal interactions, and therefore implied a very different mechanism for stability from that in simple electrolytes.

2.3 DLVO theory

The DLVO (Deryagin-Landau-Verwey-Overbeek) theory [3, 10] was introduced in the 1940s and became established as the standard description of interactions and of stability in charged colloidal suspensions. In many ways it is based on the earlier Debye-Hückel theory [11, 12] for simple electrolytes, which uses the linearised Poisson-Boltzmann equation and thermodynamic integration to determine the activity and other characteristics of electrolyte solutions in the limit of low concentration. The Poisson-Boltzmann equation assumes a model in which the microions are point particles responding to a mean field force; their equilibrium arrangement is then given by a balance, described by a Boltzmann factor, between the electrostatic potential governed by Poisson's equation, and the chemical potential.

The Debye-Hückel theory predicts that around every ion there will be found, averaged over time, an excess of ions of opposite sign. These counterions can be viewed as forming an atmosphere around the first ion, screening its interactions with other ions outside the atmosphere. The electrostatic potential due to the first ion as a function of distance r takes the form of a screened Coulomb or Yukawa potential $e^{-\kappa r}/r$ instead of the $1/r$ dependence in the potential which is found around unscreened ions (a similar mechanism operates in metals, where the free electrons screen the charges of the nuclei). The parameter κ, which will be defined in equation (3.32), depends on the charges and concentrations of all the species of ion in the solution, and is equal to the inverse of the screening length, which is regarded as the range of the screened interaction: due to its rapid decay with distance, a Yukawa

interaction is considered to operate only over a finite range, unlike the Coulomb interaction whose range is viewed as infinite.

DLVO theory uses the same techniques and physical assumptions as Debye-Hückel theory, but applies them to the interactions in colloidal systems. It expresses the electrostatic contribution to the free energy of a suspension as a sum over the pair potentials V_{mn} between every pair of colloidal particles m and n in the system; these pair interactions are usually approximated as

$$V_{mn} = \frac{Z^2 e^2}{4\pi\epsilon}\left(\frac{e^{\kappa a}}{1+\kappa a}\right)^2 \frac{e^{-\kappa R_{mn}}}{R_{mn}}, \tag{2.1}$$

where ϵ is the absolute permittivity of the solvent and R_{mn} is the distance between two colloidal particles m and n, of charge Ze and radius a. Here, the inverse screening length κ has contributions only from the microions; because the colloidal particles are so much larger, their motion is regarded separately from that of the microions, in the sense that the Poisson-Boltzmann equation is used to find the microion distribution about a fixed pair of colloidal ions. In the Debye-Hückel theory of electrolytes, on the other hand, all ions were treated on an equal footing. As in the simple electrolyte system, V_{mn} is a screened Coulomb potential, and it carries with it the same concept of a counterion atmosphere. A point which will prove to be of great importance is that κ is still regarded as a constant in the DLVO theory, independent of the separations of the colloidal particles. The form of the DLVO pair potential is shown in figure 2.1.

The DLVO theory thus asserts that stability against coagulation is provided by repulsive electrostatic forces. The theory also takes account of the short range attractive van der Waals forces between the colloidal particles; it is these forces that are responsible for coagulation into the primary minimum of the potential if the electrostatic barrier can be overcome. At high added salt concentrations (large κ), the range of the screened Coulomb repulsion is reduced so much that it is shorter than that of the van der Waals forces, leading to a secondary minimum in the interaction potential (see figure 2.1). This secondary minimum is taken to be responsible for the phenomenon of flocculation, in which colloidal particles form a low density, easily dispersed aggregate. The ability of added salt to cause flocculation is strongly dependent on the valence of the ions added (the Schulze-Hardy rule [1]); this is explained by the fact, easily seen from equation (3.32), that the contribution to κ of a particular ion species is proportional to the square of the valence but only linearly dependent on the concentration.

The success of the DLVO theory in qualitatively describing known aspects of col-

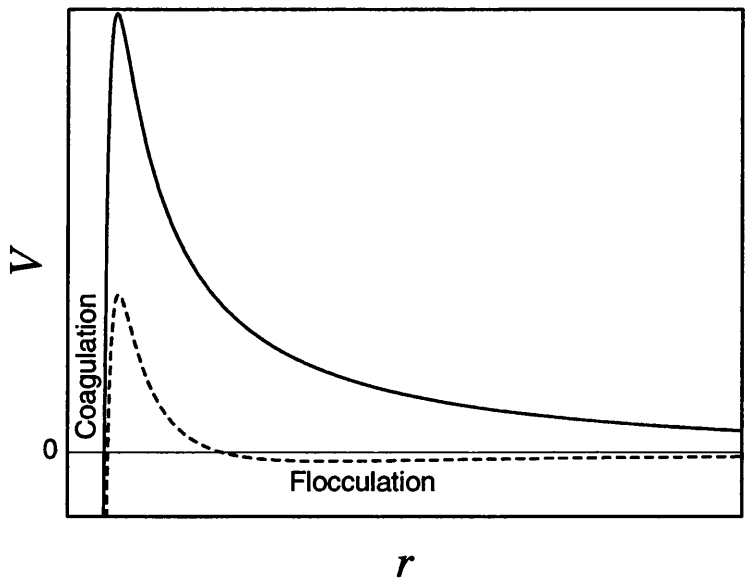

Figure 2.1: Representation of DLVO pair potential V as a function of particle separation r. Solid line: low added salt concentration; dashed line: high added salt concentration. After reference [13].

loidal stability led to its adoption as the standard theory of interactions in charged colloidal dispersions [1]. Exact quantitative description would not be expected, due to the various approximations in the physical model and to the linearisation of the Poisson-Boltzmann equation, although Verwey and Overbeek showed [3] by comparison with numerical results that, for spherical colloidal particles, the linearised approximation produces good results even outside its region of strict validity.

There exists experimental evidence that the interaction between two otherwise isolated particles or surfaces in an aqueous solution takes the DLVO form. Experiments have used surfaces such as sapphire [14], as well as dispersions of polystyrene latex [15] and polystyrene sulphate [16] particles.

2.4 Experimental evidence for the phase behaviour

The existence of ordered structures in charged colloidal dispersion was known at least as early as the 1950s [17]. Kose *et al.* later produced optical images of such ordered dispersions [18], showing the presence of defects and dislocations, and Hachisu *et al.* [19] showed that ordered and disordered (solid- and liquidlike) regions can coexist;

the phase diagram was later investigated systematically by Monovoukas and Gast [20]. The existence of an ordered (crystalline or solidlike) state and even its coexistence under some conditions with a dense disordered (liquidlike) state are compatible in principle with a repulsive effective electrostatic pair potential, as simulations have shown [21, 22, 23].

However, in 1979 Ise *et al.* found evidence, from small-angle X-ray scattering (SAXS) experiments on dilute solutions of sodium polyacrylate, of an ordered structure in which the particle separation $2D_{exp}$ was much smaller than the value $2D_0$ which it would have taken if the structure had filled the available space homogeneously [24, 25]. This was interpreted as evidence that the solidlike structure was coexisting with a void or with a much less dense (gaslike) structure. The phenomenon occurred away from the range of densities in which flocculation due to the secondary minimum in DLVO theory would be expected, and it was therefore suggested that an attractive effective electrostatic interaction was required to explain the results. The same effect was seen with highly charged latex particles [26]; it appeared that the phenomenon occurred only for colloidal particles of high surface charge density and at low salt concentrations. At low surface charge density, and at high salt concentrations with particles of high charge density, $2D_{exp} \approx 2D_0$, implying a single phase.

Subsequent studies produced images of metastable crystallites [27] and of voids in liquidlike phases [28, 29, 30]; these voids may, of course, be gaslike phases containing particles at very low concentrations, and evidence of liquid-gas phase separation, reentrant with respect to salt concentration at fixed macroion charge in the sense that higher or lower salt concentrations led to a homogeneous suspension, was reported [31, 32]. This latter claim was disputed [33], and there have been other studies which have found no evidence of phase separation into a dense and a rarefied phase [34]. Ise *et al.* argue that the phenomenon will occur only if the macroion surface charge density is sufficiently high [2], and that this explains negative results. However, the existence of the phase separation phenomenon is not universally accepted [35] because it conflicts with the established theory of colloidal stability.

Experiments by Yoshida *et al.* have investigated and imaged the process of formation both of voids [36] and of crystals [4, 37] from an initial liquidlike homogeneous state. The latter is the so-called 'Swiss Cheese effect', illustrated in figure 2.2; space-filling crystals form from the initial state on a timescale of seconds to minutes, and then gaslike regions form, on a timescale of minutes to hours, both within the crystals and at the interfaces between them.Two other interesting effects studied in the 1990s should be mentioned here. Matsuoka *et al.* investigated the

nearest neighbour macroion separation $2D_{exp}$ as a function of salt concentration, and found that it first increased (the crystal became less dense) with increasing salt concentration, then decreased after passing through a maximum (that is, the crystal density passed through a minimum) [38, 39]. Yamanaka *et al.* found a solid-liquid phase transition which was reentrant with respect to the macroion surface charge at fixed salt concentration and macroion density [40, 41].

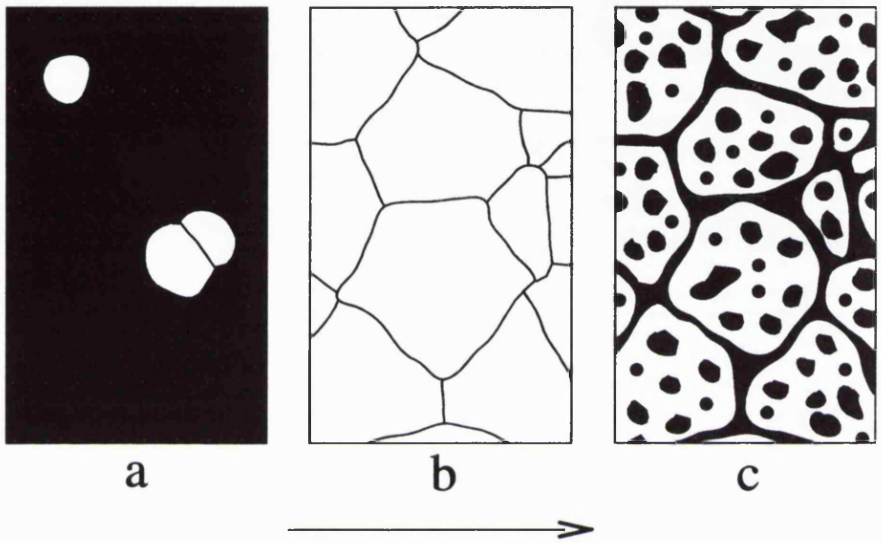

Figure 2.2: The 'Swiss Cheese effect' discovered by Yoshida *et al.* White represents solidlike (ordered) states, while black represents liquidlike and gaslike (disordered) states. A solidlike state nucleates (a) from the initial liquidlike state on a timescale of seconds to minutes, to produce space filling crystals (b). Then a gaslike state forms within the crystals and at their interfaces (c), on a timescale of minutes to hours.

2.5 Theoretical scene

Phase coexistence between a dense and a rarefied phase cannot be explained by a free energy expression that consists only of a sum over repulsive pair potentials. Therefore, experimental evidence for this phenomenon provided a challenge to the DLVO theory. There are three main strands of thought on the theoretical explanation: (1) DLVO theory is an incorrect or incomplete description of the behaviour of the Poisson-Boltzmann model, and a corrected version would predict the phase behaviour on the basis of this model; (2) effective attractive electrostatic interactions between macroions are induced by phenomena which are not covered by the Poisson-Boltzmann model, and which the DLVO theory therefore does not pretend

to consider; or (3) the electrostatic interaction between macroions is always purely repulsive, and the experimental results suggesting otherwise are spurious or have been misinterpreted.

2.5.1 Modified Poisson-Boltzmann theories

First we shall consider theories which are based on the same physical assumptions as DLVO; the microions are described throughout as point ions in a mean field treatment. The first attempt at explaining the observation of voids or gaslike phases was the theory of Sogami [42] and of Sogami and Ise [43]. These authors argued that experimental conditions approximated most closely to a system at constant pressure (due to the effects of the ion distribution and of atmospheric pressure on the volume of the suspension) rather than constant volume, and therefore that the Gibbs free energy G was the appropriate thermodynamic potential to be minimised. Starting from a linearised Poisson-Boltzmann model, they derived a pair potential for the Helmholtz free energy F, which was repulsive and took a similar form to the DLVO potential. They went on to derive a pair potential for the Gibbs free energy, which was substantially different: it combined a short-ranged electrostatic repulsion with a long-ranged electrostatic attraction to form a secondary minimum in the pair potential, caused not by van der Waals forces but by electrostatic effects. Thus, in contrast to DLVO, Sogami and Ise regarded the electrostatic free energy to be responsible both for cohesion and for stability against coagulation. The theory was extended to the one-dimensional system, applicable to clay plates, by Smalley [44].

A number of criticisms were raised against the Sogami-Ise theory. Overbeek argued that the difference between F and G should be small in a condensed system, and suggested that the difference between the two as calculated by Sogami and Ise resulted from their failure to take into account a contribution from the solvent in the derivation of G [45]. It was later pointed out [44] that the suggestion of a solvent contribution violates fundamental thermodynamics and disagrees with the DLVO theory. Woodward also criticised the Sogami-Ise derivation, on the grounds that it required the thermodynamic potentials to be first order homogeneous functions of the extensive variables, a condition that is not satisfied in inhomogeneous systems [46]. The argument that $F \approx G$ is indeed compelling, and the question of the correctness of the Sogami-Ise derivation of the Gibbs free energy remains open; the resolution of this question has perhaps been hampered by the heat of controversy over the issue. A similar attractive pair potential has been derived by Tokuyama [47] using the theory of diffusion. Other treatments have predicted a repulsive pair

potential between two otherwise isolated macroions [48, 49] and between a macroion and a surrounding 'cage' of fixed macroions [50].

Van Roij and co-workers [51, 52, 53, 54] developed an expression for the Helmholtz free energy using classical density functional theory, where the free energy functional to be minimised was based on the linearised Poisson-Boltzmann theory. The result contains a sum over pair potentials identical to those of the DLVO theory, together with a serious of additional 'volume' terms, which depend on the density of the macroions in the suspension but not on the structure (the actual macroion positions). The calculated phase diagrams display solid-, liquid- and gaslike phases, and at low salt concentrations permit coexistence between a dense and a rarefied phase, for which the volume terms are regarded as being responsible. The existence of these volume terms had been pointed out earlier [55, 56], and has been further emphasised by other authors [57, 58, 59]. It has been argued that theories which include the volume terms may in fact be equivalent to the Sogami-Ise theory [60].

The theory of RDH differed from the DLVO and Sogami-Ise theories in that it permitted the inverse screening length κ, which depends on the microion density, to vary as a function of macroion density in order to maintain charge neutrality in a given phase. This κ variation had been suggested earlier by Beresford-Smith *et al.* [61], who did not include some of the free energy contributions of the microions and therefore did not produce phase diagrams. Other theories have calculated F, taking account of the dependence of κ on the macroion density, and have showed the existence of phase separation. Warren used a development [62] of Debye-Hückel theory, and concluded that the phase separation is driven by the cohesive nature of the electrostatic free energy and opposed by the counterion entropy. Knott and Ford showed that phase coexistence in a system with no added salt results from the direct solution of the linearised Poisson-Boltzmann equation [63]; this work forms a part of this thesis. Chan *et al.* have also found phase coexistence in the zero salt system [64], using a version of Debye-Hückel theory extended for finite ion sizes.

It is has been shown that, if κ is held constant, the electrostatic part of the interaction in a system of more than two macroions is purely repulsive [61, 66, 67]. This can be seen as an extension of the DLVO conditions to a many-body system, which would not be expected to predict phase coexistence. However, Linse and Lobaskin also failed to find phase coexistence in Monte Carlo simulations [68, 69] which used fundamental electrostatic interactions.

It is interesting to note that the interpretation of the interaction as a sum of an attractive electrostatic component and an entropic repulsion was also arrived at by Sogami *et al.* on the basis of calculations of the interaction between two highly

charged plates (the one-dimensional system) in an electrolyte [70, 71]. These found an attractive effect from the Helmholtz, rather than the Gibbs, free energy, although the results have been disputed [72, 73].

2.5.2 Outside the Poisson-Boltzmann model

By introducing approximations, the Poisson-Boltzmann model of the microion distribution can potentially fail to describe some aspects of the system. The mean field approximation, which describes the microions as a continuous fluid of variable density rather than as individual particles, fails to take into account microion-microion correlations. In addition, the DLVO theory and most others are based on the linearised form of the Poisson-Boltzmann model, and therefore are not valid if the potential varies too much. It is in the region of the macroion surfaces that the potential takes its most extreme value and the linearised theory is most likely to be incorrect; since this is the location of highest microion density, correlations will also be most important in this region.

There are two main approaches to correcting the theory for these inadequacies. The first is to consider microions that are close to the surface to be, in a sense, part of the macroion: they are 'condensed' on to the surface. This eliminates the problem of describing high potentials and microion correlations at the surface with the Poisson-Boltzmann equation. Then the effective interactions between macroions are described [74, 75, 76, 77] using the DLVO potential with a reduced or 'renormalised' effective charge [78, 79] rather than the 'bare' charge. It has recently been claimed on the basis of another extended Debye-Hückel theory that, although the electrostatic contribution to the free energy is attractive, counterion condensation stabilises suspensions against the phase separation which occurs in the linearised theory [80, 81].

The second approach is explicitly to correct the theory to take account of microion correlations [82, 83]. This can introduce attractive effects in the electrostatic free energy (for a review, see [35]). However, the attractions are short-ranged, and could not explain the presence of the voids. It has been suggested that the voids are not caused by electrostatic interactions at all, but by depletion interactions involving impurities [35].

Another mechanism for phase coexistence that has been proposed is charge inversion or overcharging, in which a macroion is bound to enough counterions to change its sign. Neighbouring macroions might then have charges of opposite sign, leading to long-range electrostatic attraction [84]. However, it will be shown in this thesis

that it is not necessary to go beyond the linearised Poisson-Boltzmann model to find phase separation, because the phase separation behaviour is actually inherent even in such a simplified approach, so long as the parameters are introduced correctly.

Chapter 3

Calculation of the thermodynamics of a charged colloidal suspension

3.1 Introduction

In this chapter, we derive expressions for the free energy of a colloidal suspension, on the basis of the principles of thermodynamics which were set out in chapter 1. The technique used draws on the work of Sogami and Ise [43], who provided the backbone of a method for the solution of the linearised Poisson-Boltzmann equation for a large suspension. One problem with the method is that it permits microions to penetrate the interiors of the macroions [53], but here we eliminate this difficulty, enabling the Helmholtz free energy of a colloidal suspension, as well as the surface potential of a macroion in such a suspension, to be found analytically. This requires us to make a small number of justifiable approximations, based around the idea that the environments of all the macroions in a given phase are approximately identical and spherically symmetric.

Much of the contents of this chapter and the next has been published in Physical Review E [63].

3.2 The model

The theoretical model to be considered treats a large constant number, N_M, of identical spherical macroions of radius a, each of which has a constant charge Ze, where $|Z| \gg 1$, distributed uniformly over its surface (e is the elementary charge). Associated with the macroions are a constant number N_i of each species i of microions, which are regarded as point charges of value $z_i e$. The system overall is

charge neutral, so that $N_M Z + \sum_i N_i z_i = 0$. The ions are suspended in a solvent which is maintained at constant volume V and constant temperature T and which is described as a continuum with permittivity $\epsilon = \epsilon_r \epsilon_0$, which is unaffected by the ions. Here, ϵ_0 is the permittivity of the vacuum, and ϵ_r the relative permittivity; we regard the solvent as being water, which has a relative permittivity of around 80.

We consider the behaviour of the macroions to be adiabatically separated from that of the microions, since the macroions are much larger; the microions will be allowed to take up their equilibrium configuration about a 'fixed' system of macroions, and only then will the effect on the macroions be considered. We ignore correlations between the microions, so that they do not interact directly with one another; they behave like an ideal gas except that they interact with a mean field electrostatic potential. These last two simplifications make possible a Poisson-Boltzmann treatment of the electrostatics of the system.

There are three external constraints on the system: the temperature is constant, the volume of the solvent (that is, the total volume available to the suspension) is constant, and no exchange of ions is permitted with the surroundings. Therefore, the equilibrium state will be the state that minimises the Helmholtz free energy F. This is found by thermodynamic integration of equation (1.44), which expresses the differential of F as

$$dF = -SdT - pdV + \sum_i \int d^3\mathbf{r}\,(\mu_i(\mathbf{r}) dn_i(\mathbf{r})) + \sum_j \int d^3\mathbf{r}\,(\psi(\mathbf{r}) d\rho_j(\mathbf{r})) \qquad (3.1)$$

where S is the entropy of the microions, p is the pressure and V the volume. The third term, involving chemical potentials $\mu_i(\mathbf{r})$ and densities $n_i(\mathbf{r})$, contains an integral over an inhomogeneous system and a summation over the microion species i. The fourth term represents the electrostatic contribution; $\psi(\mathbf{r})$ is the electrostatic potential, defined so that its mean value is zero, and $\rho_j(\mathbf{r}) = z_j e n_j(\mathbf{r})$ is the charge density of species j. Here, the suffix j runs over all the microion species i, together with the macroions. We start from a fixed initial state and integrate over $n_i(\mathbf{r})$, T, V and $\rho_j(\mathbf{r})$ in turn, keeping the other integration variables constant at each stage.

Equation (3.1) can be written as

$$dF = dF_0 + dF_{el}, \qquad (3.2)$$

where dF_0, containing the first three terms on the right hand side of equation (3.1), is the non-electrostatic part of the differential of the free energy, and dF_{el} is the electrostatic part. An additional contribution to dF_0 comes from the free energy of

the colloidal particles in the absence of charge. If the particles are regarded as hard spheres, this entropic term can be calculated using the Carnahan-Starling equation of state [85, 86]; however, it is small in comparison with the other terms, and we shall ignore it. Therefore, the non-electrostatic free energy F_0 will come only from hypothetical uncharged microions.

3.3 The electrostatic free energy and the Poisson-Boltzmann equation

3.3.1 The thermodynamic integration

We calculate the electrostatic part of the free energy using its differential

$$dF_{el} = \sum_i \int d^3\mathbf{r} \left(\psi(\mathbf{r}) d\rho_j(\mathbf{r})\right). \tag{3.3}$$

The charge density of microions of species i is $\rho_i(\mathbf{r}) = z_i n_i(\mathbf{r}) e$. The charge density on the surface of a macroion must also be proportional to the elementary charge e, as the total charge on a macroion is Ze. We shall introduce a charge number density $\rho'_j(\mathbf{r})$, defined by $\rho_j(\mathbf{r}) = \rho'_j(\mathbf{r})e$; for microion species i, $\rho'_i(\mathbf{r}) = z_i n_i(\mathbf{r})$. In order to change $\rho_j(\mathbf{r})$ in equation (3.3) during the thermodynamic integration, it is necessary to change e (theoretically) rather than $\rho'_j(\mathbf{r})$, since the latter would also introduce changes in free energy which will be dealt with in other stages of the thermodynamic integration. The equation can be rewritten as

$$dF_{el} = \sum_j \int d^3\mathbf{r} \left(\psi(\mathbf{r}) \rho'_j(\mathbf{r}) de'\right), \tag{3.4}$$

where de' represents an infinitesimal change in e. The electrostatic energy U_{el} is defined as $U_{el} = \frac{1}{2}\sum_j \int d^3\mathbf{r}\psi(\mathbf{r})\rho_j(\mathbf{r})$, so that

$$dF_{el} = \frac{2U_{el}(e')}{e'} de'. \tag{3.5}$$

For convenience later we substitute $de'^2/2e'$ for de', to give the expression which we will use for the electrostatic part of the Helmholtz free energy in terms of the electrostatic energy

$$F_{el} = \int_0^{e^2} \frac{U_{el}(e')}{e'^2} de'^2, \tag{3.6}$$

where e' is being taken from zero to its physical value e. This leads to the following well known expression for the total free energy

$$F = F_0 + \int_0^{e^2} \frac{U_{el}(e')}{e'^2} de'^2. \tag{3.7}$$

This is Debye's charging equation; to use it, we need to calculate U_{el}. The standard expression, in terms of the total charge density $\rho(\mathbf{r}) = \sum_j \rho_j(\mathbf{r})$, is

$$U_{el} = \frac{1}{2} \int \psi(\mathbf{r}) \rho(\mathbf{r}) d^3\mathbf{r}. \tag{3.8}$$

Combining this with Poisson's equation $\nabla^2\psi = -\rho/\epsilon$ gives

$$U_{el} = -\frac{\epsilon}{2} \int \psi(\mathbf{r}) \nabla^2\psi(\mathbf{r}) d^3\mathbf{r}, \tag{3.9}$$

and with some vector manipulation and the use of the divergence theorem, we find

$$U_{el} = \frac{\epsilon}{2} \int_V [\nabla\psi(\mathbf{r})]^2 d^3\mathbf{r} - \frac{\epsilon}{2} \oint_S [\psi(\mathbf{r}) \nabla\psi(\mathbf{r})] \cdot d\mathbf{S}, \tag{3.10}$$

where surface S envelopes volume V. But the second term, as a surface term, becomes negligible in a large system, and so the result is the familiar expression for the electrostatic energy

$$U_{el} = \frac{\epsilon}{2} \int_V [\nabla\psi(\mathbf{r})]^2 dV. \tag{3.11}$$

It can be seen that equation (3.11) depends only on the gradient of the potential, while equation (3.8) depends on its absolute value. Consider a redefinition of the zero of potential, so that a constant $\Delta\psi$ is added to the potential at each point: the value of the energy given by equation (3.11) would not change. It might appear that the energy given by equation (3.8) would change. However, since the system is neutral overall, the energy increase of the positive charges in the system would be exactly balanced by the energy decrease of the negative charges.

3.3.2 Mean field theory for the microions

The adiabatic separation of the macroions from the microions and the neglect of microion-microion correlations permit the use of a mean field Poisson-Boltzmann description of the microion distribution. This means that the microions are modelled as a continuous fluid of charge (of varying density) rather than as a collection of discrete particles. To simplify the following discussion about the interpretation of the Boltzmann factor, we shall temporarily ignore the macroions altogether. The

phase space probability density $p_i(\mathbf{r}, \mathbf{p})$ for each microion of species i is given by the canonical distribution,

$$p_i(\mathbf{r}, \mathbf{p}) = \frac{e^{-\beta H_i(\mathbf{r},\mathbf{p})}}{\int d\Omega e^{-\beta H_i(\mathbf{r},\mathbf{p})}}, \tag{3.12}$$

where $\mathbf{r}$ and $\mathbf{p}$ are the position and momentum, respectively, $H_i(\mathbf{r}, \mathbf{p})$ is the Hamiltonian, and $\beta = 1/k_B T$, where k_B is the Boltzmann constant and T the absolute temperature. The integral is performed over the phase space Ω. We make the assumption that the Hamiltonian H_i of a microion of species i is a sum of two independent terms: a term $H_i^r(\mathbf{r})$ which depends only on the position $\mathbf{r}$, and a term $H_i^p(\mathbf{p})$ which depends only on the momentum $\mathbf{p}$. Then equation (3.12) becomes

$$p_i(\mathbf{r}, \mathbf{p}) = \frac{e^{-\beta H_i^r(\mathbf{r})} e^{-\beta H_i^p(\mathbf{p})}}{\int dV e^{-\beta H_i^r(\mathbf{r})} \int d\mathbf{p} e^{-\beta H_i^p(\mathbf{p})}}, \tag{3.13}$$

where the volume integral is taken over the whole available volume and the momentum integral is taken over the whole space of possible momenta. The probability density as a function of position is found by integrating out the momentum contributions: $p_i(\mathbf{r}) = \int d\mathbf{p} p_i(\mathbf{r}, \mathbf{p})$. Only the top right hand exponential of equation (3.13) depends on $\mathbf{p}$, and when integrated this cancels with the bottom right hand integral, to leave

$$p_i(\mathbf{r}) = \frac{e^{-\beta H_i(\mathbf{r})}}{\int dV e^{-\beta H_i(\mathbf{r})}}. \tag{3.14}$$

Assume that there are N_i identical ions in the space; their number density will be given by a Boltzmann factor,

$$n_i(\mathbf{r}) = \frac{N_i e^{-\beta H_i(\mathbf{r})}}{\int dV e^{-\beta H_i(\mathbf{r})}} = n_{i0} e^{-\beta H_i(\mathbf{r})}, \tag{3.15}$$

where $n_{i0} = \frac{N_i}{\int dV e^{-\beta H_i(\mathbf{r})}}$. This is a statistical mechanical justification for the expression (1.42) which was derived from thermodynamics in the chapter 1. The Hamiltonian is taken to be $H_i(\mathbf{r}) = z_i e \psi(\mathbf{r})$, where $\psi(\mathbf{r})$ is the electrostatic potential.

3.3.3 Interpretation of the Boltzmann factor

The microion number density is

$$n_i(\mathbf{r}) = n_{i0} e^{-\beta z_i e \psi(\mathbf{r})}. \tag{3.16}$$

It is clear that if n_{i0} is replaced by some different value $n_{i0} + \Delta n_{i0}$, the same ion distribution can still be produced, provided that $\psi(\mathbf{r})$ is also shifted by the appropriate constant amount. There is no physical significance in such a constant shift in $\psi(\mathbf{r})$, since the physics depends only on the gradient of the potential; the potential has no natural zero value, and its absolute value is of no importance. Consider

$$n_i'(\mathbf{r}) = (n_{i0} + \Delta n_{i0})\, e^{-\beta z_i e(\psi(\mathbf{r}) + \Delta\psi(\mathbf{r}))}. \tag{3.17}$$

This will be the same density distribution as $n_i(\mathbf{r})$, provided that

$$\Delta\psi(\mathbf{r}) = \frac{1}{\beta z_i e} \ln\left(1 + \frac{\Delta n_{i0}}{n_{i0}}\right), \tag{3.18}$$

which is independent of $\mathbf{r}$ and therefore represents a constant shift $\Delta\psi$.

This shifting of the electrostatic potential is a little like a gauge transformation [87], with the 'gauge condition' being a condition on an integral of the potential,

$$\int dV e^{-\beta z_i e\psi(\mathbf{r})} = \frac{N}{n_{i0}}, \tag{3.19}$$

which can be satisfied by setting the potential zero to the appropriate value. As an example of a 'gauge', consider that in which n_{i0} is equal to $\overline{n_i}$, the mean density of ions of species i. This requires the zero of the potential to be set so that

$$\int dV e^{-\beta z_i e\psi(\mathbf{r})} = V. \tag{3.20}$$

Note that, since the ion density can be represented in the $n_{i0} = \overline{n_i}$ gauge as

$$n_i(\mathbf{r}) = \overline{n_i} e^{-\beta z_i e\psi(\mathbf{r})}, \tag{3.21}$$

it can also be represented as

$$n_i(\mathbf{r}) = n_{i0} e^{-\beta z_i e(\psi(\mathbf{r}) + \Delta\psi)}, \tag{3.22}$$

where $n_{i0} = c_i \overline{n_i}$, with $c_i = e^{\beta z_i e \Delta\psi}$, for any $\Delta\psi$. This means that, whatever gauge is being used, n_{i0} is some constant multiple of the mean ion density. This is significant for the consideration of colloidal suspensions: in the present model, the total number of microions is a constant, and therefore so is their mean density. Consequently, in a given fixed gauge, n_{i0} is also a constant.

In systems containing several species of microion it is impossible, in any given gauge, to have $c_j = c_i$ unless $z_j = z_i$. That is, equation (3.19) can only be satisfied

simultaneously for ion species having unequal charges if we interpret n_{i0} differently for each species. For example, we could define the potential zero so as to make the n_{i0} associated with ions of charge z_i equal to the mean density $\overline{n_i}$, but then the n_{j0} associated with ions of charge $z_j \neq z_i$ would not be equal to $\overline{n_j}$. This point would need to be taken into account in the application of solutions to the full Poisson-Boltzmann equation.

3.3.4 The linearised Poisson-Boltzmann equation

Poisson's equation for the electrostatic potential states that

$$\nabla^2\psi(\mathbf{r}) = -\frac{1}{\epsilon}\rho(\mathbf{r}), \tag{3.23}$$

where $\rho(\mathbf{r})$ is the charge density. If we consider a system in which the only charges are those on the microions, this charge density is

$$\rho(\mathbf{r}) = \sum_i z_i e n_i(\mathbf{r}) = \sum_i z_i e n_{i0} e^{-\beta z_i e \psi(\mathbf{r})}. \tag{3.24}$$

Inserting this into Poisson's equation gives the Poisson-Boltzmann equation for the electrostatic potential in an ionic system,

$$\nabla^2\psi(\mathbf{r}) = -\frac{1}{\epsilon}\sum_i z_i e n_{i0} e^{-\beta z_i e \psi(\mathbf{r})}. \tag{3.25}$$

The full Poisson-Boltzmann equation is, unfortunately, too difficult to solve analytically for any but the simplest geometries. However, we can expand the exponential as a power series, and if we assume that the potential is everywhere sufficiently close to zero for the conditions $|\beta z_i e \psi(\mathbf{r})| \ll 1$ to be met (the Debye-Hückel approximation), we can keep only the first two terms, leading to the linearised Poisson-Boltzmann equation,

$$\nabla^2\psi(\mathbf{r}) = -\frac{1}{\epsilon}\sum_i z_i e n_{i0} \left(1 - \beta z_i e \psi(\mathbf{r})\right). \tag{3.26}$$

It is clear that the extent to which this linearised equation is a good approximation to the original depends not only on the gradient of the potential, but also on the gauge. The equivalence between gauges that exists in the full equation is lost: it is no longer true that an arbitrary change Δn_{i0} can be compensated for by a constant shift $\Delta\psi$ in $\psi(\mathbf{r})$. The best gauge to use, if we wish to convert to the linearised equation, is one which keeps $\psi(\mathbf{r})$ as close as possible to zero in as much of the

system as possible. The one mentioned above, in which $n_{i0} = \overline{n_i}$, seems to be quite a good candidate: if we integrate the density (using a linearised Boltzmann factor),

$$N_i = \int dV n_i(\mathbf{r}) = n_{i0}V - \beta z_i e n_{i0} \int dV \psi(\mathbf{r}), \tag{3.27}$$

we see that this gauge correponds to the condition $\int dV \psi(\mathbf{r}) = 0$, or $\overline{\psi} = 0$.

Now it can be seen that this linearised system possesses an advantage to set against the disadvantage of the restriction on our choice of potential zero. It is possible to write $n_{i0} = c\overline{n_i}$, where c is the same for every species of microion, provided that the gauge used is $\overline{\psi} = 0$ (so $n_{i0} = \overline{n_i}$ and $c = 1$). This means that we can put the same interpretation on n_{i0} for each ion species, irrespective of their charge.

There is a third, and conclusive, reason for choosing $\overline{\psi} = 0$ in the linearised system (and this also applies, in fact, to the nonlinear system). We wish to calculate the Helmholtz free energy of a colloidal system from the electrostatic energy using equation (3.7), Debye's charging equation. This involves integrating the elementary charge e from zero to its physical value. Therefore, we should consider the behaviour of a system of ions described by a Boltzmann factor as e is changed. The ion density at some charge $e^{(1)}$ is given by the linearised Boltzmann factor as

$$n_i^{(1)}(\mathbf{r}) = n_{i0}^{(1)} \left(1 - \beta z_i e^{(1)} \psi^{(1)}(\mathbf{r})\right). \tag{3.28}$$

There is no reason to expect the density distribution to remain the same as e changes to $e^{(2)}$; however, we require the total number of ions to stay the same,

$$n_{i0}^{(1)} \left(V - \beta z_i e^{(1)} \int dV \psi^{(1)}(\mathbf{r})\right) = n_{i0}^{(2)} \left(V - \beta z_i e^{(2)} \int dV \psi^{(2)}(\mathbf{r})\right). \tag{3.29}$$

During the e-integration, we wish to keep n_{i0} constant, that is, $n_{i0}^{(2)} = n_{i0}^{(1)}$; applying this condition and considering the situation when $e^{(1)}$ is equal to zero, we see that equation (3.29) can only be satisfied if $\overline{\psi}^{(2)} = \overline{\psi}^{(1)} = 0$. It appears that Debye's charging-up theorem only makes sense if $\overline{\psi} = 0$, so we shall assume this gauge in the remainder of the paper.

3.3.5 Representation of the macroions

Before we can model a colloidal suspension, we must add the macroions. The total surface charge density $\rho_M(\mathbf{r})$ is given [43] by a sum over a set of spherical delta

functions of radius a, the nth of which represents a macroion centred on $\mathbf{R}_n$,

$$\rho_M(\mathbf{r}) = \sum_n \rho_n(\mathbf{r}) = \sum_n \frac{Ze}{4\pi a^2}\delta(|\mathbf{r} - \mathbf{R}_n| - a). \tag{3.30}$$

The next step is to modify the available volume (and hence the phase space) to exclude microions from the interior of the macroions. We encode this exclusion by multiplying the Boltzmann factor by a product of Heaviside step functions $\prod_n \theta_n \equiv \prod_n \theta(|\mathbf{r} - \mathbf{R}_n| - a)$,

$$n_i(\mathbf{r}) = n_{i0}\left(1 - \beta z_i e\psi(\mathbf{r})\right)\prod_n \theta_n. \tag{3.31}$$

This change requires the volume integrals mentioned above to be taken over all space except the interiors of the macroions.

Introducing a constant quantity κ^2, defined, in the same way as the square of the inverse screening length in Debye-Hückel theory, to be

$$\kappa^2 \equiv \frac{\beta}{\epsilon}\sum_i z_i^2 e^2 n_{i0}, \tag{3.32}$$

allows the linearised Poisson-Boltzmann equation, taking the macroions into account, to be written as

$$\left(\nabla^2 - \kappa^2 \prod_n \theta_n\right)\psi(\mathbf{r}) = -\frac{1}{\epsilon}\sum_n \rho_n(\mathbf{r}) - \frac{1}{\epsilon}\sum_i z_i e n_{i0}\prod_n \theta_n. \tag{3.33}$$

The dielectric constant of the macroion interiors will obviously be different from that of the solution, but in these regions the charge density, and therefore $\nabla^2\psi$, will be zero, so the difference in the dielectric constants will have no effect on our results. Consequently, we use for ϵ its value in the solution.

3.4 Solution of the Poisson-Boltzmann equation

3.4.1 A shifted potential

The first step is to simplify equation (3.33) by changing variables to a new potential $\phi(\mathbf{r})$, which is given by

$$\phi(\mathbf{r}) = \psi(\mathbf{r}) - \frac{e}{\epsilon\kappa^2}\sum_i z_i n_{i0}, \tag{3.34}$$

so that

$$\left(\nabla^2 - \kappa^2 \prod_n \theta_n\right)\phi(\mathbf{r}) = -\frac{1}{\epsilon}\sum_n \rho_n(\mathbf{r}). \tag{3.35}$$

Since the shift is a constant, the gradient of $\phi(\mathbf{r})$ is equal to that of $\psi(\mathbf{r})$. This shift in the potential is not the same as the 'gauge transformation' introduced earlier in the chapter. There, we shifted the potential in order to describe the system with the same form of equation, but with a different value for n_{i0}. Here, we shift the potential in order to describe the system with a different, simpler, form of equation, but with the *same* value for n_{i0}.

What is the interpretation of this shifted potential $\phi(\mathbf{r})$? The value of $\psi(\mathbf{r})$ at some (possibly hypothetical) location far from any macroions can be found from the condition of local charge neutrality,

$$\sum_i z_i n_i(\mathbf{r}) = 0; \tag{3.36}$$

we substitute (3.31) into (3.36), remembering that $\Pi_n \theta_n = 1$ outside the macroions, to give

$$\sum_i z_i n_{i0} \left(1 - \beta z_i e \psi_\infty\right) = 0, \tag{3.37}$$

and therefore

$$\psi_\infty = \frac{1}{\beta e} \frac{\sum_i z_i n_{i0}}{\sum_i z_i^2 n_{i0}} = \frac{e}{\epsilon \kappa^2} \sum_i z_i n_{i0}. \tag{3.38}$$

So $\phi(\mathbf{r}) = \psi(\mathbf{r}) - \psi_\infty$; that is, $\phi(\mathbf{r})$ is the potential relative to a zero point located at some point far outside the system of macroions. This is the potential zero used by Verwey and Overbeek [3]; however, the n_{i0} in the definition of the κ^2 which appears in equation (3.35) is still to be interpreted as the mean microion density. The above interpretation of $\phi(\mathbf{r})$ is not correct when only a single species of microion is present, because in these circumstances (3.36) implies $n_i = 0$, which can be satisfied in the true nonlinear Poisson-Boltzmann regime only by an infinite potential: the linearisation approximation (which we used to justify the interpretation) cannot then be valid in a region of the system where (3.36) is satisfied.

3.4.2 Solving for the potential in Fourier space

In order to solve equation (3.35), we follow Sogami and Ise [43] in Fourier transforming it; our convention for the Fourier transform $\mathcal{F}[\alpha(\mathbf{r})]$ of a function $\alpha(\mathbf{r})$ is

$$\mathcal{F}[\alpha(\mathbf{r})] = \frac{1}{(2\pi)^{3/2}} \int d^3\mathbf{r} \alpha(\mathbf{r}) e^{-i\mathbf{k}\cdot\mathbf{r}}, \tag{3.39}$$

where the volume integral is to be taken over the whole of the system. The term involving ∇^2 is easily dealt with using $\mathcal{F}[\nabla^2 \phi(\mathbf{r})] = -k^2 \tilde{\phi}(\mathbf{k})$, where the meaning of

the tilde is that $\tilde{\alpha}(\mathbf{k}) \equiv \mathcal{F}[\alpha(\mathbf{r})]$. For the second term in equation (3.35), we use the fact that $\prod_n \theta_n$ is zero inside macroions and unity outside to write

$$\mathcal{F}\left[\kappa^2 \prod_n \theta_n \phi(\mathbf{r})\right] = \kappa^2 \tilde{\phi}(\mathbf{k}) - \frac{\kappa^2}{(2\pi)^{3/2}} \int_{int} dV \phi(\mathbf{r}) e^{-i\mathbf{k}\cdot\mathbf{r}}, \tag{3.40}$$

where the integral is over the interiors of all the macroions. To perform this integration, we introduce an approximation by assuming that the field surrounding each macroion is spherically symmetric. Then the potential inside the macroions will be constant, and will in fact be equal to the surface potential ϕ_s. If we also write $\mathbf{r} = \mathbf{R}_n + \mathbf{r}'$, the integral can be rewritten as

$$\int_{int} dV \phi(\mathbf{r}) e^{-i\mathbf{k}\cdot\mathbf{r}} = \phi_s \sum_n e^{-i\mathbf{k}\cdot\mathbf{R}_n} \int_{|\mathbf{r}'|=0}^{a} d^3\mathbf{r}' e^{-i\mathbf{k}\cdot\mathbf{r}'}. \tag{3.41}$$

The integral on the right hand side of equation (3.41) is identical for each macroion, and can be evaluated by elementary methods, yielding

$$\mathcal{F}\left[\kappa^2 \prod_n \theta_n \phi(\mathbf{r})\right] = \kappa^2 \tilde{\phi}(\mathbf{k}) - \left(\frac{2}{\pi}\right)^{1/2} \kappa^2 \phi_s \left(\frac{\sin ka}{k^3} - \frac{a \cos ka}{k^2}\right) \sum_n e^{-i\mathbf{k}\cdot\mathbf{R}_n}. \tag{3.42}$$

To find the Fourier transform of the right hand side of equation (3.35), we once again introduce $\mathbf{r} = \mathbf{R}_n + \mathbf{r}'$, resulting in an integral which is the same for each macroion. After we integrate over the angular coordinates of $\mathbf{r}'$, a delta function picks out the value $r' = a$ in the r'-integration, with the result,

$$\tilde{\rho}_n(\mathbf{k}) = \frac{1}{(2\pi)^{3/2}} \frac{Ze \sin ka}{ka} e^{-i\mathbf{k}\cdot\mathbf{R}_n}. \tag{3.43}$$

Collecting equations (3.35), (3.42) and (3.43) leads to the result for the Fourier transform of the potential,

$$\tilde{\phi}(\mathbf{k}) = \frac{1}{(2\pi)^{3/2}} \frac{Ze}{\epsilon} \frac{1}{k^2 + \kappa^2} g(k) \sum_n e^{-i\mathbf{k}\cdot\mathbf{R}_n}, \tag{3.44}$$

where, to lighten the equations, we have defined $g(k)$ by

$$g(k) \equiv \frac{\sin ka}{ka} + \frac{4\pi\epsilon\kappa^2\phi_s}{Ze} \left(\frac{\sin ka}{k^3} - \frac{a \cos ka}{k^2}\right). \tag{3.45}$$

3.4.3 The potential around a single macroion

Before considering a large suspension, it is instructive to apply the results derived above to the calculation of the electrostatic field around a single isolated spherical macroion, although this can, of course, be calculated more simply [3]. The assumption that the field surrounding the particle is spherically symmetric will be exactly true for a single macroion. Without loss of generality, we can assume that the centre of the macroion is at $\mathbf{R} = 0$, so that, from equation (3.44),

$$\tilde{\phi}(\mathbf{k}) = \frac{1}{(2\pi)^{3/2}} \frac{Ze}{\epsilon} g(k) \frac{1}{k^2 + \kappa^2}. \tag{3.46}$$

Now we use the inverse Fourier transform,

$$\phi(\mathbf{r}) = \frac{1}{(2\pi)^{3/2}} \int d^3\mathbf{k} \tilde{\phi}(\mathbf{k}) e^{i\mathbf{k}\cdot\mathbf{r}}; \tag{3.47}$$

substituting equation (3.46) into this and integrating over the angular part of $\mathbf{k}$ gives

$$\phi(r) = \frac{1}{2\pi^2} \frac{Ze}{\epsilon r} \int_0^\infty dk \frac{k}{k^2 + \kappa^2} g(k) \sin kr. \tag{3.48}$$

This integral can be evaluated by contour integration in the complex plane. We rewrite it as a sum of two separate contour integrals, of which one contains terms of the form e^{ikC}, where C is a positive constant, while the other contains terms of the form e^{-ikC}. The former must be integrated around the upper half plane, the latter around the lower. However, the group into which a given term falls depends on the relative values of a and r, with the result that equation (3.48) has two different solutions: one valid for $r < a$ (that is, inside the macroion),

$$\phi_{r<a}(r) = \phi_s + \left(\frac{Ze}{4\pi\epsilon\kappa a} - \phi_s \left(\frac{1}{\kappa} + a \right) \right) \frac{\sinh \kappa r}{r} e^{-\kappa a}, \tag{3.49}$$

which results from poles at zero and $+i\kappa$ in the upper half plane and at zero and $-i\kappa$ in the lower half plane, and one for $r > a$ (outside the macroion),

$$\phi_{r>a}(r) = \left(\left(\frac{Ze}{4\pi\epsilon\kappa a} - \frac{\phi_s}{\kappa} \right) \sinh \kappa a + a\phi_s \cosh \kappa a \right) \frac{e^{-\kappa r}}{r}, \tag{3.50}$$

which results from poles at $+i\kappa$ in the upper half plane and at $-i\kappa$ in the lower half plane. To make the link between the two solutions, we consider the boundary

condition on the second solution, at the surface,

$$\phi_{r>a}(a) = \phi_s. \tag{3.51}$$

This leads to the condition

$$\frac{Ze}{4\pi\epsilon\kappa a} = \phi_s\left(\frac{1}{\kappa} + a\right); \tag{3.52}$$

applied to the first solution, this condition produces, as expected, a constant potential $\phi_{r<a} = \phi_s$, while applied to the second solution it produces

$$\phi_{r>a}(r) = \phi_s a e^{\kappa a}\frac{e^{-\kappa r}}{r}, \tag{3.53}$$

which is the potential derived by Verwey and Overbeek [3]. It is also worth noting that the boundary condition is equivalent to

$$\phi_s = \frac{Ze}{4\pi\epsilon a}\frac{1}{1+\kappa a}; \tag{3.54}$$

allowing for differences in the electromagnetic units, this is Verwey's and Overbeek's relation between the surface potential ϕ_s and the surface charge Ze.

3.4.4 The surface potential in a suspension

Now we wish to consider the surface potential of a macroion in a suspension of identical macroions. The main motivation for doing this is to provide an approximate expression for ϕ_s which can be used in calculations of the free energy of such a system. The inverse Fourier transform is applied to equation (3.44), but now with many macroions. This leads to

$$\phi(\mathbf{r}) = \frac{1}{(2\pi)^3}\frac{Ze}{\epsilon}\sum_n \int d^3\mathbf{k}\frac{1}{k^2+\kappa^2}e^{i\mathbf{k}\cdot(\mathbf{r}-\mathbf{R}_n)}g(k), \tag{3.55}$$

which is a sum of potentials, the nth of which has the same form of equation as the single macroion potential in equation (3.48), but centred on $\mathbf{R}_n$ rather than on zero. Thus, we can use the results derived in the previous section to express the solutions for the potential in real space as sums of the single macroion solutions, as follows: inside macroion m, we have a sum of the internal solution for macroion m and the

external solutions for all the other macroions,

$$\phi_{int}(\mathbf{r}) = \phi_s + \left(\frac{Ze}{4\pi\epsilon\kappa a} - \phi_s\left(\frac{1}{\kappa} + a\right)\right)\frac{\sinh\kappa\left|\mathbf{r}-\mathbf{R}_m\right|}{\left|\mathbf{r}-\mathbf{R}_m\right|}e^{-\kappa a}$$

$$+\left(\left(\frac{Ze}{4\pi\epsilon\kappa a} - \frac{\phi_s}{\kappa}\right)\sinh\kappa a + a\phi_s\cosh\kappa a\right)\sum_{n\neq m}\frac{e^{-\kappa|\mathbf{r}-\mathbf{R}_n|}}{|\mathbf{r}-\mathbf{R}_n|}, \tag{3.56}$$

while, outside all macroions, we have a sum over the external solutions for all the macroions,

$$\phi_{ext}(\mathbf{r}) = \left(\left(\frac{Ze}{4\pi\epsilon\kappa a} - \frac{\phi_s}{\kappa}\right)\sinh\kappa a + a\phi_s\cosh\kappa a\right)\sum_{n}\frac{e^{-\kappa|\mathbf{r}-\mathbf{R}_n|}}{|\mathbf{r}-\mathbf{R}_n|}. \tag{3.57}$$

In this system, the assumption that the field around each macroion is spherically symmetric is only an approximation. Consequently, the potential inside the macroions will not be exactly constant, and nor will the surface potential ϕ_s be constant over the surface. However, in the present approximate treatment we assume that it is constant, and consider the value taken at the surface of one particular macroion m by the external solution for the potential. We introduce the further approximation that the effect of the other macroions on the potential at this surface is the same as it is at the centre (that is, $|\mathbf{r}-\mathbf{R}_n| \approx |\mathbf{R}_n - \mathbf{R}_m|$ for all n; this approximation can be justified by noting that the effect of a macroion located on one side of macroion m being nearer to an element of the surface of m than it is to the centre of m will be partially cancelled by the effect of a macroion on the opposite side being further from the surface than it is from the centre). The result is

$$\phi_s = \left(\left(\frac{Ze}{4\pi\epsilon\kappa a} - \frac{\phi_s}{\kappa}\right)\sinh\kappa a + a\phi_s\cosh\kappa a\right)\frac{e^{-\kappa a} + \Sigma^Y}{a}, \tag{3.58}$$

where Σ^Y is the sum over the Yukawa potentials,

$$\Sigma^Y \equiv a\sum_{n\neq m}\frac{e^{-\kappa R_{mn}}}{R_{mn}} = \sum_{n\neq m}\frac{e^{-\kappa a S_{mn}}}{S_{mn}}; \tag{3.59}$$

here, $R_{mn} \equiv |\mathbf{R}_m - \mathbf{R}_n|$, and $S_{mn} \equiv R_{mn}/a$ is a dimensionless separation between the centres of macroions m and n. Equation (3.58) can be rearranged to yield a simple expression for the surface potential,

$$\phi_s = \frac{Ze}{4\pi\epsilon a}\frac{e^{-\kappa a} + \Sigma^Y}{(1+\kappa a)\,e^{-\kappa a} + (1 - \kappa a\coth\kappa a)\,\Sigma^Y}. \tag{3.60}$$

It is easy to see that in the limit of a single macroion ($\Sigma^Y = 0$), this expression for ϕ_s reduces to equation (3.54), as expected.

We can also introduce a dimensionless surface potential Φ_s, which is the ratio of the surface potential to that of an isolated macroion with the same charge,

$$\Phi_s = \frac{4\pi\epsilon a\,(1+\kappa a)}{Ze}\phi_s; \tag{3.61}$$

then equation (3.60) takes the form

$$\Phi_s = \frac{(1+\kappa a)\left(e^{-\kappa a}+\Sigma^Y\right)}{(1+\kappa a)\,e^{-\kappa a}+(1-\kappa a\coth\kappa a)\,\Sigma^Y}, \tag{3.62}$$

while equation (3.45) becomes

$$g(k) = \frac{\sin ka}{ka} + \frac{\kappa^2\Phi_s}{a\,(1+\kappa a)}\left(\frac{\sin ka}{k^3} - \frac{a\cos ka}{k^2}\right). \tag{3.63}$$

3.4.5 The electrostatic free energy of a suspension

Now we are in a position to find the electrostatic energy using the gradient of the potential and equation (3.11). This is given by an inverse Fourier transform,

$$\nabla\phi(\mathbf{r}) = \frac{1}{(2\pi)^{3/2}}\int d^3\mathbf{k}\mathcal{F}[\nabla\phi(\mathbf{r})]e^{i\mathbf{k}\cdot\mathbf{r}}; \tag{3.64}$$

using equation (3.44) and given that $\mathcal{F}[\nabla\phi(\mathbf{r})] = i\mathbf{k}\tilde{\phi}(\mathbf{k})$, this can be written explicitly as

$$\nabla\phi(\mathbf{r}) = \frac{1}{(2\pi)^3}\frac{Ze}{\epsilon}\sum_n\int d^3\mathbf{k}\frac{i\mathbf{k}}{k^2+\kappa^2}g(k)e^{i\mathbf{k}\cdot\mathbf{r}}e^{-i\mathbf{k}\cdot\mathbf{R}_n}, \tag{3.65}$$

which leads, through equation (3.11), to

$$U_{el} = -\frac{1}{(2\pi)^6}\frac{Z^2e^2}{2\epsilon}\sum_m\sum_n\int d^3\mathbf{r}\int d^3\mathbf{k}\int d^3\mathbf{k}'\frac{\mathbf{k}\cdot\mathbf{k}'}{(k^2+\kappa^2)\,(k'^2+\kappa^2)}$$

$$\times g(k)g(k')e^{i(\mathbf{k}+\mathbf{k}')\cdot\mathbf{r}}\left(e^{-i\mathbf{k}\cdot\mathbf{R}_n}\right)\left(e^{-i\mathbf{k}'\cdot\mathbf{R}_m}\right). \tag{3.66}$$

Performing the integral over $\mathbf{r}$, we get a delta function which picks out $\mathbf{k}' = -\mathbf{k}$ in the integral over $\mathbf{k}'$, giving, since $g(k)$ is an even function,

$$U_{el} = \frac{1}{(2\pi)^3}\frac{Z^2e^2}{2\epsilon}\sum_m\sum_n\int d^3\mathbf{k}\frac{k^2}{(k^2+\kappa^2)^2}\left(g(k)\right)^2e^{i\mathbf{k}\cdot(\mathbf{R}_m-\mathbf{R}_n)}. \tag{3.67}$$

For the range of parameters in which we will be interested (the low salt concentration regime), the term in $g(k)$ in equation (3.63) which depends on Φ_s appears to be well approximated by

$$\frac{\kappa^2\Phi_s}{a\,(1+\kappa a)} \approx A\kappa^2 + B, \tag{3.68}$$

where $A = \ln v/9a$ and $B = 7/2va^3$. Now U_{el}/e^2 depends on the elementary charge e only through κ^2. Recalling that $\kappa^2 = \frac{\beta}{\epsilon}\sum_i z_i^2 e^2 n_{i0}$, we can perform the integral in equation (3.7), with the result

$$F = F_0 + \frac{1}{(2\pi)^3}\frac{Z^2e^2}{2\epsilon}\sum_m\sum_n\int d^3\mathbf{k}\left(\frac{(g(k))^2}{k^2+\kappa^2} - \kappa^2 Y\right.$$

$$\left.+2\left(X - k^2Y\right)\left(\frac{k^2}{\kappa^2}\ln\left(1+\frac{\kappa^2}{k^2}\right) - 1\right)\right)e^{i\mathbf{k}\cdot(\mathbf{R}_m - \mathbf{R}_n)}, \tag{3.69}$$

where

$$X = AB\left(\frac{\sin ka}{k^3} - \frac{a\cos ka}{k^2}\right)^2 + A\frac{\sin ka}{ka}\left(\frac{\sin ka}{k^3} - \frac{a\cos ka}{k^2}\right) \tag{3.70}$$

and

$$Y = A^2\left(\frac{\sin ka}{k^3} - \frac{a\cos ka}{k^2}\right)^2. \tag{3.71}$$

The electrostatic part of the free energy in equation (3.69) can be split into two sets of terms: terms where $m \neq n$ (pair free energy) and terms where $m = n$ (self free energy),

$$F_{el} = F_{pair} + F_{self}. \tag{3.72}$$

After the angular integration, F_{pair} can conveniently be rewritten as

$$F_{pair} = -\frac{i}{(2\pi)^2}\frac{Z^2e^2}{2\epsilon}\sum_n\sum_{m\neq n}\left(\int_{-\infty}^{\infty} kdk\left(\frac{(g(k))^2}{k^2+\kappa^2} - \kappa^2 Y\right)\frac{e^{ikR_{mn}}}{R_{mn}}\right.$$

$$\left.+4i\int_0^{\infty} kdk\left(X - k^2Y\right)\left(\frac{k^2}{\kappa^2}\ln\left(1+\frac{\kappa^2}{k^2}\right) - 1\right)\frac{\sin kR_{mn}}{R_{mn}}\right). \tag{3.73}$$

While the second integral must be evaluated numerically, the first can be evaluated by contour integration; since we do not wish the macroions to be able to interpenetrate one another, we can assume $R_{mn} > 2a$, and take into account only a pole at $+i\kappa$. Assuming all macroions to have identical environments, the pair free energy

per macroion, f_{pair}, can be written

$$f_{pair} = \frac{Z^2e^2}{8\pi\epsilon a}\left(\left(\frac{\sinh\kappa a}{\kappa a} + \frac{\Phi_s}{1+\kappa a}\left(\cosh\kappa a - \frac{\sinh\kappa a}{\kappa a}\right)\right)^2 \Sigma^Y \right.$$

$$\left. + \frac{4\ln v}{9\pi\kappa^2 a}\sum_{m\neq n}\int_0^\infty I(k)dk\frac{\sin kaS_{mn}}{kaS_{mn}}\right), \tag{3.74}$$

where Φ_s is to be calculated from equation (3.62), and

$$I(k) = \left(\frac{7}{2v\,(ka)^2} - \frac{\ln v}{9}\right)(\sin ka - ka\cos ka)^2 + \sin ka\,(\sin ka - ka\cos ka)\,. \tag{3.75}$$

These results can be compared with the equivalent result of Sogami and Ise [43],

$$F_{pair} = \frac{Z^2e^2}{8\pi\epsilon}\left(\frac{\sinh\kappa a}{\kappa a}\right)^2 \sum_n \sum_{m\neq n} \frac{e^{-\kappa R_{mn}}}{R_{mn}}; \tag{3.76}$$

the exclusion of the microions from the interiors of the macroions has introduced additional terms.

In F_{self}, $\mathbf{R}_m = \mathbf{R}_n$, and so the exponential in equation (3.69) goes to unity. The result is a spherically symmetric function in k-space, which is identical for each macroion; after the angular integration, we find

$$F_{self} = \frac{1}{(2\pi)^2}\frac{Z^2e^2}{2\epsilon}\sum_n\left(\int_{-\infty}^\infty k^2dk\left(\frac{(g(k))^2}{k^2+\kappa^2} - \kappa^2 Y\right)\right.$$

$$\left. + 4\int_0^\infty k^2dk\left(X - k^2Y\right)\left(\frac{k^2}{\kappa^2}\ln\left(1+\frac{\kappa^2}{k^2}\right) - 1\right)\right). \tag{3.77}$$

Once again, the second integral has to be evaluated numerically, while the first can be evaluated using contour integration. We split this first integral into three separate integrals, of which the first (containing no complex exponential terms) involves a pole at $+i\kappa$, the second (containing a positive complex exponential) involves poles at $+i\kappa$ and zero, and the third (containing a negative complex exponential) involves poles at $-i\kappa$ and zero. The result for the self free energy per macroion is

$$f_{self} = \frac{Z^2e^2}{8\pi\epsilon a}\left(\frac{1}{1+\kappa a} + \frac{1}{3}\left(\frac{\kappa a}{1+\kappa a}\right)^2\Phi_s^2 + \frac{e^{-\kappa a}}{1+\kappa a}\left(\frac{\sinh\kappa a}{\kappa a} - \cosh\kappa a\right)(\Phi_s - 1)^2\right.$$

$$\left. - \frac{1}{3}\left(\frac{\kappa a\ln v}{9}\right)^2 + \frac{4\ln v}{9\pi\kappa^2 a}\int_0^\infty I(k)dk\right). \tag{3.78}$$

The role of the macroion surface potential is twofold. Firstly, it provides a boundary condition to link the potential in the two regions (inside and outside macroions), in the same way as it did in the treatment of a single, isolated macroion. Secondly, it introduces many-body interactions. The linearised Poisson-Boltzmann equation is often considered to lead only to pairwise interactions, and to ignore many-body effects; however, while F_{pair} looks rather like a sum of pairwise interactions, it actually takes account, through Φ_s, of the positions of all the macroions in the suspension (as does F_{self}; in this sense, the distinction we have made between F_{pair} and F_{self} is rather artificial, and is largely a consequence of the form of the equations rather than of any physical feature of the system).

We should also consider the role of the parameter κ defined in equation (3.32). Although this is defined in the same way as the inverse screening length in Debye-Hückel theory, it has no physical meaning at any particular point in this inhomogeneous system, since it depends on the mean microion densities n_{i0} rather than on the local densities. In a sense, it is a 'mean inverse screening length'. κ is related to the number of microions, and therefore, because of the overall neutrality of the system, to the total charge on the macroions, but it is also related to the choice of gauge. Changing the value of κ at constant macroion density can thus represent two possible situations. If accompanied by the appropriate change in the value of Z, it represents a change in the charge on the macroions, and therefore in the total number of microions. If κ is varied without changing Z, it represents a change of gauge, and the resulting alteration in the results is not an indication of any physical change in the system, but of an alteration in the extent to which the linearised Poisson-Boltzmann equation is a good approximation to the full version. However, changing the gauge away from $\overline{\psi} = 0$ invalidates results for the free energy obtained using equation (3.7).

3.5 The microion ideal gas

In the absence of electrostatic effects, the microions are described as an ideal gas. The free energy of an inhomogeneous mixture of ideal gases with densities $n_i(\mathbf{r})$ is given by

$$F_{id} = k_B T \sum_i \int n_i(\mathbf{r}) \left(\ln n_i(\mathbf{r}) \Lambda_i^3 - 1 \right) d^3\mathbf{r}, \tag{3.79}$$

where $\Lambda_i = (h^2/2\pi m_i k_B T)^{1/2}$ is the thermal wavelength of species i; note that this depends on the masses m_i, and therefore on the chemical nature, of the microions. h is Planck's constant. Expanding the free energy in the inhomogeneities in microion

density $\Delta n_i = n_i - \overline{n_i}$, where $\overline{n_i}$ is the mean microion density, we find that the first order term vanishes because of the condition $\int \Delta n_i d^3\mathbf{r} = 0$; we can conclude that the free energy of the inhomogeneous ideal gas differs from that of the homogeneous ideal gas of the same mean density only to the second and higher orders of the inhomogeneities [53]. Since we shall calculate the electrostatic energy using the linearised version of the Poisson-Boltzmann equation, we are effectively assuming that inhomogeneities are small, and it is consistent with this approximation to write

$$F_{id} = k_B T \sum_i N_i \left(\ln \frac{N_i}{V} \Lambda_i^3 - 1 \right), \tag{3.80}$$

where N_i is the total number of microions of species i. We are approximating the free energy of an inhomogeneous ideal gas by the free energy of a homogeneous ideal gas.

A few words should be added in defence of this procedure. It appears that the ion distribution obtained from the linearised Poisson-Boltzmann equation can also be derived using classical density functional theory (DFT), if the microion ideal gas free energy is expanded to second order. It might be argued that it is consistent to expand the ideal gas free energy to second (rather than first) order if the electrostatic free energy is calculated using the linearised Poisson-Boltzmann equation, and therefore that the present treatment is inconsistent.

This argument would be incorrect. A DFT treatment requires the ideal gas free energy to be expanded to second order because an expansion to first order does not depend on the detail of the microion distribution around a macroion, and therefore would provide no entropic term to prevent the collapse of the counterion atmosphere on to the surface of the macroion. There are no grounds to believe that this level of approximation is somehow uniquely 'consistent': the DFT calculation combines an almost exact calculation of the electrostatic free energy of a system which conforms to the linearised Poisson-Boltzmann theory, and an approximate (to second order) calculation of the ideal gas free energy of the same system. By way of comparison, the present treatment combines a (presumably equivalent) almost exact calculation of the electrostatic free energy of the linearised system and an approximate (to first order) calculation of the ideal gas free energy of the same system. The degrees of approximation are different, but neither degree of approximation can be described as the 'consistent' one.

Equation (3.80) gives the free energy of a homogeneous ideal gas in state (N_i, V, T), given that we already have N_i microions of each species i. Now let us establish the change in free energy due to creating such a gas of microions from a

suitable source. The free energy F_0 associated with the microions is calculated by thermodynamic integration of its differential

$$dF_0 = -SdT - pdV + \sum_i \mu_i dN_i, \tag{3.81}$$

where S is the entropy associated with the microions (now regarded as spatially homogeneous) and μ_i is the chemical potential of microions of species i (ignoring electrostatic effects). We integrate from an initial state ($N_i^0 = 0$, V^0, T^0) to the physical state (N_i, V, T), by integrating first across N_i with V and T held constant, then across T with N_i and V held constant, and finally across V with N_i and T held constant. For the first integral, we take the chemical potential to be

$$\mu(N_i, V^0, T^0) = \mu_i^{ref} + k_B T^0 \ln\left(\frac{N_i/V^0}{N_i^{ref}/V^0}\right). \tag{3.82}$$

where $\mu_i^{ref} = \mu(N_i^{ref}, V^0, T^0)$ is the chemical potential in some reference state (the density of which we shall not need to specify). After all three integrals have been performed, the result for the microion free energy is

$$F_0 = \sum_i N_i \left[u_i + k_B T \left(\ln \frac{N_i}{V}\Lambda_i^3 - 1\right)\right]; \tag{3.83}$$

here, $u_i = u_i^0 - \frac{3}{2}k_B T^0$, where u_i^0 is the energy required to create a microion of species i at temperature T^0. This result contains a new term in addition to the density dependent term in equation (3.80); this is because we have taken account of the free energy cost of forming the microions in the first place. Equation (3.83) can also be written, less concisely but more illuminatingly, as

$$F_0 = \sum_i N_i \left[u_i^0 + \frac{3}{2}k_B\left(T - T^0\right) + k_B T \left(\ln \frac{N_i}{V}\Lambda_i^3 - \frac{5}{2}\right)\right], \tag{3.84}$$

where the first term is the energy required to create the microions at temperature T^0, the second is the energy required to increase their temperature from T^0 to T, and the third is the Sackur-Tetrode entropy multiplied by $-T$.

We shall now consider the interpretation of u_i. A microion formed at temperature T^0 will automatically possess kinetic energy $\frac{3}{2}k_B T^0$, so the energy cost of creating the microion is $u_i^0 - \frac{3}{2}k_B T^0$, which is equal to u_i. Therefore, we regard u_i as the temperature-independent energy cost of forming a microion of species i. Finally, using the ideal gas equation and the definition of the Gibbs free energy, we find that

u_i is related to the reference chemical potential μ_i^{ref} according to

$$u_i = \mu_i^{ref} - k_B T^0 \ln \frac{N_i^{ref}}{V^0} \left(\Lambda_i^0\right)^3 , \tag{3.85}$$

where Λ_i^0 is the thermal wavelength of species i at temperature T^0.

Chapter 4

An idealised system: the zero salt limit

4.1 The free energy

We wish to specify the thermodynamics of a region which is in a single phase (that is, homogeneous with respect to the macroion density), in order to investigate the possibility that two such regions, with different macroion densities, might coexist. Before we can calculate the Helmholtz free energy using equations (3.59), (3.62), (3.74), (3.75), (3.78) and (3.83), it is necessary to do two things: first, to relate the microion densities to the macroion density, and second, to choose an approximate distribution for the macroions around any given macroion, in order to calculate Σ^Y in equation (3.59). The task of relating the microion density to the macroion density is simplest if the system contains only one species of microion, which we take to be a monovalent counterion. The absence of coions implies that the system contains no added salt. In this chapter, we shall investigate the phase behaviour of this idealised zero salt system, which has important implications for our view of the mechanism of phase separation in charged colloidal suspensions.

Each region (phase) of the system should be charge neutral, and this requirement will be satisfied if the number of microions in a given region is equal to $|Z|$ multiplied by the number of macroions: we consider the microion density to behave as though each microion were associated with a particular macroion, and confined to the region in which that macroion is located. That is, we consider each region to be approximately equivalent to a hypothetical system comprising an identical region surrounded by an impenetrable wall, which confines the microions to that region.

Why is this local charge neutrality assumption necessary? Whatever method is used for the calculation of the free energy of a charged colloidal suspension, it appears

necessary to simplify the calculation by considering only a region which is in a single phase, and ignoring any surrounding regions which are in a different phase with a different macroion density. (If we wish to consider two coexisting phases, we simply repeat the calculation at two different densities.) But the free energy calculation for a given single-phase region requires knowledge of the counterion density in that region, which can only be determined precisely if we take account of any other regions in which the macroion density is different, for example by minimising the total free energy with respect to the movement of counterions between regions.

Some simplifying assumption is required in order to escape from this trap. The charge neutrality assumption is based on the idea that, if this minimisation were performed, the number of counterions in each region of the system would be such as to produce charge neutrality; any significant departure from this distribution would create a macroscopic electrostatic field, and would be energetically unfavourable.

In the zero salt system, the charge neutrality assumption allows us to write the mean microion density $\overline{n}$ as $\overline{n} = |Z|/\tilde{V}$, where $\tilde{V}$ is equal to the volume available to the microions associated with one macroion: that is, the total volume in a region available to the microions, divided by the number of macroions in the region. Substituting this $\overline{n}$ for n_{i0} in the definition of κ^2, equation (3.32), we find that the parameter κa, which appears frequently in the expressions for the electrostatic free energy, varies with $\tilde{V}$ according to

$$\kappa a = \left(\frac{|Z| e^2 a^2}{\epsilon k_B T} \frac{1}{\tilde{V}} \right)^{1/2} . \tag{4.1}$$

This dependence of κa on the density of the macroions has an important effect on the form of the electrostatic free energy expressed in equations (3.74) and (3.78).

We can introduce a dimensionless volume v per macroion, expressed in units of the volume of one macroion, $(4/3)\pi a^3$; this dimensionless volume is given by $v = \left(3\tilde{V}/4\pi a^3\right) + 1$ and is equal to $1/\eta$, where η is the colloid volume fraction. Equation (4.1) then becomes

$$\kappa a = \left(\frac{3|Z| e^2}{4\pi\epsilon k_B T a} \frac{1}{(v-1)} \right)^{1/2} . \tag{4.2}$$

The presence here of $(v-1)$ instead of v accounts for the exclusion of the microions from the interiors of the macroions.

The microion ideal gas free energy per macroion, from equation (3.83), is

$$f_0 = |Z| \left[u + k_B T \left(\ln \frac{|Z|}{\widetilde{V}} \Lambda^3 - 1 \right) \right], \tag{4.3}$$

where u is the energy of formation of a microion and Λ is the thermal wavelength. In terms of v, this gives

$$f_0 = |Z| \left\{ u + k_B T \left[\ln \frac{3|Z|}{4\pi} \left(\frac{\Lambda}{a} \right)^3 - \ln (v-1) - 1 \right] \right\}. \tag{4.4}$$

Most of the parameters in the expression for the ideal gas free energy are constants; we can simplify the calculations and avoid having to consider the chemical nature of the microions by taking only the v-dependent part Δf_0:

$$\Delta f_0 = -|Z| k_B T \ln (v-1). \tag{4.5}$$

The second prerequisite for the calculation of the free energy is an approximate form for the distribution of macroions around a particular macroion. This is to enable the calculation of Σ^Y in equation (3.59). The relation between v and the dimensionless nearest neighbour macroion separation S (in units of the macroion radius a) depends on the structure. We shall regard a face centred cubic structure as an approximate model of both solidlike and fluidlike phases of different densities; for this structure,

$$S = \left(\frac{4\sqrt{2}\pi}{3} v \right)^{1/3}. \tag{4.6}$$

4.2 Phase coexistence

The total electrostatic free energy per macroion can now be calculated as $f_{el} = f_{pair} + f_{self}$, and the total free energy per macroion as $f = f_{el} + \Delta f_0$. Our investigation of the dependence of the free energy on $|Z|$ and a is made simpler by the observation that, at constant v,

$$f(C|Z|, Ca) = Cf(|Z|, a), \tag{4.7}$$

where C is a constant. This is made plausible by consideration of the expressions for f. The electrostatic terms f_{pair} and f_{self} both consist largely (though not entirely) of a function of κa multiplied by Z^2/a; equation (4.2) shows that the parameter κa can be expressed, at constant v, as a function of $|Z|/a$. Meanwhile, Δf_0 is equal to a constant (at constant v) multiplied by $|Z|$. The fact that equation (4.7)

appears to be exactly true, according to our numerical results, suggests that all the contributions to the electrostatic free energy, written in units of Z^2/a, could be expressed (at constant v) as functions of κa, even if this is not apparent from the form in which they are written.

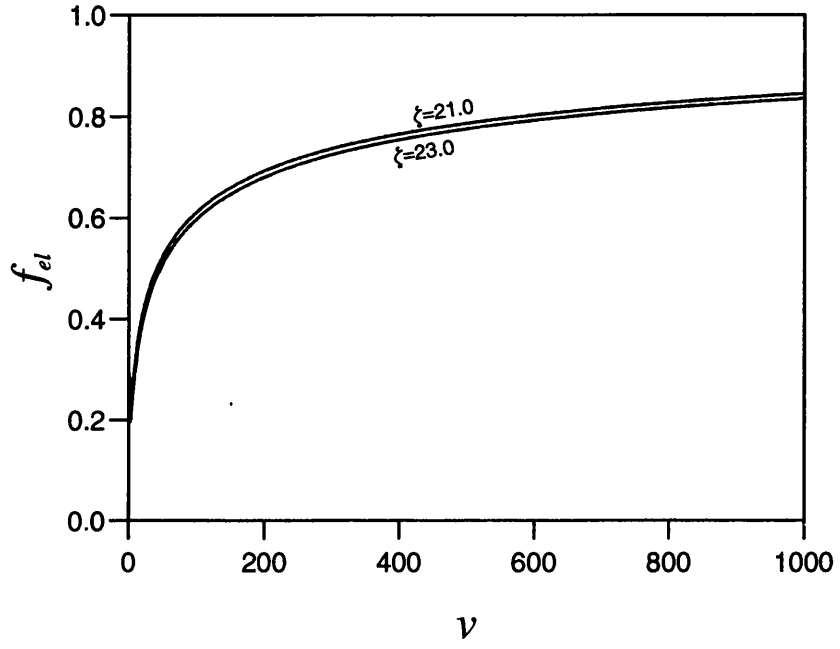

Figure 4.1: The electrostatic part f_{el} of the free energy per macroion in units of $Z^2e^2/8\pi\epsilon a$.

The relation in equation (4.7) makes the various components of the free energy, if they are expressed in units of $Z^2e^2/8\pi\epsilon a$, dependent only on a parameter $\zeta = |Z|/a$ (we use a expressed in nm in the definition of ζ) and not on Z and a separately. The dependence on $|Z|$ and a reduces to ζ-dependence. Figure 4.1 shows f_{el} as a function of v for two different values of ζ, which has units of nm^{-1}. The results show clearly that this part of the free energy increases monotonically with increasing v (decreasing macroion density), and therefore that it makes a cohesive contribution to the total Helmholtz free energy of the system. This is opposed by the free energy Δf_0 of the microion ideal gas, which becomes more negative logarithmically as the volume increases.

In the theory of the phase behaviour of molecular fluids associated with van der Waals, the free energy contains two terms: an intermolecular interaction which is attractive at long distances and has a repulsive hard core, and the ideal gas term, which is always repulsive. At sufficiently low temperatures, so that the ideal gas

term does not overwhelm the intermolecular interaction, the graph of the total free energy F as a function of V may develop an upward bulge, where $\partial^2 F/\partial V^2$ becomes negative; since the pressure is given by $p = -\partial F/\partial V$, this leads to a so-called van der Waals loop in the pV diagram [7]. A horizontal line drawn across the loop ensures mechanical stability (the two phases, at the end points of the horizontal line, are at the same pressure); drawing this line according to Maxwell's equal area construction ensures that the free energy is globally minimised (the two phases have the same chemical potential). This situation was introduced in chapter 1 and illustrated in figures 1.2 and 1.3.

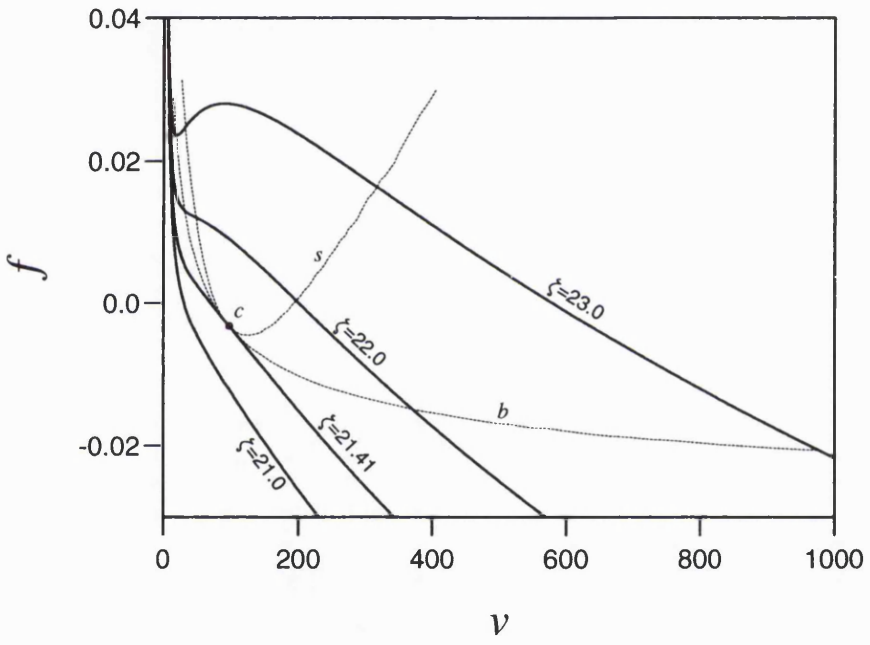

Figure 4.2: The free energy f per macroion in units of $Z^2e^2/4\pi\epsilon a$, for various values of ζ. Compare with figure 1.2.

In the present two-component system, the free energy per macroion f contains two important terms, f_{el} and Δf_0, which take similar forms and similar roles to the the intermolecular interaction and the ideal gas term, respectively, in a molecular fluid. At low densities Δf_0 dominates, while for certain values of ζ, the cohesive nature of f_{el} strongly influences the shape of $f(v)$ at high densities. The result is that an upward bulge appears in the graph of f as a function of v. The corresponding pV diagram shows a van der Waals loop, which indicates coexistence between two phases with different densities.

We are lead, then, towards Warren's conclusion [62] that the electrostatic free energy has a destabilising effect, tending to push a suspension towards inhomogeneity, while stability against phase separation or aggregation is provided by the counterion entropy. Indeed, the value of the theoretical zero salt system is that it permits us to use this analogy with molecular fluids, making very clear the mechanism by which competition between the electrostatic and ideal gas contributions to the free energy results in phase coexistence.

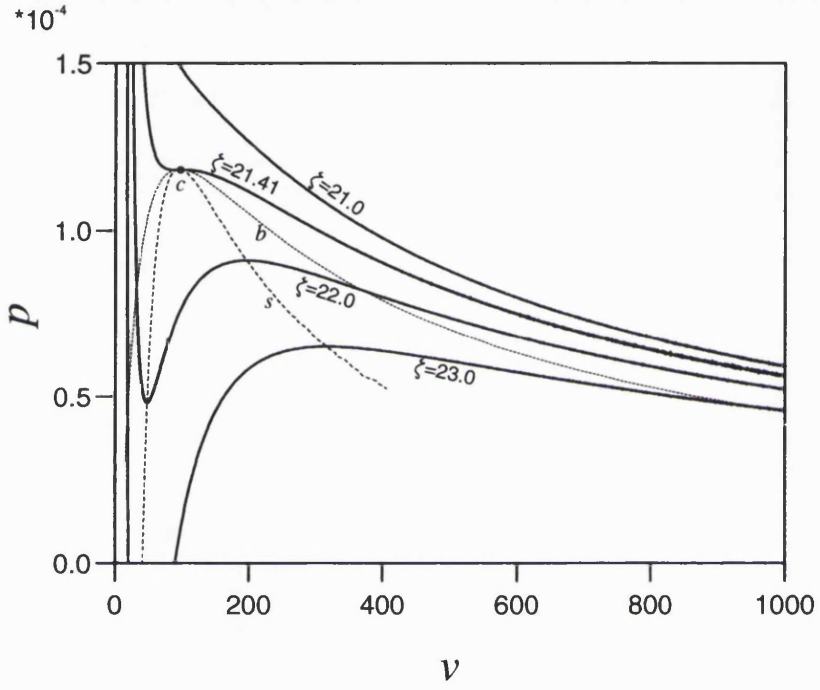

Figure 4.3: pV diagram, showing van der Waals loops, for various values of ζ. The pressure has units of $3Z^2e^2/32\pi^2\epsilon a^4$. Compare with figures 1.3 and 1.4.

Figure 4.2 shows the dependence of $f = \Delta f_0 + f_{el}$ on v for various different values of ζ, while the pV diagram is plotted in figure 4.3. The binodal is marked b, the spinodal s, and the critical point c. Because of the relation (4.7), the values of v at the binodal and spinodal in a system with given $|Z|$ and a depend only on ζ, not on $|Z|$ and a separately. The value of ζ at the critical point is $\zeta_c = 21.41$ nm^{-1}; at each value of the macroion radius a, phase coexistence between a dense and a rarefied region emerges as the charge is increased above a critical value $Z_c = \zeta_c a$. These results agree with other theoretical treatments [43, 53, 62, 64] in predicting on the basis of linearised Poisson-Boltzmann theory that dense and rarefied phases can coexist in a colloidal suspension. However, a notable unexplained difference is that the phenomenon has been shown to occur in the limit of zero added salt; two

recent treatments [53, 62] found that the phase coexistence vanishes in this limit, although a third [64] agreed with the present results in predicting phase coexistence at zero salt.

Chapter 5

Added salt: the Donnan effect and the phase diagram

5.1 Introduction

The previous chapter considered the phase behaviour of a suspension which contained only one species of microion. While this restriction simplifies theoretical investigation of the system, it must be lifted in a more realistic model, since real colloidal systems contain added salt. The salt concentration is, in fact, the most easily varied experimental parameter in such a system, and the phase behaviour is most usefully expressed as a function of colloid density and salt concentration. The present chapter will concentrate on the role of added salt in charged colloidal suspensions. The aims are, first to consider two coexisting regions (phases) with differing colloid densities and to determine theoretically how added salt will be partitioned between the regions (as seen, for example, in the Donnan effect) and second to produce phase diagrams as a function of the densities of the macroions and the salt. Finally, we shall discuss the implications which our results have for theories describing interactions in colloidal suspensions.

5.2 Expressions for the free energy

As in the zero salt system, we have a large number N_M of colloidal particles of radius a and constant charge Ze. These are balanced by $N_c = |Z| N_M$ point univalent counterions (with charge $z_c e$, where $|z_c| = 1$). We take the macroions to be negative (that is, $Z < 0$) and the counterions to be positive, but it makes no difference to the results if the signs are interchanged. The system now also contains N_s pairs of added

salt ions, each pair consisting of a point univalent counterion and a point univalent coion (a microion carrying charge of the same sign as that of the macroions). All the counterions are taken to be identical; the system contains in total $N_c + N_s$ counterions and N_s coions.

Calculations of the free energy of this added salt system can proceed in much the same way as in the zero salt system; that is, using equations (3.59), (3.62), (3.74), (3.75), (3.78) and (3.83). However, the task of relating the microion densities to the macroion density is more complicated than it is in the zero salt system. Recall that the microion densities enter the formalism in two places: in the definition of the parameter κa, and in the microion ideal gas contribution to the free energy. If the system divides into two regions having different macroion densities, the densities of the various species of microions will also be different in the two phases. The charge neutrality assumption, requiring that each region of the system should be neutral, leads to $|Z|+\widetilde{N}_s$ counterions and $\widetilde{N}_s$ coions being associated with each macroion. $\widetilde{N}_s$ is just the number of pairs of salt ions associated with each macroion. The charge neutrality assumption does not provide us with a simple way of fixing this number, which is why added salt makes the calculations more complicated.

The parameter κa varies, through its dependence on the mean microion densities $\overline{n}_i$, as a function of the dimensionless volume v

$$\kappa a = \left(\frac{3e^2}{4\pi\epsilon k_B T a} \frac{|Z| + 2\widetilde{N}_s}{v - 1} \right)^{1/2} . \tag{5.1}$$

This is the equivalent, in a system with added salt, of equation (4.2). From equation (3.83), the ideal gas part of the free energy per macroion can be expressed as

$$f_0 = \left(|Z| + \widetilde{N}_s\right) \left[u_+ + k_B T \left(\ln \frac{|Z| + \widetilde{N}_s}{\widetilde{V}} \Lambda_+^3 - 1 \right) \right] + \widetilde{N}_s \left[u_- + k_B T \left(\ln \frac{\widetilde{N}_s}{\widetilde{V}} \Lambda_-^3 - 1 \right) \right], \tag{5.2}$$

where Λ_+ and Λ_- are the thermal wavelengths of counterions and coions, respectively, and u_+ and u_- are their energies of formation. Both the thermal wavelengths and the energies of formation depend on the chemical nature of the microion species. The free energy can be rewritten as

$$f_0 = \left(|Z| + \widetilde{N}_s\right) k_B T \ln \left(\frac{|Z| + \widetilde{N}_s}{\widetilde{V}} \right) + \widetilde{N}_s k_B T \ln \left(\frac{\widetilde{N}_s}{\widetilde{V}} \right)$$

$$+ |Z| \left[u_+ + k_B T \left(\ln \Lambda_+^3 - 1 \right) \right] + \widetilde{N}_s \left[u_- + k_B T \left(\ln \Lambda_+^3 \Lambda_-^3 - 2 \right) \right] . \tag{5.3}$$

The third term in equation (5.3) is a constant for constant Z and T, and therefore it can be ignored in the determination of the thermodynamics. The fourth term depends on the number of salt pairs $\widetilde{N}_s$ per macroion. However, the contribution of this term to the ideal gas free energy of the whole system is $N_s\left[u_- + k_BT\left(\ln\Lambda_+^3\Lambda_-^3 - 2\right)\right]$, which is a constant. It is, of course, the free energy of the whole system which we wish to calculate and minimise: the free energy per macroion is merely a convenient route to this. Therefore, the fourth term makes no contribution to the thermodynamics of the system, and can be ignored. This is convenient, as it means we do not have to consider the chemical nature of any of the microions. We can consider only the $\tilde{V}$- and $\widetilde{N}_s$-dependent part Δf_0 of the ideal gas free energy,

$$\Delta f_0 = \left(|Z| + \widetilde{N}_s\right) k_BT \ln\left(\frac{|Z| + \widetilde{N}_s}{\tilde{V}}\right) + \widetilde{N}_s k_BT \ln\left(\frac{\widetilde{N}_s}{\tilde{V}}\right). \tag{5.4}$$

Expressed in terms of the dimensionless volume v per macroion, this becomes

$$\Delta f_0 = k_BT\left[\left(|Z| + \widetilde{N}_s\right)\ln\left(|Z| + \widetilde{N}_s\right) + \widetilde{N}_s \ln\widetilde{N}_s + \left(|Z| + 2\widetilde{N}_s\right)\ln\left(\frac{3}{4\pi a^3}\frac{1}{v-1}\right)\right]. \tag{5.5}$$

As in the previous chapter, the relation between v and the macroion nearest neighbour separation S is expressed by equation (4.6).

5.3 Salt partition: The Donnan equilibrium

Given two coexisting phases α and β of colloidal particles, at different densities, how is the added salt distributed between the two phases? This is equivalent to the problem of two suspensions separated by a membrane through which the microions can pass but the macroions cannot. Let phase X contain N_M^X macroions, N_+^X counterions and N_-^X coions, and let the total Helmholtz free energy be F. To maintain charge neutrality, counterions and coions cannot cross the membrane individually, but only in counterion-coion pairs. The condition for equilibrium is for the total Helmholtz free energy of the system to be a minimum with respect to the passage of these pairs across the membrane,

$$\left(\frac{\partial F}{\partial N_+^\alpha} + \frac{\partial F}{\partial N_-^\alpha}\right) - \left(\frac{\partial F}{\partial N_+^\beta} + \frac{\partial F}{\partial N_-^\beta}\right) = 0, \tag{5.6}$$

or in terms of the chemical potentials μ_+^X and μ_-^X of the counterions and coions,

$$\mu_+^\alpha + \mu_-^\alpha = \mu_+^\beta + \mu_-^\beta. \tag{5.7}$$

If we regard the microions as an ideal gas, and ignore the consequences of electrostatic effects for their distribution between the two phases, the chemical potential of microion species i in phase X is given by $\mu_i^X = \mu_i^0 + k_B T \ln \overline{n}_i^X$, and so

$$\overline{n}_+^\alpha \overline{n}_-^\alpha = \overline{n}_+^\beta \overline{n}_-^\beta, \tag{5.8}$$

which looks like a law of mass action. The electroneutrality condition in phase X, recalling that $Z < 0$, is $N_M^X |Z| + N_-^X = N_+^X$, or

$$\overline{n}_+^X = \frac{|Z|}{\widetilde{V}^X} + \overline{n}_-^X; \tag{5.9}$$

substituting this into equation (5.8) and noticing that $\overline{n}_-^X$ is equal to the mean density $\overline{n}_s^X$ of salt pairs, we find

$$\overline{n}_s^\alpha \left(\frac{|Z|}{\widetilde{V}^\alpha} + \overline{n}_s^\alpha \right) = \overline{n}_s^\beta \left(\frac{|Z|}{\widetilde{V}^\beta} + \overline{n}_s^\beta \right). \tag{5.10}$$

Rearranging gives

$$\frac{1}{\overline{n}_s^\beta - \overline{n}_s^\alpha} \left(\frac{1}{\widetilde{V}^\alpha} - \frac{1}{\widetilde{V}^\beta} \right) = \frac{1}{|Z| \, \overline{n}_s^\beta} \left(\overline{n}_s^\beta + \overline{n}_s^\alpha + \frac{|Z|}{\widetilde{V}^\alpha} \right). \tag{5.11}$$

Using the electroneutrality condition (5.9), we find

$$\frac{1}{\overline{n}_s^\beta - \overline{n}_s^\alpha} \left(\frac{1}{\widetilde{V}^\alpha} - \frac{1}{\widetilde{V}^\beta} \right) = \frac{1}{|Z|} + \frac{1}{\overline{n}_s^\beta \widetilde{V}^\alpha}. \tag{5.12}$$

Finally, we introduce the volume fraction $\eta^X = 1/v^X$, where $\widetilde{V}^X = (4/3)\pi a^3 \left(v^X - 1 \right)$ is approximated by $\widetilde{V}^X \approx (4/3)\pi a^3 v^X$; the approximation is reasonable provided that $v^X \gg 1$. The result is

$$\frac{\eta^\alpha - \eta^\beta}{\overline{n}_s^\beta - \overline{n}_s^\alpha} \approx \frac{4\pi a^3}{3\,|Z|} + \frac{\eta^\alpha}{\overline{n}_s^\beta}. \tag{5.13}$$

All the variables in equation (5.13) are positive, which means that the sign of $\left(\overline{n}_s^\beta - \overline{n}_s^\alpha \right)$ must be the same as the sign of $\left(\eta^\alpha - \eta^\beta \right)$. That is, the salt density will be higher in the phase where the macroion density is lower: if the system separates into phases of different macroion density, there will be a macroion-rich and a salt-rich phase. This 'repulsion' of the salt by the macroions is the Donnan effect.

However, the above calculation is based on the assumption that the microions behave as an ideal gas. We expect the result to change if we take electrostatic

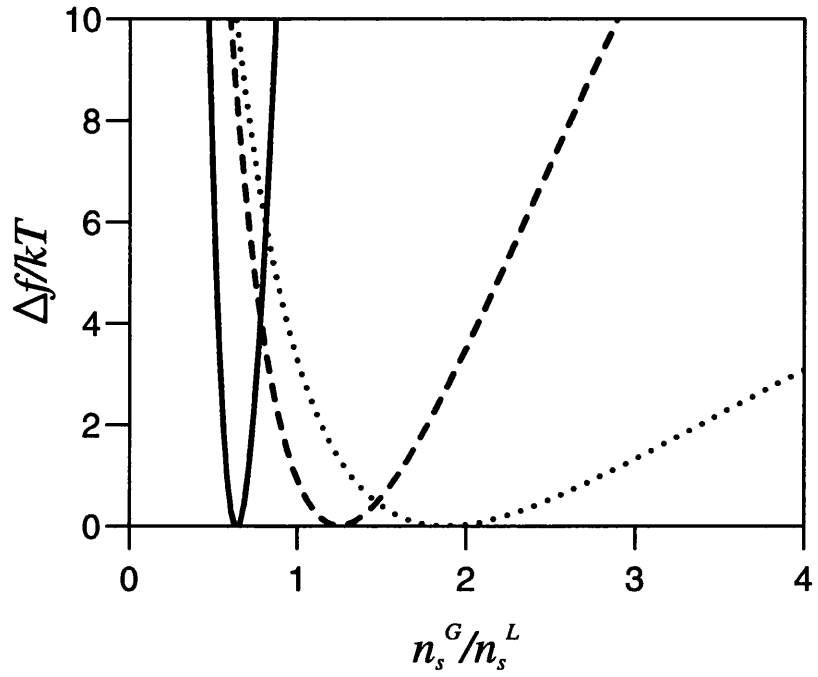

Figure 5.1: The variation of the mean Helmholtz free energy per macroion Δf in a two phase system, relative to its minimum, as a function of the ratio of the mean salt density n_s^G in the rarefied (gas) colloidal phase to the mean salt density n_s^L in the dense (liquid) colloidal phase. Macroions have radius $a = 50$ nm. Mean number of salt pairs per macroion $N_s = 100$. Mean $\eta = 0.05$, dense phase has $\eta = 0.1$, rarefied phase has $\eta = 0.002$. Solid line: $|Z| = 1500$; dashed line: $|Z| = 1250$; dotted line: $|Z| = 1000$.

effects into consideration, as correlations between positive and negative charges lead to a reduction in the free energy. The correlations in question are not the microscopic correlations between microions, which are neglected in the mean-field Poisson-Boltzmann treatment, but the mesoscopic correlations represented by the tendency of counterions to congregate in an atmosphere around a macroion. These electrostatic effects will tend to push salt towards the macroion-rich phase. Figures 5.1 and 5.2 show how the Helmholtz free energy depends on the ratio n_s^G/n_s^L of the salt densities in the two phases (n_s^G is the mean salt density in the rarefied colloidal phase and n_s^L is the mean salt density in the dense colloidal phase), when other variables such as the macroion densities are held constant. For low $|Z|$, the minimum of Δf is at $n_s^G/n_s^L > 1$, but as $|Z|$ increases, the minimum moves to $n_s^G/n_s^L < 1$. The resulting salt partition, obtained by minimising the free energy with respect to the transfer of salt between the two phases, is shown in figure 5.3. It can be seen that, for sufficiently high values of the macroion charge $|Z|$ and of the mean number of

salt pairs per macroion N_s/N_M, the electrostatic effects can overcome the entropic effects and lead to the salt density being higher in the macroion-rich phase: a kind of 'reverse Donnan effect'. In principle, this could be observed experimentally.

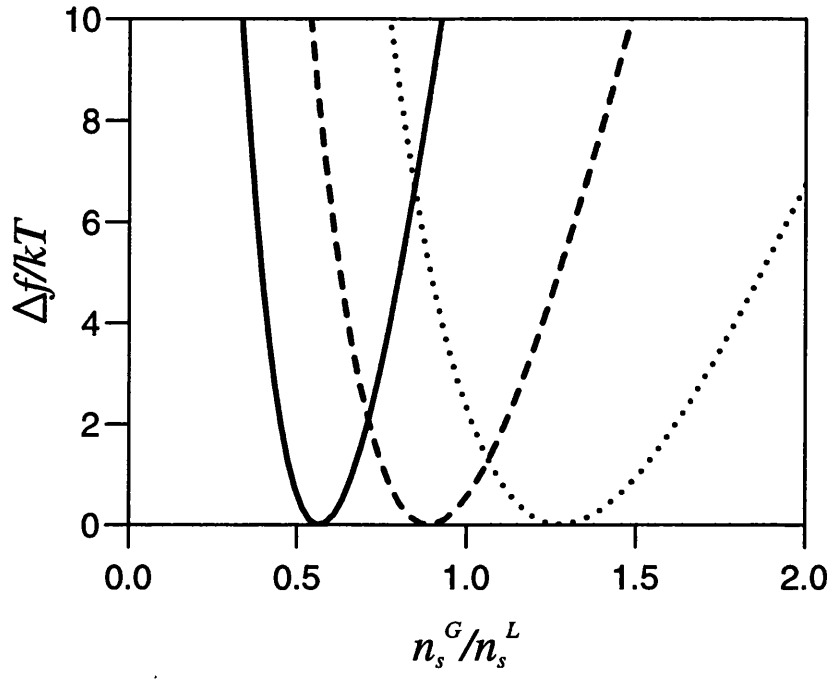

Figure 5.2: The variation of the mean Helmholtz free energy per macroion Δf in a two phase system, relative to its minimum, as a function of the ratio of the mean salt density n_s^G in the rarefied (gas) phase to the mean salt density n_s^L in the dense (liquid) phase. Macroions have radius $a = 50$ nm and $|Z| = 1500$. Mean $\eta = 0.05$, dense phase has $\eta = 0.1$, rarefied phase has $\eta = 0.002$. Solid line: mean number of salt pairs per macroion $N_s = 500$; dashed line: $N_s = 100$; dotted line: $N_s = 50$.

The technique of minimising the free energy with respect to the passage of salt between the phases is used in the calculations leading to the phase diagrams, detailed in the following section, in order to find how the salt is partitioned.

5.4 Phase diagrams

5.4.1 Free energy curves and phase separation

Chapter 4 showed that an analogy can be drawn between the phase behaviour of a molecular fluid and that of a charged colloidal suspension in the zero salt regime. In both systems, the graph of the Helmholtz free energy expressed as a function of

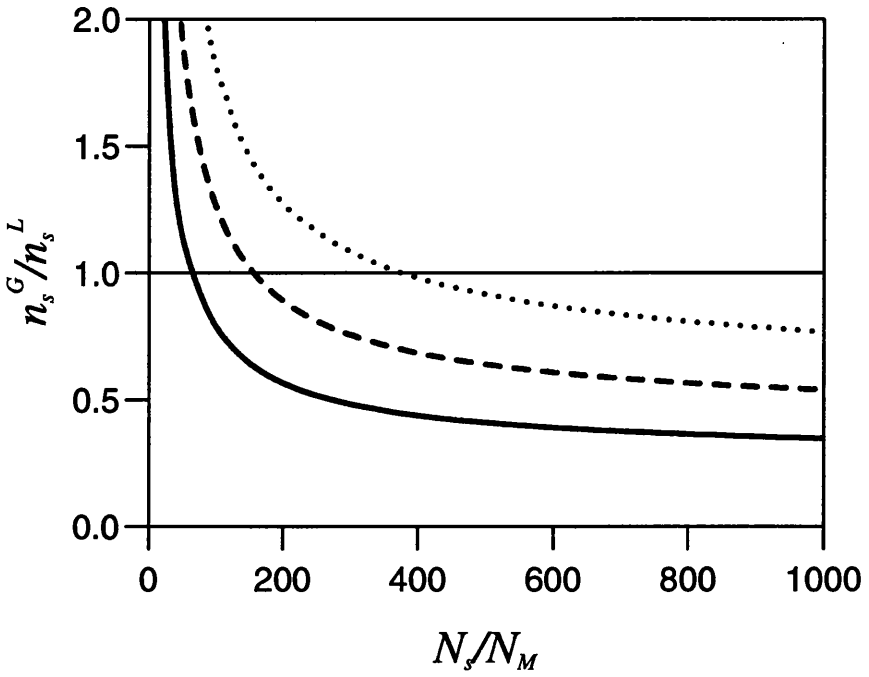

Figure 5.3: Ratio of the mean salt density n_s^G in the rarefied phase to the mean salt density n_s^L in the dense phase, as a function of the mean number of salt pairs N_s per macroion. Macroions have radius $a = 50$ nm. Mean $\eta = 0.05$, dense phase has $\eta = 0.1$, rarefied phase has $\eta = 0.002$. Solid line: $|Z| = 1500$; dashed line: $|Z| = 1250$; dotted line: $|Z| = 1000$.

the volume per particle shows, under certain conditions, an upward bulge in which its second derivative becomes negative, leading to a van der Waals loop in the pV diagram. This type of situation was illustrated schematically in figure 1.2.

However, the situation is more complicated when the system contains added salt. In addition to having the same pressure and macroion chemical potential, the coexisting states must also have the same salt chemical potential if they are to coexist in equilibrium. The nearest approach at nonzero salt to the graphically neat situation which exists at zero salt would be to replace the Helmholtz free energy with the semigrand potential

$$\omega = f - \mu_s \widetilde{N}_s \tag{5.14}$$

suggested by van Roij, Dijkstra and Hansen (RDH) [53]. This fixes the salt chemical potential μ_s externally. The total number of salt pairs will then depend on the chemical potential and on the proportions of the total number of macroions that are in each of the two phases. However, we consider the explicit phase separation of a fixed amount of material in a closed system. This model requires the total number

of salt pairs, rather than their chemical potential, to be fixed. So with ω as the dependent variable in figure 1.2, a homogeneous system at B will not, in general, phase separate into a mixture of A and C, since that would involve changing the total amount of salt, and therefore, effectively, changing into a different system. Instead, a system starting at B would conserve the amount of salt, and separate (if at all) into states A' and C', with a different salt chemical potential μ_s'. This means that figure 1.2 only provides us with a pair of states A and C which can coexist. It does not immediately tell us which unstable or metastable homogeneous states B will separate into A and C. Thus, the graphical interpretation of phase coexistence phenomena is more complicated if added salt is present, and the simple analogy with the van der Waals theory of molecular fluids is lost.

5.4.2 Calculation of the phase diagrams

The method used here to establish the phase diagram was to choose a point with some $\overline{n}_s$ and $\overline{\eta}$, the mean salt density and colloid volume fraction of the system, and to minimise the total Helmholtz free energy with respect to two variables v^α and λ^α. These are, respectively, the dimensionless volume per macroion in phase α and the proportion of the total number of macroions which are in phase α. This two-dimensional minimisation was performed using the downhill simplex method [88]. The free energy per macroion, $f = f_{el} + \Delta f_0$, was calculated using equations (3.74), (3.78) and (5.5), and required the salt distribution to be found as explained in the previous section. Calculations for an appropriately chosen line of such points allow the boundary of a region of phase coexistence to be established.

The phase diagrams produced by this method demonstrate that, at certain values of the macroion charge Z and radius a, there is a region of coexistence between phases of different density. Figures 5.4, 5.5 and 5.6 show how the boundary of this region changes with Z, for macroions of radius 50 nm. The phase diagrams are displayed as a function of mean colloid volume fraction $\overline{\eta}$ and salt density $\overline{n}_s'$; the salt density is expressed as the number of pairs of salt ions in a volume equivalent to the volume $(4/3)\pi a^3$ of one macroion, and therefore has the same units as $\overline{\eta}$. Note that 1 unit of $\overline{n}_s'$ corresponds to about 3.2 μM (3.2×10^{-6} moles per litre). The thick lines represent the phase coexistence boundary, and the thinner lines are the tie lines, which join points on the boundary which can coexist. The tie lines must be straight in order to conserve the total number of colloidal particles and salt ions. A hypothetical homogeneous system within the coexistence region would phase separate into the two states at either end of the tie line on which it lay. The

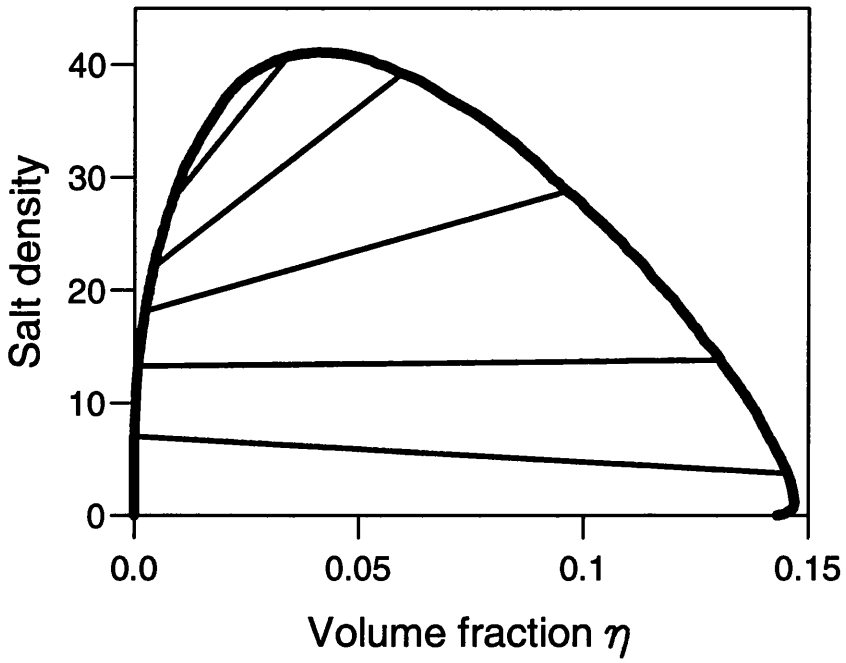

Figure 5.4: Phase diagram for macroions of radius $a = 50$ nm and $|Z| = 1500$, as a function of volume fraction and salt density. The salt density is expressed as the number of pairs of salt ions in a volume equivalent to the volume $(4/3)\pi a^3$ of one macroion, and therefore is in the same units as the volume fraction.

phase coexistence region increases in size with increasing $|Z|$. For $|Z| > 1070$, it has an upper critical point but the bottom of the region sits on the line of zero salt. As $|Z|$ falls below 1070, the region rises away from the zero salt line, and a lower critical point appears; the two critical points merge as the phase coexistence region vanishes when $|Z|$ is just below 1000.

We should consider the possibility that the result (4.7), mentioned in the context of a zero salt suspension in chapter 4, also holds when the suspension contains added salt. This would have the consequence that increasing both $|Z|$ and a by some constant factor C would leave the phase diagram, expressed as a function of η and $\overline{n}'_s$, unchanged; this is approximately true (compare figure 5.7 with 5.5). Figures 5.4, 5.5 and 5.6 could then be regarded as phase diagrams for $\zeta = 30$, $\zeta = 25$ and $\zeta = 20$, respectively, with the two critical points merging slightly below $\zeta = 20$. The validity of (4.7) begins to break down as the concentration of salt is increased, although this could be a consequence of the approximation in equation (3.68), which becomes progressively less valid as the salt concentration is increased.

How do these predictions compare with other experimental evidence? The phase

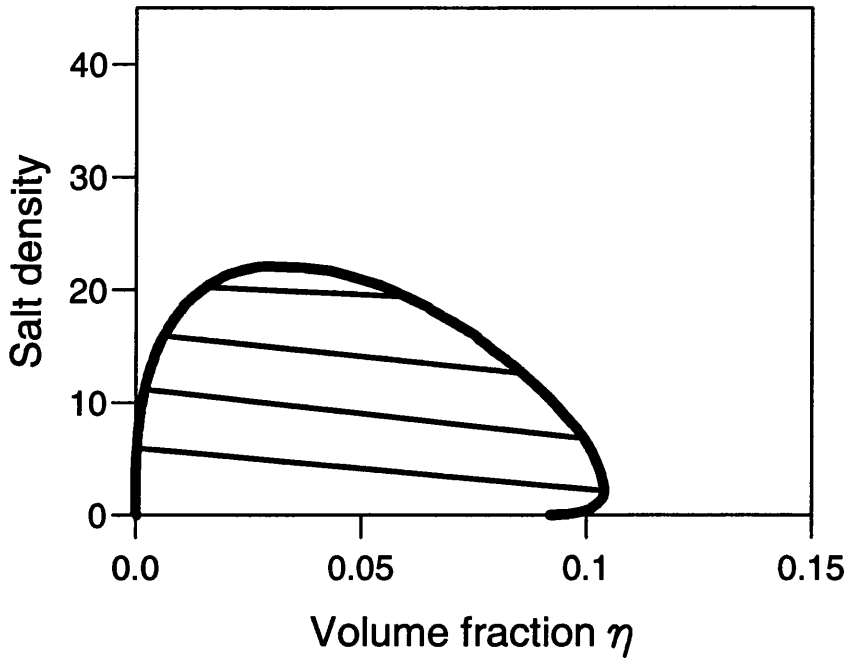

Figure 5.5: Phase diagram for macroions of radius $a = 50$ nm and $|Z| = 1250$.

separation is predicted only above a certain critical macroion charge, and only in the low salt regime. These characteristics are in agreement with experiment. The parameter whose value governs the occurrence or non-occurrence of the phase separation appears to be $\zeta = |Z|/a$, rather than the macroion surface charge density (proportional to $|Z|/a^2$) which was suggested by Ise *et al.* [26, 2]. The critical value $\zeta = 20$ is of a reasonable order of magnitude, but experimental data in reference [2] suggest that phase coexistence can be observed in the region of $\zeta = 9$ to $\zeta = 10$. The reentrant phase coexistence with respect to added salt [31, 32] can perhaps be represented as vertical movement across the coexistence region in a phase diagram like that in figure 5.6, or across the right hand side of the coexistence region in a phase diagram like those in figures 5.4, 5.5 and 5.7.

We can also compare our theoretical results with the those of RDH [53] and of Warren [62]. Qualitatively, the behaviour is the same: a region of phase coexistence appears when the macroion charge is higher than a certain critical value, increases in size as the macroion charge is increased, and decreases in size as the macroion radius is increased. The differences in the actual values of parameters such as the critical charge (which is significantly lower in the other two treatments) are perhaps of only limited significance, since neither the present treatment nor the others are exact. The

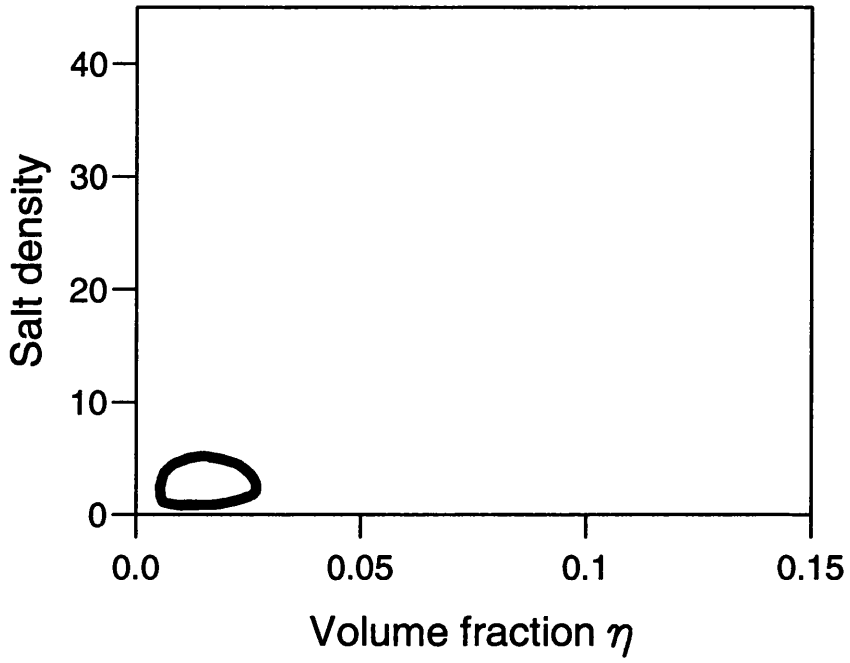

Figure 5.6: Phase diagram for macroions of radius $a = 50$ nm and $|Z| = 1000$.

volume fractions and salt concentrations of the phase coexistence region are similar in the different treatments. Broadly, then, these results confirm the conclusions of other authors. However, there are two important differences which should be pointed out. First, the phase diagrams presented here, together with the results of the previous chapter, suggest, as mentioned there, that phase coexistence can occur even in the limit of zero added salt, whereas the earlier treatments require at least some salt to be present in the system. The second difference concerns the way that the salt is partitioned between the two coexisting phases. The earlier treatments show only phase diagrams in which the salt density is higher in the macroion-poor phase, whereas the phase diagrams in the present volume indicate that, at higher salt concentration and higher macroion charge, the electrostatic interactions involving the salt ions are sufficient to reverse the Donnan effect and cause the salt density to be higher in the macroion-rich phase. This 'reverse Donnan effect' should, in principle, be observable.

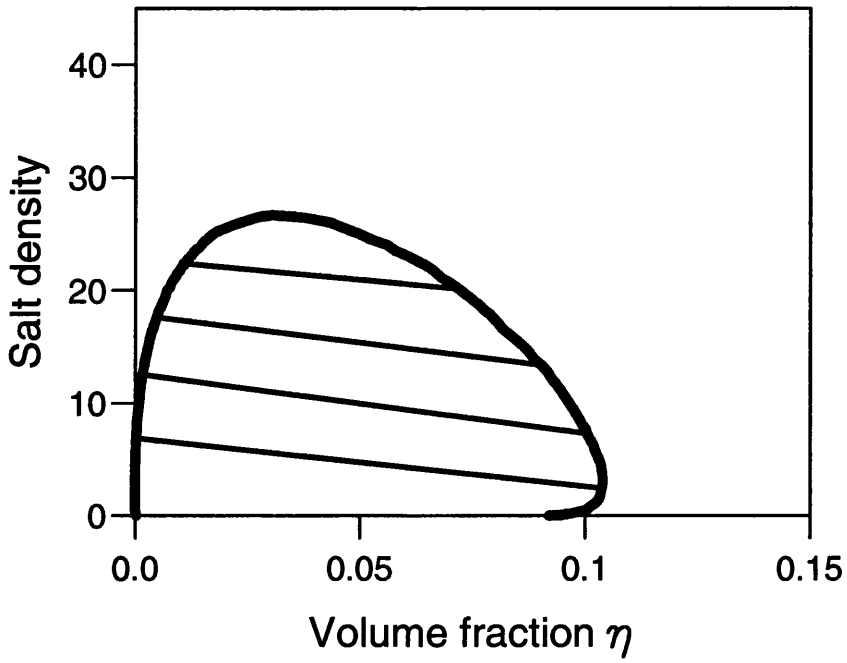

Figure 5.7: Phase diagram for macroions of radius $a = 60$ nm and $|Z| = 1500$.

5.5 The theory of interactions in colloidal suspensions

We might ask, what are the implications of these results for our view of the interactions and free energy of this type of system? A good place to start is with the DLVO theory, which describes the electrostatic part of the Helmholtz free energy as a sum of pair interactions of the form

$$V_{mn} = \frac{Z^2 e^2}{4\pi\epsilon} \left(\frac{e^{\kappa a}}{1 + \kappa a} \right)^2 \frac{e^{-\kappa R_{mn}}}{R_{mn}}, \tag{5.15}$$

where R_{mn} is the separation of macroions m and n. According to the DLVO theory, the pair interactions are repulsive; they provide for stability against coagulation, although this stability is lost when the interaction is weakened by large amounts of added salt, allowing the attractive van der Waals force to draw the colloidal particles together.

The theoretical treatment of the thermodynamics of colloidal suspensions which has been presented in this thesis makes it clear that there is a problem with the DLVO theory as describe above: if two parts of a system have different colloid

densities, they must also have different microion densities in order to maintain charge neutrality in each part. The parameter κ will then change as a function of the colloid density, through its dependence on the microion densities as in equation (4.2). (This change was first applied to the calculation of phase diagrams by van Roij and Hansen [51], although it had been pointed out somewhat earlier [61].)

Equation (5.15) is quite similar in form to the pair contribution f_{pair} to the electrostatic free energy, equation (3.74). Figure 5.8 compares the two at various salt concentrations, taking into account the macroion density dependence of κ, for macroions of radius $a = 50$ nm and charge $|Z| = 1150$. The DLVO free energy f_{DLVO} per macroion is here given by

$$f_{DLVO} = \frac{Z^2 e^2}{8\pi\epsilon a}\left(\frac{e^{\kappa a}}{1+\kappa a}\right)^2 \Sigma^Y, \tag{5.16}$$

where the extra factor of $1/2$ relative to equation (5.15) is inserted because each pair interaction V_{mn} is 'divided' between two macroions. At high salt concentrations, we cannot use the full equation (3.74) to calculate f_{pair}, since an approximation used in its derivation is only valid at low salt. Instead, we use the corresponding expression from Sogami and Ise [43],

$$f'_{pair} = \frac{Z^2 e^2}{8\pi\epsilon a}\left(\frac{\sinh \kappa a}{\kappa a}\right)^2 \Sigma^Y, \tag{5.17}$$

which differs from (3.74) in that it permits microions to penetrate the interiors of the macroions. The two expressions (3.74) and (5.17) should be equivalent for high values of v. The v-dependence of κ is calculated as in equation (5.1); we use here the approximation that the system of macroions and counterions exists against a background of salt of constant density.

Figure 5.8 suggests that the DLVO potential should be interpreted as an approximation to the pair contribution to the electrostatic free energy. When the macroion density dependence of κ is taken into account, the form of the expression is, of course, very different from the Yukawa repulsion traditionally associated with the theory. In addition, the DLVO theory ignores the two other contributions to the free energy: the self free energy f_{self} and the ideal gas contribution f_0. This problem, too, is caused by the failure to allow κ to vary: equations (3.78) and (3.83) make it clear that f_0 would be a constant, and f_{self} nearly so, if the microion density were a constant. Figure 5.9 illustrates that $f_{el} = f_{pair} + f_{self}$ is cohesive, not only at zero salt as mentioned in the previous chapter, but even when salt is present. Here, the components f_{pair} and f_{self} of the free energy are approximated by the corresponding

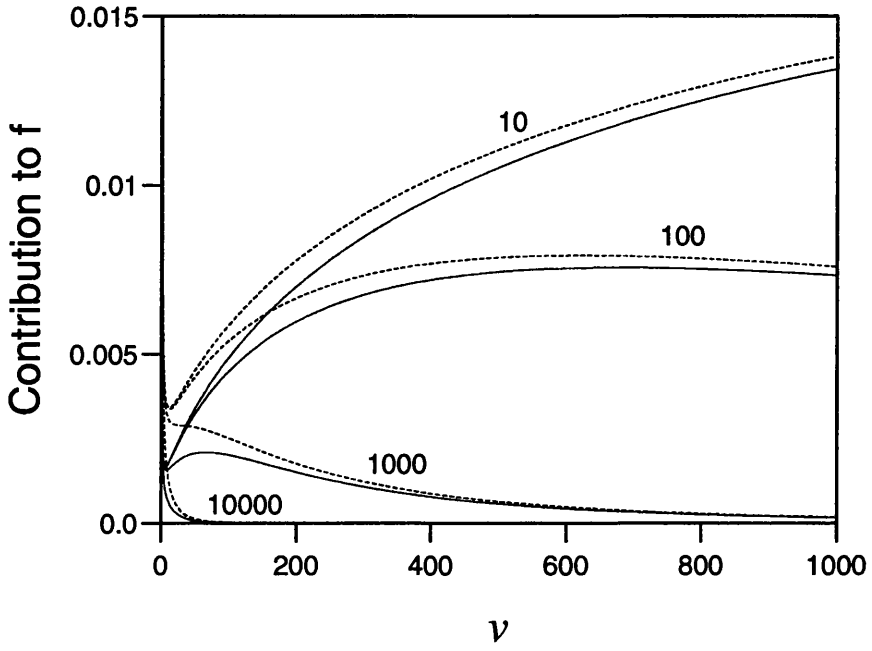

Figure 5.8: Comparison of f_{DLVO} (dashed lines) and f'_{pair} (solid lines), in units of $Z^2e^2/8\pi\epsilon a$. Macroions have radius $a = 50$ nm and charge $|Z| = 1150$. Salt density is held constant; the numbers refer to the number of pairs of salt ions per macroion when $v = 500$.

f'_{pair} and f'_{self} in a simplified system where the microions are not excluded from the macroion interiors [43]:

$$f'_{self} = \frac{Z^2e^2}{8\pi\epsilon a}\left(\frac{e^{-\kappa a}\sinh\kappa a}{\kappa a}\right). \tag{5.18}$$

The pair contribution is in fact considerably less important numerically than the self free energy, which always makes a cohesive contribution to the total electrostatic free energy f_{el} (compare magnitudes in figures 5.8 and 5.9).

It would be tempting to think that DLVO theory is approximately valid at high added salt concentrations, because the dependence of κa on the macroion density becomes weaker as the salt concentration is increased. Then f_{self} and f_0 would become constants at high salt concentrations, while f_{pair} would take the form of a Yukawa potential. However, this conclusion would be incorrect. The parameter κa only becomes a constant in the limit of infinite salt concentration, and in this limit both f_{pair} and f_{self} tend to zero. Figure 5.9 shows how f_{el} changes as the salt concentration is increased.

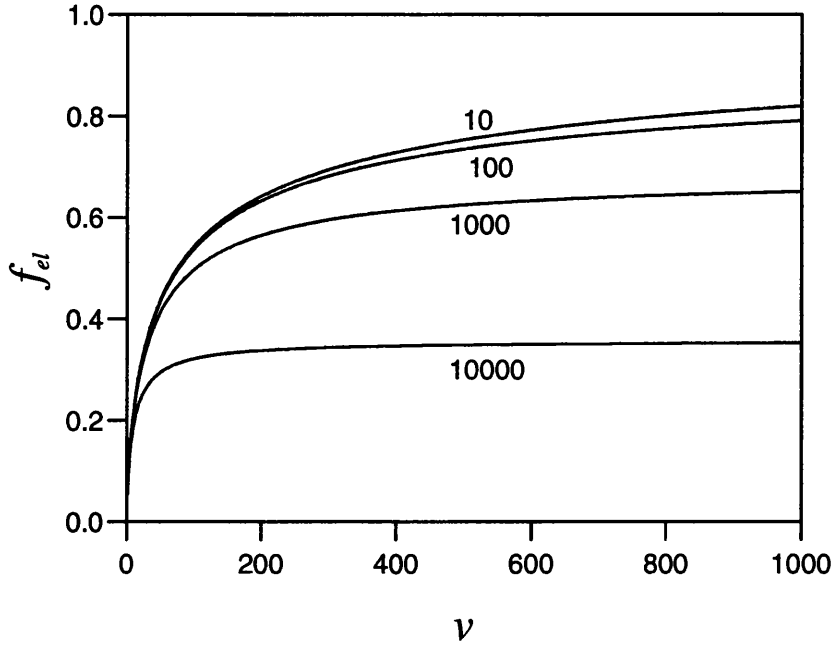

Figure 5.9: Electrostatic free energy f_{el} in units of $Z^2e^2/8\pi\epsilon a$, for macroions of radius $a = 50$ nm and charge $|Z| = 1150$. Salt density is held constant; the numbers indicate the number of pairs of salt ions per macroion when $v = 500$.

We are forced to conclude that, as a description of colloidal stability and phase behaviour, DLVO theory is wrong not just at low salt but in all suspensions. Essentially, its failure to take into account the link between the microion and macroion densities causes it to ignore two of the contributions to the free energy of the system and to predict incorrectly the form of the one contribution which it does not ignore. Any correlations between the DLVO theory and experimental results on colloidal stability must be regarded as coincidence; the theory was originally arrived at from theoretical considerations, and we have shown from theoretical considerations, based on the same physical assumptions, that it is incorrect.

In place of the traditional view of charged colloidal suspensions stabilised by repulsive effective electrostatic interactions, we have a view of cohesive effective electrostatic interactions in a system stabilised by the ideal gas free energy of the counterions. The physical interpretation of the cohesive nature of the electrostatic free energy is that increasing the macroion density brings the counterions closer to the (oppositely charged) macroions, resulting in a lower electrostatic energy. This can be seen from a thought experiment involving point microions and cubic macroions with charged surfaces: the lowest level of electrostatic energy would be achieved by

packing the macroions together so that all the positive and negative charges were confined to the surfaces. From a mesoscopic point of view, the system would then contain no charge density and therefore no electric fields at all.

The fact that DLVO theory is incorrect when applied to colloidal stability does not make it inappropriate for the description of other phenomena. If the counterion density is taken to be constant, f_{self} and f_0 are also constants, while f_{pair} takes the repulsive form traditionally ascribed to it by DLVO theory. One can draw a distinction between phenomena that involve density changes in the whole system, and phenomena which involve only the motion of particular macroions relative to one another. The former require the effects of changes in the counterion density to be taken into account, while the latter do not. The separation of a system into a dense and a rarefied phase is a phenomenon of the former type, and cannot be described by the DLVO theory. On the other hand, when we come to consider phenomena of the second type, such as separation into phases of equal or near-equal density but different symmetry, or the motion of macroions in a crystal phase about their equilibrium positions, or the interaction between an isolated pair of macroions, it seems likely that we should regard κ as approximately constant. This leaves us with a pair contribution which approaches the DLVO form, and also allows us to neglect the self and ideal gas terms. Experimental results show that the effective interaction between a pair of otherwise isolated colloidal particles is repulsive [16, 15]. Calculations using the nonlinear Poisson-Boltzmann theory of the force experienced by a single colloidal particle in a suspension when it is moved independently of its neighbours also support these conclusions [50].

The new stabilisation mechanism, like the old one, will be destroyed by high concentrations of added salt, since the changes in counterion density caused by changes in macroion density will have progressively less effect on f_0 as the salt density is increased. Thus, the view of interactions in colloidal suspensions set out here appears to be capable of describing phenomena which DLVO theory can describe, in addition to permitting phase separation between dense and rarefied phases at low added salt, which is observed experimentally and which DLVO theory does not permit.

The ideal gas part of the free energy should not be regarded as entirely non-electrostatic, since its dependence on macroion density is a consequence of the variations in the counterion density that are required to maintain charge neutrality. It is also probable that the division of phenomena into those involving bulk density changes and those involving the motion of individual macroions is a simplification; presumably, these two types represent hypothetical extremes, while real phenomena

will involve a combination of the two.

Finally, we shall consider the implications of this discussion for two theories of colloidal interactions: the theory of van Roij, Dijkstra and Hansen (RDH) [53], and that of Sogami and Ise (SI) [43]. The expression for the free energy derived by RDH contains DLVO pair interactions together with a density-dependent, but structure-independent, volume term. There, the pair interactions are interpreted as repulsive, but as the macroion density dependence of κ is correctly taken into account, this is probably not the correct interpretation. It should be noted that the misinterpretation does not affect either the mathematical results or the phase diagrams derived by RDH. The volume term would correspond to the two terms which in the present volume are called f_{self} and f_0.

The form of expression derived by SI for the Helmholtz free energy is clearly justified on thermodynamic grounds; it was used earlier in the present discussion, and the methods underlying it have been of great importance to the results of this chapter and the previous two. However, the SI theory, like the DLVO theory, does not take into account the dependence of the microion densities on the macroion density, and therefore ignores two of the contributions to the free energy. Therefore, our conclusions probably do not support the argument that the attractive tail in the Gibbs pair potential derived from the SI theory is equivalent [60] to the volume terms in other theories; however, we have not considered the question of the SI calculation of the Gibbs free energy. The SI expressions for the Helmholtz free energy (5.17) and (5.18) lead to the electrostatic contribution being cohesive, as shown above, if they are correctly applied.

Chapter 6

The effect of density-dependent macroion charge

6.1 Introduction

The treatment of the thermodynamics of a colloidal suspension which is set out in chapters 3-5 makes the simplifying assumption that the surface charge on a macroion is independent of the macroion density. Other approaches to the problem have also made this assumption. However, since the macroion charge is caused by dissociation of surface groups, its value should depend on the surroundings, and a faithful representation of the system would reflect this. It is therefore pertinent to ask how good the constant charge assumption is, and what additional effects on the predicted behaviour of the suspension might arise from allowing the charge to vary. It would also be reassuring if we could confirm that the phase behaviour predicted by the theoretical treatments mentioned above is genuine and not an artefact of the constant charge assumption.

The issue here is variation in the actual bare surface charge on the macroion; this is conceptually distinct from the ideas of counterion condensation and charge renormalisation [78, 79]. Problems involving the variation of a surface charge in contact with a liquid have generally been addressed using the concept of a charge regulating surface [89]. In this chapter we take a different approach. At a given macroion density, we minimise the free energy with respect to the surface charge Z to find the physical value of Z at that density, and finally this physical value of the surface charge can be used to calculate the free energy as a function of the density, so that the phase behaviour can be investigated. In the process, we demonstrate how the usual equation for the charge regulating surface can be derived by minimising the free energy which results from our simple but physically plausible model for the

system.

6.2 Calculation of the free energy

6.2.1 The model

The theoretical system to be considered here contains a constant number of colloidal particles of radius a, each of which has Z_0 surface groups which can, in principle, be ionised. The number of surface groups which are actually ionised is $|Z|$, and there are also $|Z|$ oppositely charged monovalent point microions associated with each macroion. The key difference between this model and the models used in previous chapters is that Z is permitted to depend on the density of the macroions. The surface boundary condition which constrains the behaviour of the system is therefore not the charge density, but the dissociation constant of the reaction at the surface. This reaction is of the form

$$\mathrm{MX} \rightleftharpoons \mathrm{M}^+ + \mathrm{X}^- \tag{6.1}$$

where M^+ represents a microion, X^- a surface ion, and MX an undissociated surface group (but it makes no difference to the model if instead the microions are negative and the surface ions positive). The X^- and MX are taken to be homogeneously distributed over the surface of each macroion. We regard the dissociation process and the electrostatic field which results from its products as making separate contributions to the thermodynamics, although in fact the bond in the MX group may be largely electrostatic in origin. The system contains no added salt.

In this system, it is necessary for the calculation of the thermodynamics to take into account the existence of the X^- and MX, instead of just regarding the macroion surfaces as shells of charge. This requires a number of changes in equation (3.1) for the differential of the Helmholtz free energy: an additional term σdA must be added, where σ and A are the surface tension and area of the macroion-solvent interfaces; the entropy must include contributions both from the microions and from the macroion surfaces; and the summations over species must cover the M^+, X^- and MX. Equation (3.1) becomes

$$dF = -SdT - pdV + \sigma dA + \sum_i \int d^3\mathbf{r}\,(\mu_i(\mathbf{r})dn_i(\mathbf{r})) + \sum_i \int d^3\mathbf{r}\,(\psi(\mathbf{r})d\rho_i(\mathbf{r}))\,. \tag{6.2}$$

This can be written as

$$dF = dF_{\mathrm{M}^+} + dF_{el} + dF_{surf}. \tag{6.3}$$

The first term in equation (6.3) is the differential of the microion ideal gas free energy,

$$dF_{\mathrm{M}^+} = -S_{\mathrm{M}^+}dT - pdV + \int d^3\mathbf{r}\left(\mu_{\mathrm{M}^+}(\mathbf{r})dn_{\mathrm{M}^+}(\mathbf{r})\right), \tag{6.4}$$

where S_{M^+}, μ_{M^+} and $n_{\mathrm{M}^+}(\mathbf{r})$ are the entropy, chemical potential and density, respectively, of the microions. The second term is the differential of the electrostatic free energy,

$$dF_{el} = \sum_i \int d^3\mathbf{r}\left(\psi(\mathbf{r})d\rho_i(\mathbf{r})\right). \tag{6.5}$$

The third term is the differential of the non-electrostatic free energy of the surface species X^- and MX,

$$dF_{surf} = -S_{surf}dT + \sigma dA + \mu_{\mathrm{X}^-}dN_{\mathrm{X}^-} + \mu_{\mathrm{MX}}dN_{\mathrm{MX}}, \tag{6.6}$$

where S_{surf} is the entropy of the surface species, and μ_i and N_i are the chemical potential and total particle number of the surface species i. The volume integral in the third and fourth terms on the right hand side of equation (6.6) has been performed implicitly, because the X^- and MX are confined to the surfaces, where their densities are homogeneous.

Now, dF_{M^+} is identical to the dF_0 which is defined in equation (3.2), if dF_0 is specialised to a system containing only one species of microion. In addition, dF_{el} is the same as in chapter 3. This means that two of the three components in the Helmholtz free energy can be calculated using expressions derived earlier. The free energy f per macroion can be written as

$$f = f_{\mathrm{M}^+} + f_{el} + f_{surf}, \tag{6.7}$$

where f_{el} is calculated using equations (3.59), (3.62), (3.74), (3.75) and (3.78), while f_{M^+} is found from equation (3.80) to be

$$f_{\mathrm{M}^+} = |Z|\left[u_{\mathrm{M}^+} + k_BT\left(\ln\frac{|Z|}{\widetilde{V}}\Lambda^3_{\mathrm{M}^+} - 1\right)\right], \tag{6.8}$$

where u_{M^+} is the temperature-independent energy cost of formation of a microion

and Λ_{M^+} is the thermal wavelength. In terms of the dimensionless volume v, this is

$$f_{M^+} = |Z| \left\{ u_{M^+} + k_B T \left[\ln \frac{3|Z|}{4\pi} \left(\frac{\Lambda_{M^+}^3}{a} \right)^3 - \ln(v-1) - 1 \right] \right\}. \tag{6.9}$$

Equation (6.9) is effectively identical to equation (4.4); however, an important difference between the present system and the same system with constant Z is that here it is impossible to ignore any of the terms in the free energy of the microion ideal gas. This makes it necessary to specify the chemical nature of the microions through the values chosen for u_{M^+} and Λ_{M^+}.

Just as in the constant Z system, the parameter κa varies with v according to equation (4.2), while the relation between v and the nearest neighbour macroion separation S is given by equation (4.6).

6.2.2 The free energy of the surface groups

Now we must calculate f_{surf}. We consider the surface of each macroion to contain Z_0 discrete locations, of which $N_{X^-} = |Z|$ contain a surface ion X^-, while the remaining $N_{MX} = (Z_0 - |Z|)$ contain an undissociated surface group MX. The ions do not interact with one another except through the mean electrostatic field; this electrostatic contribution is included in f_{el}, and so the energy to be included in the calculation of f_{surf} is just $|Z| \left(u^0_{X^-} - u^0_{MX} \right)$, where $u^0_{X^-}$ and u^0_{MX} are the temperature-independent energy costs of creating one X^- or one MX. Therefore the canonical partition function Q_1 for the surface groups on a single macroion is

$$Q_1 = \sum_{\Omega} \exp\left[-|Z| \left(u^0_{X^-} - u^0_{MX} \right) / k_B T \right]. \tag{6.10}$$

The number of states (each with the same energy) in the phase space Ω is equal to the number of ways of distributing $|Z|$ indistinguishable objects between Z_0 boxes, so that

$$Q_1 = \frac{Z_0!}{Z!\,(Z_0 - |Z|)!} \exp\left[-|Z| \left(u^0_{X^-} - u^0_{MX} \right) / k_B T \right], \tag{6.11}$$

and, using $f_{surf} = -kT \ln Q_1$ and Stirling's approximation, we find

$$f_{surf} \approx |Z| \left(u^0_{X^-} - u^0_{MX} \right) - k_B T \left[Z_0 \ln Z_0 - |Z| \ln |Z| - (Z_0 - |Z|) \ln (Z_0 - |Z|) \right] \tag{6.12}$$

for the surface contribution to the free energy per macroion. This calculation is equivalent to the performance of the thermodynamic integration of dF_{surf} in equa-

tion (6.6). The integration would be performed along a path from ($N_{X^-} = 0$, $N_{MX} = Z_0$, $A = A_s$, $T = T^0$) to ($N_{X^-} = |Z|$, $N_{MX} = Z_0 - |Z|$, $A = A_s$, T): note that the σdA term makes no contribution, since the surface area remains fixed at A_s during the integration. Equation (6.12) allows the chemical potential, in the absence of electrostatic effects, to be calculated as

$$\mu_i = u_i^0 + k_B T \left(1 + \ln N_i\right), \tag{6.13}$$

where i represents X^- or MX.

6.2.3 The total free energy

The total free energy per macroion, collecting equations (6.7), (6.9) and (6.12), is

$$f = f_{el} + |Z| \left(u^0 + \frac{3}{2} k_B T\right) + |Z| \, k_B T \ln \left[\frac{3}{4\pi} e^{-5/2} \left(\frac{\Lambda_{M^+}}{a}\right)^3 \frac{|Z|}{v-1}\right]$$

$$+ k_B T \left[(Z_0 - |Z|) \ln (Z_0 - |Z|) + |Z| \ln |Z| - Z_0 \ln Z_0\right], \tag{6.14}$$

where $u^0 = u^0_{M^+} + u^0_{X^-} - u^0_{MX} - \frac{3}{2} k T^0$ is a temperature-independent parameter which depends on the chemical nature of the macroions and microions and which must be defined externally; it is actually equal to the energy cost of the dissociation reaction (6.1). For the purpose of inserting tabulated chemical data, we could assume $u^0 = \Delta G$, where the dissociation free energy per molecule ΔG is related to the dissociation constant K by

$$K = e^{-\Delta G / k_B T}. \tag{6.15}$$

The second term on the right hand side of equation (6.14) is the non-electrostatic energy, while the third and fourth terms come from the entropy associated with the microion ideal gas and the macroion surface, respectively.

If the charge Z on a macroion is regarded as a constant, equation (6.14) reduces to the results of chapter 4; we can ignore the terms which do not depend on the volume, and consider only a free energy Δf, given by

$$\Delta f = f_{el} - |Z| \, k_B T \ln (v - 1). \tag{6.16}$$

However, in this chapter we wish to consider the variation of Z with macroion density, and so the extra contributions to the free energy must be taken into account.

6.3 Minimisation of the free energy

6.3.1 Macroion surface charge as a function of density

The next step is to find the state of the system at fixed v: that is, to find the value which Z will take when the macroions are imagined as held at a given fixed density. This is accomplished by minimising the Helmholtz free energy given in equation (6.14) with respect to Z, holding v constant. The fixed parameter expressing the nature of the macroion surface is here u^0 rather than Z. The minimisation process gives $df/dZ = 0$, and so it is equivalent to

$$\frac{\partial f}{\partial N_{\mathrm{M}^+}} + \frac{\partial f}{\partial N_{\mathrm{X}^-}} - \frac{\partial f}{\partial N_{\mathrm{MX}}} = 0. \tag{6.17}$$

This provides the expected condition on the electrochemical potentials $\tilde{\mu}_i$ of the different species: $\tilde{\mu}_{\mathrm{M}^+} + \tilde{\mu}_{\mathrm{X}^-} - \tilde{\mu}_{\mathrm{MX}} = 0$. At the surface, the contributions of the electrostatic field to the electrochemical potentials of the M^+ and X^- will be equal and opposite and will cancel one another, while its contribution to the electrochemical potential of the uncharged MX will clearly be zero everywhere (equation (1.41)). Therefore we have the following condition on the chemical potentials $\mu_i^{(s)}$ at the surface:

$$\mu^{(s)}_{\mathrm{M}^+} + \mu^{(s)}_{\mathrm{X}^-} - \mu^{(s)}_{\mathrm{MX}} = 0. \tag{6.18}$$

Using equations (3.82), (3.85) and (6.13), we find

$$\frac{\Lambda^3_{\mathrm{M}^+} n^{(s)}_{\mathrm{M}^+} N_{\mathrm{X}^-}}{N_{\mathrm{MX}}} = e^{-u^0/k_B T}, \tag{6.19}$$

where $n^{(s)}_{\mathrm{M}^+}$ is the density of microions at the macroion surface. This makes the link with the charge regulating surface treatment of this type of equilibrium [89]. An expression of this form can be derived from the dissociation equilibrium

$$\frac{a^{(s)}_{\mathrm{M}^+} a_{\mathrm{X}^-}}{a_{\mathrm{MX}}} = K \tag{6.20}$$

(where a_{X^-} and a_{MX} are the activities of surface ions and undissociated surface groups and $a^{(s)}_{\mathrm{M}^+}$ is the activity of the microions at the surface) by assuming that the activities of the various species at the surface are proportional to their concentrations; here we have shown that this is compatible with our simple model of the system. The thermal wavelength Λ_{M^+} maintains the correct dimensions on the left

hand side of equation (6.19); its presence results from the ideal gas characteristics of the microions in our model, since an ideal gas has activity $a = \Lambda^3 n$.

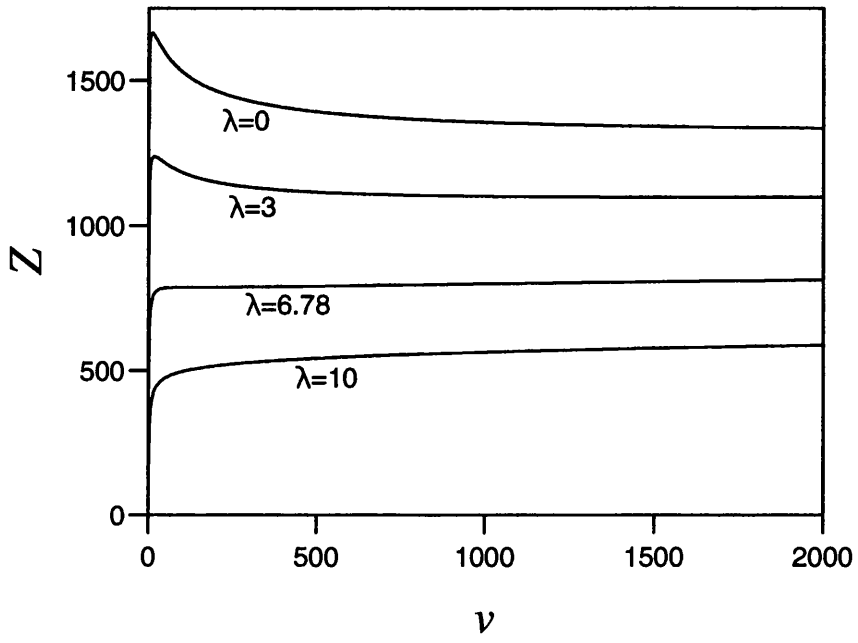

Figure 6.1: Macroion surface charge Z as a function of dimensionless volume v for $a = 50$ nm, $Z_0 = 10000$ and various values of λ.

At fixed a and v, we find that $|Z|$ does not depend on u^0 or m (the mass of a microion) separately, but only on a parameter λ which we define by $\lambda = (u^0 - u_c^0)/kT$. The energy u_c^0 is defined only up to an additive constant; for $a = 50$ nm we choose

$$u_c^0 = 6.67 + \frac{3}{2} \ln\left(\frac{m}{m_p}\right), \tag{6.21}$$

where m_p is the mass of a proton. The reason for the choice of 6.67 as the additive constant will be explained in the next section. Figure 6.1 shows the dependence of $|Z|$ on v for macroions of radius 50 nm and $Z_0 = 10000$. For these calculations, we ignore those parts of equations (3.74) and (3.78) which require a numerical integral to be performed, since the effect on the results is small and the calculational cost large. Figure 6.2 is a larger scale view of the high macroion density ends of the curves shown in figure 6.1. For small values of v the $|Z|(v)$ curves fall into two groups according to the value of λ. For the regime with $\lambda > 6.78$, the surface charge increases monotonically with increasing v (decreasing macroion density). However, for $\lambda < 6.78$, it displays a different behaviour: as v increases, the charge initially

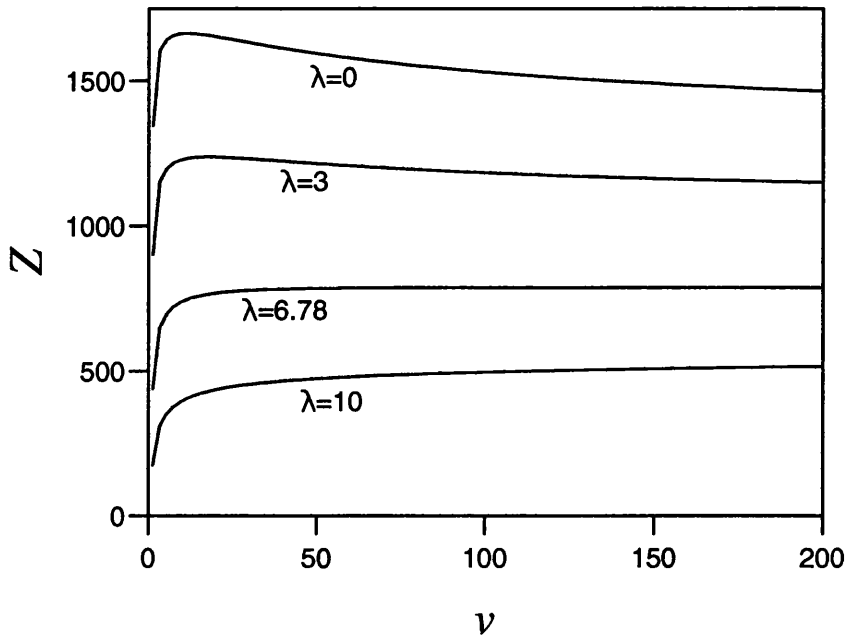

Figure 6.2: Macroion surface charge Z as a function of dimensionless volume v for $a = 50$ nm, $Z_0 = 10000$ and various values of λ (larger scale view of high macroion density end of graph in figure 6.1).

increases, then decreases, then finally begins to increase once more. There is a crossover in the behaviour in the region with $\lambda \approx 6.78$, in which Z is broadly constant over a wide range of values of v; it is in this region that the constant charge approximation would be most valid.

The behaviour of Z results from the competition between terms in the free energy which become more positive with increasing $|Z|$, and therefore act against the formation of microions (f_{el} and the non-electrostatic energy), and the entropic terms, which become more negative with increasing $|Z|$ for relevant values of the parameters. For large values of u^0, and therefore of λ, the $u^0 |Z|$ term dominates; as u^0 decreases, the entropic terms come to dominate, initially at intermediate densities.

The large v (low macroion density) behaviour of Z is more uniform across the range of values of λ: it shows a slow increase in $|Z|$ with increasing v. In fact, Z is not expected to level off (saturate) as $v \to \infty$, except eventually at $|Z| = Z_0$. This is because taking the $v \to \infty$ limit in a zero salt system is equivalent to putting it in contact with an infinite microion reservoir of zero density, so that a microion density profile described by a Boltzmann distribution will never reach equilibrium: microions will be dissipated into the reservoir until the surface saturates [90].

6.3.2 Free energy as a function of density: the phase diagram

Having found the physical value of the macroion surface charge at a given macroion density, we can then specify the Helmholtz free energy at that density, and produce a plot of the free energy per macroion against the volume per macroion, as in figure 6.3. As was the case with $|Z|$, we find that f does not depend on u^0 and m separately, but only on λ.

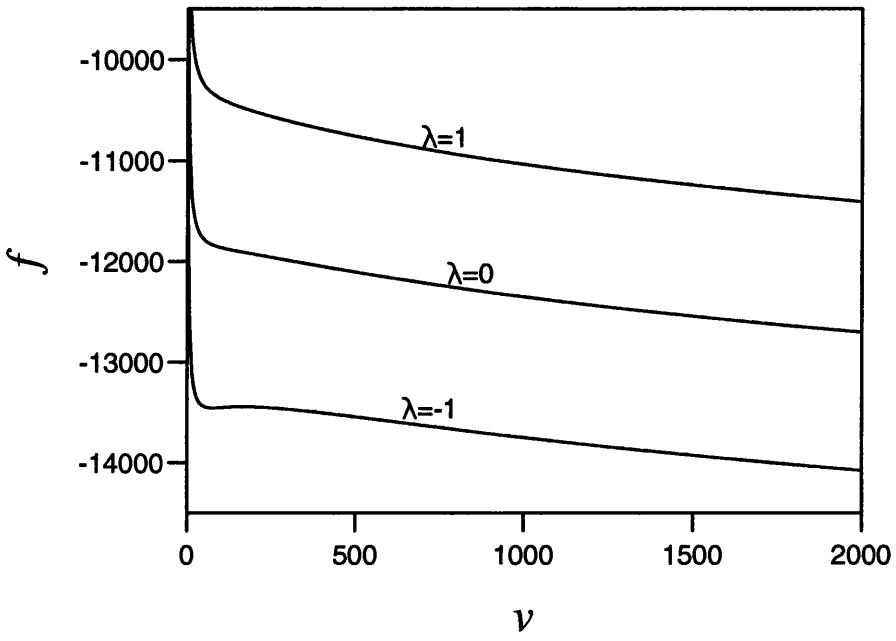

Figure 6.3: Free energy f per macroion, in units of k_BT, as a function of dimensionless volume v for $a = 50$ nm, $Z_0 = 10000$ and various values of λ.

For $\lambda > 0$, the free energy f per macroion decreases monotonically with increasing v (decreasing macroion density), while the second derivative of f with respect to v remains positive. Systems with these values of λ will expand to fill all the available space: their interaction will be observed to be repulsive, and no phase coexistence will occur. On the other hand, if $\lambda < 0$ a region appears in which the second derivative of the free energy becomes negative (deepening to a local minimum as λ is decreased further); as for a molecular fluid, this is the sign of coexistence between a dense and a rarefied phase. Therefore, we can interpret u_c^0 as the critical dissociation energy at a given a and m: phase separation is possible only if $u^0 < u_c^0$. This is the reason for our choice of the additive constant in equation (6.21) which defines u_c^0.

If a pressure $p = -\partial f/\partial v$ is plotted against v, as shown in figure 6.4, a van der Waals loop is observed for $\lambda < 0$. Maxwell's equal area construction allows the physical 'isotherm' (in this case, curve of constant dissociation energy and microion mass) to be plotted across this loop; parts of the pressure curve which lie away from the physical isotherm represent metastable or unstable states. A system will phase separate if its mean macroion density lies within the range of values covered by the loop. As λ decreases below zero, the difference in density between the two phases rapidly becomes very large; it is only in the immediate vicinity of the critical point that two phases of comparable density are predicted.

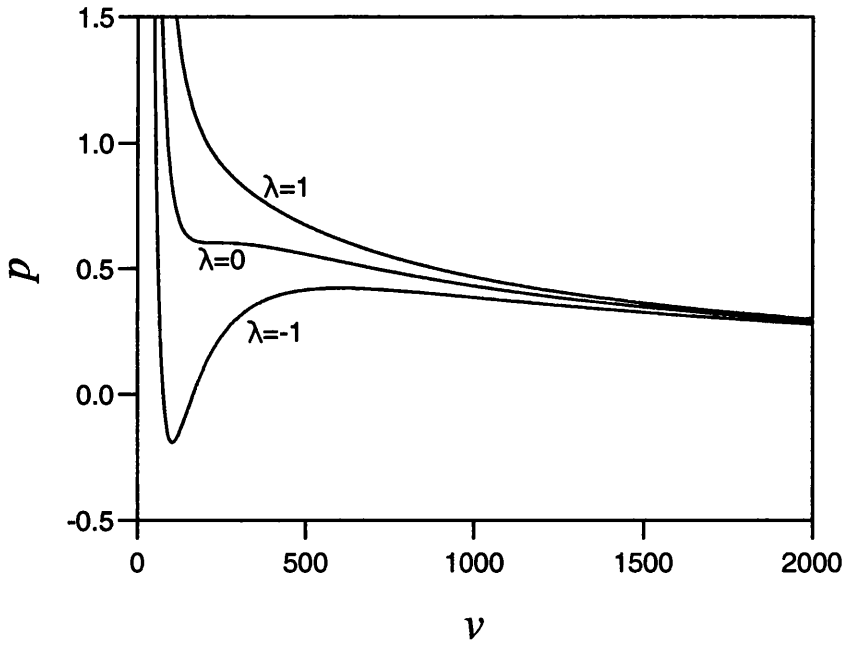

Figure 6.4: pV diagram for $a = 50$ nm, $Z_0 = 10000$ and various values of λ.

The value of u_c^0 depends on the mass of the microions, and the values we choose for the mass depend upon whether we consider a bare microion or include up to six water molecules from a hydration shell. H^+ ions have a mass $m/m_p = 1$, if we take a bare ion, or $m/m_p = 109$, if we include six water molecules. The corresponding values of u_c^0 can be calculated, using equation (6.21), as $6.67k_BT$ and $13.71k_BT$. Potassium (K^+) ions have a mass of $m/m_p = 39$ (unhydrated) or $m/m_p = 147$ (hydrated); the critical dissociation energies are $12.17k_BT$ and $14.16k_BT$, respectively. These values for u_c^0 are reasonable for dissociation energies in aqueous solution.

To summarise: these results predict that the variation of the surface charge with

macroion density should have an effect on the phase behaviour of charged colloidal suspensions. However, we find the same qualitative behaviour as with the constant charge assumption: a van der Waals loop appears when the value of the parameter λ falls below the critical value of zero. Hence we would expect colloidal gas-liquid coexistence, provided that a real experimental system can be found for which $\lambda < 0$. This is an important conclusion, as it shows that the recent theoretical predictions of phase coexistence are not merely an artefact of the constant charge assumption. The results also emphasise the point that, when two phases coexist in this manner, the surface charges on the macroions may be significantly different in the two phases.

Chapter 7

Homogeneous nucleation theory

7.1 Introduction

As mentioned in chapter 1, a homogeneous fluid which is metastable with respect to another phase or mixture of phases may persist temporarily. This is because of the free energy barrier associated with the formation of a surface: before a large region of the new phase can exist, a small droplet must nucleate, and this droplet will have a large surface area relative to its volume. As a result, the free energy cost of forming the surface of a small droplet outweighs the free energy gain of forming the bulk of the droplet, and the droplet is unstable with respect to the surrounding metastable phase.

Consider a small liquidlike cluster containing i particles, surrounded by its vapour. We wish to consider the work ΔW required to form such a cluster from the vapour. Recall from chapter 1 that, in a system whose constraints (constant temperature and volume, and no exchange of matter with the surroundings) are such as to make the Helmholtz free energy F a minimum at equilibrium, the work ΔW required to cause a reversible process to happen is equal to the change ΔF in the Helmholtz free energy during the process. With a view to applying the results to the colloidal system discussed in previous chapters, we will consider nucleation under these external constraints, and so $\Delta W = \Delta F$. This makes the assumption that the states before and after the formation of the cluster can be joined by a reversible path.

We make the assumptions of classical nucleation theory: that is, the cluster can be described as a very small spherical droplet of liquid of radius R, which behaves in the same way as a macroscopic spherical drop in the sense that it has a well-defined surface whose area, because of the geometry of the sphere, is proportional to $i^{2/3}$. The surface tension σ and density n_l are regarded as equal to those of a macroscopic quantity of liquid under the same conditions. We shall see that, if the cluster is

sufficiently small that its formation from the vapour produces a negligible change in the density of the vapour, the free energy cost of forming the cluster from the vapour can be expressed as

$$\Delta F = \Delta f_b i + f_s i^{2/3}, \tag{7.1}$$

where Δf_b is the free energy cost of transferring one particle from the vapour to the liquid phase, and f_s is a parameter proportional to the free energy cost of creating unit area of surface. f_s is positive while, if the vapour is metastable, Δf_b will be negative.

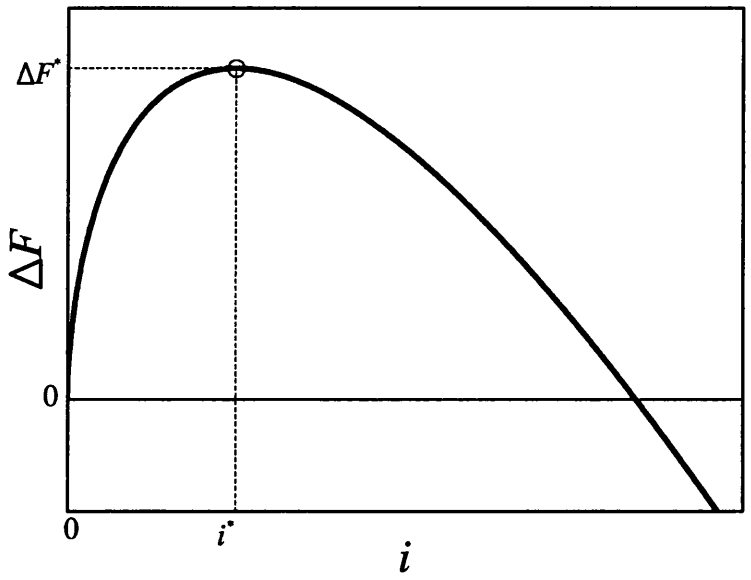

Figure 7.1: Illustration of the dependence of the free energy cost of forming a cluster from the vapour, ΔF, on the cluster size i.

The shape of $\Delta F(i)$ is shown in figure 7.1; it possesses a peak at a critical cluster size i^*. Clusters larger than i^* will tend to grow, but a cluster can only reach this size by means of random fluctuations: clusters smaller than i^* are unstable with respect to the vapour. The formation probability of a critical cluster is proportional to the exponential of the negative of the work of formation ΔF^* of the critical cluster, and since a cluster which exceeds the critical size will tend to grow into a macroscopic droplet, we consider the probability of formation of a droplet also to be proportional to this. The Becker-Döring equations relate the nucleation rate J (the

rate of formation of droplets) to the formation probability [91], giving, to a good approximation,

$$J = J_0 \exp\left(-\Delta F^*/k_B T\right), \tag{7.2}$$

where the prefactor J_0 emerges from a detailed consideration of the condensation rate of monomers on to a cluster and their evaporation rate from a cluster. J_0 is only weakly dependent on the cluster size, for a given substance under given conditions.

In this chapter, we outline the classical theory of nucleation, in preparation for its application to colloidal systems in chapter 8. We first show how the free energy change can be calculated using thermodynamics, in order to justify the form of equation (7.1). The second part of the chapter explains how the characteristics of the critical cluster can be determined from physically measurable quantities in nucleation experiments. Calculations involving simple fluids are used to illustrate this; although there do not yet appear to have been any experiments directed specifically at investigating nucleation phenomena in colloidal suspensions, the results of this chapter will be relevant for any future experiments.

7.2 The thermodynamic model

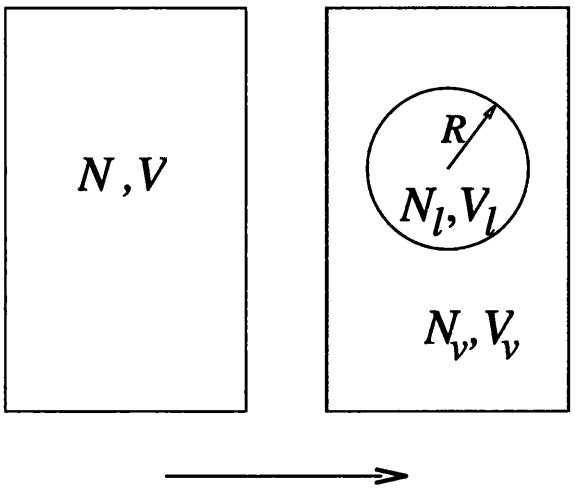

Figure 7.2: Schematic of the process of formation of a liquid droplet from a metastable vapour.

Now we wish to justify equation (7.1) on the basis of thermodynamics. Figure 7.2 illustrates schematically the process of formation of an arbitrary droplet or cluster (not necessarily the critical cluster). The initial state consists of a homogeneous metastable vapour of N particles in volume V. The final state comprises a spherical liquid cluster of radius R and volume V_l, containing $N_l = i$ particles at constant

density i/V_l, and a vapour of volume V_v, containing N_v particles at constant density $n_v = N_v/V_v$. This is the Gibbsian view of the structure of a cluster. The temperature T, the total number of particles N and the total volume V are held constant throughout the process. Using equation (1.25) and the definition $F = U - TS$, the free energy F_h of the initial homogeneous state can be written as

$$F_h = -p_h V + \mu_h N, \tag{7.3}$$

where p_h and μ_h are, respectively, the pressure and chemical potential in the homogeneous metastable vapour. The free energy after the formation of the cluster is $F = F_l + F_v + F_s$, where the bulk free energy of the liquid cluster is $F_l = -p_l V_l + \mu_l N_l$ (p_l is the pressure in the liquid and μ_l the chemical potential) and that of the remaining vapour is $F_v = -p_v V_v + \mu_v N_v$ (p_v and μ_v are the pressure and chemical potential in the vapour). The free energy F_s of the (theoretically infinitesimally thin) interface is given by

$$F_s = \sigma A_s + \mu_s N_s, \tag{7.4}$$

where σ is the surface tension, A_s the surface area of the cluster, μ_s the chemical potential in the surface, and N_s the number of particles associated with the surface. (This does not mean that N_s particles are actually located within the infinitesimally thin interface: see below.) The σA_s term has been added to the energy, and therefore to the Helmholtz free energy, in place of a $-pV$ term.

We define the *excess* of a quantity such as the energy or Helmholtz free energy to be the difference between the actual value of that quantity and the value which is calculated if we ignore the contributions of interfaces. Thus, the excess value F^x of the free energy after the cluster has formed is F_s. The choice of the position of the theoretical dividing surface between the phases is arbitrary: a general dividing surface that separates a volume of vapour V_v and a volume of liquid V_l, where $V_v + V_l = V$, will lead to values of $N_v = n_v V_v$ and $N_l = n_l V_l$ that do not add up to N. The shortfall is the excess number of particles N_s. From the point of view of our theoretical model of the surface, these particles have no spatial location, but we regard them as associated with the interface, whose position determines how many of them there are. If we choose the interface to correspond to the so-called Gibbs dividing surface (which is defined by $N_l + N_v = N$) the excess number of particles N_s is zero, and $F_s = \sigma A_s$. This allows the parameter f_s which was introduced in equation (7.1) to be expressed as

$$f_s = (36\pi)^{1/3} \frac{\sigma}{n_l^{2/3}}. \tag{7.5}$$

Here, of course, we have made the classical assumption that the surface tension is independent of the size of the cluster.

Since $d(\Delta F) = 0$ at $i = i^*$, the critical cluster is in equilibrium with its vapour. This is an unstable equilibrium: the system is unstable against arbitrarily small changes in the size of the cluster. Now we shall show that the critical cluster is equally likely to grow or to decay. The rate of change with respect to time t of the number N_i of clusters of size i can be written as [91]

$$\frac{dN_i}{dt} = C_{i-1}N_{i-1} - E_iN_i - C_iN_i + E_{i+1}N_{i+1}, \tag{7.6}$$

where C_j and E_j are, respectively, the rate of condensation of monomers on to a cluster of arbitrary size j and the rate of evaporation of monomers from a cluster of the same size. If the populations N_i of clusters of various sizes are in thermal equilibrium (denoted N_i^{eq}), we can be assured of microscopic reversibility between all 'nearest neighbour' transitions $i \to i+1$ and $i+1 \to i$:

$$C_{i-1}N_{i-1}^{\mathrm{eq}} = E_iN_i^{\mathrm{eq}}. \tag{7.7}$$

(Note that $dN_i^{\mathrm{eq}}/dt = 0$: the cluster size distribution remains constant over time, which is of course a feature of thermal equilibrium). Equation (7.7) implies that $E_i = \left(N_{i-1}^{\mathrm{eq}}/N_i^{\mathrm{eq}}\right) C_{i-1}$ and, since the number of clusters of a given size in thermal equilibrium at temperature T will be proportional to the exponential of the negative of the work of formation, as in the justification for equation (7.2), we find

$$\frac{E_i}{C_{i-1}} = \exp\left[-\left(\Delta F_{i-1} - \Delta F_i\right)/k_BT\right], \tag{7.8}$$

where ΔF_j is the work of formation of a cluster of size j. From the shape of the nucleation barrier in figure 7.1, it can be seen that if $i < i^*$ then $E_i > C_{i-1}$; if $i \gg 1$ (so that we can approximate $i - 1 \approx i$) this can be interpreted as meaning that the cluster is more likely to decay than to grow. Similarly, if $i > i^*$ we have $E_i < C_{i-1}$, and the cluster is more likely to grow than to decay. Around $i = i^*$, the condensation and evaporation rates are equal, and so the critical cluster is equally likely to grow or to decay.

We can now consider the pressure and chemical potential when the cluster is at the critical size. Using the facts that $V_l + V_v = V$ and $N_l + N_v = N$, we can write the total free energy of a system containing an arbitrary cluster (not necessarily critical) as

$$F = -\left(p_l - p_v\right)V_l + \left(\mu_l - \mu_v\right)N_l - p_vV + \mu_vN + \sigma A_s. \tag{7.9}$$

Requiring the unstable equilibrium condition $\partial F/\partial N_l = 0$ to hold, we find that the critical cluster corresponds to equality of the chemical potentials: $\mu_l^* = \mu_v^*$. However, the same is not true of the pressure. Since the surface area A_s depends on V_l,

$$\frac{\partial F}{\partial V_l} = -(p_l - p_v) + \sigma \frac{\partial A_s}{\partial V_l}, \tag{7.10}$$

and because, from the geometry of the sphere, $\partial A_s/\partial V_l = 2/R$, setting $\partial F/\partial V_l = 0$ leads to the Laplace relation,

$$p_l^* - p_v^* = \frac{2\sigma}{R}. \tag{7.11}$$

This shows that the pressures of the two components are not equal at equilibrium. This conclusion (although not the precise form of equation (7.11)) holds for any situation in which the area of the interface depends on the volumes of the components.

7.3 The free energy of formation of a liquid cluster: classical theory

Subtracting equation (7.3) from (7.9), the free energy cost of forming an arbitrary spherical cluster can be expressed as

$$\Delta F = -(p_l - p_v) V_l + (\mu_l - \mu_v) N_l - (p_v - p_h) V + (\mu_v - \mu_h) N + \sigma A_s. \tag{7.12}$$

The metastable vapour can reasonably be treated as an ideal gas, both before and after the formation of the cluster. Thus we can use equation (1.40) to write

$$\mu_v - \mu_h = k_B T \ln\left(\frac{p_v}{p_h}\right) = k_B T \ln\left(1 + \frac{p_v - p_h}{p_h}\right). \tag{7.13}$$

Provided the cluster is small enough that the perturbations to the vapour due to its formation are small (that is, $p_v \approx p_h$), we can take only the first term in the expansion of $\ln(1+x)$ in powers of x, to give

$$\mu_v - \mu_h \approx k_B T \left(\frac{p_v - p_h}{p_h}\right) = (p_v - p_h)\frac{V}{N}, \tag{7.14}$$

where the second step follows from the ideal gas equation of state, (1.35). Thus, the third and fourth terms of equation (7.12) cancel one another, and we are left with

$$\Delta F = -(p_l - p_v) V_l + (\mu_l - \mu_v) N_l + \sigma A_s. \tag{7.15}$$

The pressure p_l and chemical potential μ_l of the liquid cluster will not have the same values as the pressure and chemical potential in the bulk equilibrium liquid (the liquid that would eventually appear in the final, mixed equilibrium state), which we will denote by p_l^{eq} and μ_l^{eq}, respectively. However, a relation between the two states can be found, in order to eliminate explicit reference to p_l and μ_l. We rewrite (7.15) as

$$\Delta F = -\left(p_l - p_l^{\mathrm{eq}}\right) V_l - \left(p_l^{\mathrm{eq}} - p_v\right) V_l + \left(\mu_l - \mu_v\right) N_l + \sigma A_s. \tag{7.16}$$

Thermodynamic integration of the Gibbs-Duhem relation (1.28) between the bulk equilibrium liquid state and the state of the liquid in the cluster, under the constraints that the temperature T and volume per particle v_l are held constant (the latter constraint implies that the liquid is incompressible, which is clearly an approximation), leads to the relation

$$p_l - p_l^{\mathrm{eq}} = n_l \left(\mu_l - \mu_l^{\mathrm{eq}}\right), \tag{7.17}$$

where we have used the fact that $v_l = 1/n_l$. Inserting (7.17) into (7.16), recalling that $n_l V_l = N_l$, and making the assumption that the vapour is perturbed only slightly by the formation of the cluster ($p_v \approx p_h$ and $\mu_v \approx \mu_h$), we find

$$\Delta F = -\left(p_l^{\mathrm{eq}} - p_h\right) V_l + \left(\mu_l^{\mathrm{eq}} - \mu_h\right) N_l + \sigma A_s. \tag{7.18}$$

Using the relation $f = \mu - pv$, which results from the definitions of the Helmholtz free energy and the chemical potential, equation (7.18) can be rewritten as

$$\Delta F = \left[f_l^{\mathrm{eq}} - f_h + p_h \left(v_l - v_h\right)\right] N_l + \sigma A_s. \tag{7.19}$$

Equation (7.19), together with (7.5), justifies the form for ΔF given in (7.1), with

$$\Delta f_b = f_l^{\mathrm{eq}} - f_h + p_h \left(v_l - v_h\right). \tag{7.20}$$

Figure 7.3 illustrates on an $f(v)$ diagram the physical plausibility of the above expression for Δf_b. The line BD is tangential to the analytic free energy curve at v_h. The length of line AE is equal to $f_l^{\mathrm{eq}} - f_h$, while the length of DE is equal to $-p_h \left(v_l - v_h\right)$ since p_h is $-\partial f / \partial v$ evaluated at B. So

$$\Delta f_b = |AE| - |DE|. \tag{7.21}$$

If an upward bulge, indicating phase coexistence, is present, Δf_b will clearly be negative; its magnitude will be the length of the line AD. The maximum value of the magnitude of Δf_b corresponds to the locally most negative value for $\partial f/\partial v$ (the local maximum of p), which is located at the spinodal. As B approaches C (the binodal), Δf_b will diminish; when B and C coincide ($v_h = v_v^{\mathrm{eq}}$), the tangents BD and AC will coincide, and $\Delta f_b = 0$. For $v_h > v_v^{\mathrm{eq}}$, Δf_b is positive, corresponding to a single phase equilibrium state. Finally, BD and AC will coincide also at the critical point, where the analytic free energy curve between A and C becomes a straight line. Δf_b is zero here, and becomes negative the other side of the critical point, where the equilibrium state is a single phase.

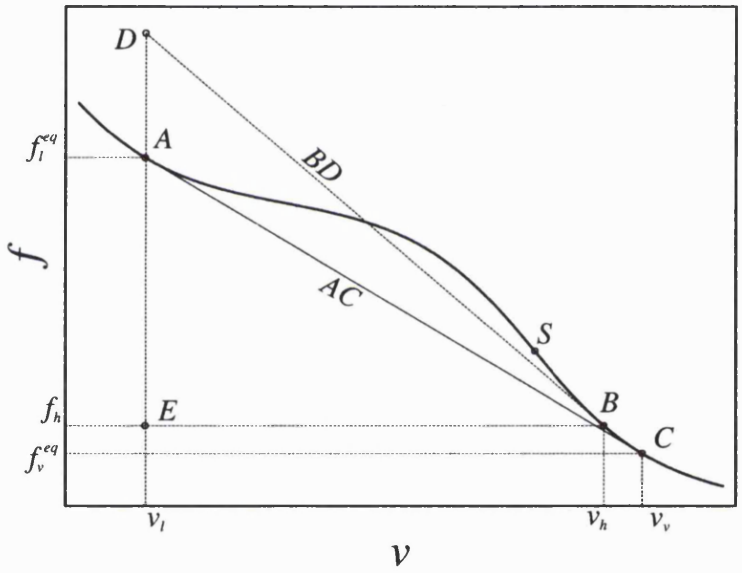

Figure 7.3: Graph of the free energy f per particle against the volume v per particle, illustrating the qualitative correctness of equation (7.20) for Δf_b.

Having justified the form of equation (7.1), we can use it to calculate the critical cluster size and work of formation within the classical approximation. The critical cluster is located at the maximum of $\Delta F(i)$, so

$$\left(\frac{\partial(\Delta F)}{\partial i}\right)_{i=i^*} = 0, \tag{7.22}$$

which leads to

$$i^* = -\frac{8}{27}\left(\frac{f_s}{\Delta f_b}\right)^3 \tag{7.23}$$

(recall that Δf_b is negative if the vapour is metastable) and therefore

$$\Delta F^* = \frac{4}{27}\frac{f_s^3}{(\Delta f_b)^2} = -\frac{1}{2}\Delta f_b i^*. \tag{7.24}$$

Inserting equation (7.5) produces

$$i^* = -\frac{32\pi}{3n_l^2}\left(\frac{\sigma}{\Delta f_b}\right)^3 \tag{7.25}$$

and

$$\Delta F^* = \frac{16\pi}{3n_l^2}\frac{\sigma^3}{(\Delta f_b)^2}. \tag{7.26}$$

7.4 The link with other formulations

A number of other expressions are used in the literature to calculate the critical work of formation. Therefore, it is important to compare the expression given in equations (7.18) and (7.19) for the Helmholtz free energy of formation of the cluster with an analogous expression using the grand potential, and also to consider the form of both these expressions when the homogeneous metastable vapour is close to the binodal ($p_h \approx p_v^{\text{eq}}$ and $\mu_h \approx \mu_v^{\text{eq}}$). Using equation (1.25) and the definition of the grand potential $\Omega = U - TS - \mu N$, we find, by an argument analogous to that applied to the Helmholtz free energy in the previous section,

$$\Delta\Omega = -\left(p_l - p_v\right)V_l - \left(p_v - p_h\right)V + \sigma A_s. \tag{7.27}$$

Following a similar line of development to that which produced (7.18) from (7.15), we find

$$\Delta\Omega = -\left(p_l^{\text{eq}} - p_h\right)V_l + \left(\mu_l^{\text{eq}} - \mu_l\right)N_l - \left(p_v - p_h\right)V + \sigma A_s. \tag{7.28}$$

These expressions have been calculated using the assumption that the total grand potential of a system is the sum of the grand potentials of the components of that system. As pointed out by Abraham [91], this assumption is only true of thermodynamic potentials if the intensive parameter which must be held constant in order for the thermodynamic potential to be a minimum at equilibrium, is constant across

the system. For the grand potential, this thermodynamic parameter is the chemical potential. This means that, unlike its analogue (7.18), equation (7.28) is only true for the critical cluster or other equilibrium situation. Remembering that under these conditions $\mu_l = \mu_v$, and assuming once again that $\mu_v \approx \mu_h$, we find

$$\Delta\Omega^* = -\left(p_l^{\mathrm{eq}} - p_h\right) V_l^* + \left(\mu_l^{\mathrm{eq}} - \mu_h\right) N_l^* + \left(p_v - p_h\right) V + \sigma A_s^*, \tag{7.29}$$

where the star denotes a value associated with the system containing a critical cluster.

The grand potential of formation is a valid expression for the work of formation only if the external chemical potential is held constant. Since the vapour is modelled as an ideal gas, this leads to the external pressure being held constant, so $p_v = p_h$. The result is that, for a critical cluster, equation (7.29) takes exactly the same form as equation (7.18). So, in the limit that negligible perturbation of the vapour results from the formation of the critical cluster in a closed system, either the Helmholtz free energy or the grand potential can be used to calculate the critical work of formation. That is to say, in this limit the closed system is equivalent to the open system, and either thermodynamic approach might be justified as an approximation to experimental conditions. However, the derivation of the equation for ΔF assumes only that the perturbation in the vapour is small, not that it is negligible. Since $V \gg V_l$, a small value for $p_v - p_h$ might still have a significant effect on the value of $\Delta\Omega$ given by (7.29), if it is applied to a closed system. This means that the limit in which the two approaches are equivalent might not exist in reality. Therefore, we shall use the Helmholtz free energy rather than the grand potential to calculate the work of formation.

Now consider equation (7.18) in the limit that the initial homogeneous metastable vapour is close to the binodal. Since $p_l^{\mathrm{eq}} = p_v^{\mathrm{eq}}$ and $\mu_l^{\mathrm{eq}} = \mu_v^{\mathrm{eq}}$, we have

$$\Delta F = -\left(p_v^{\mathrm{eq}} - p_h\right) V_l + \left(\mu_v^{\mathrm{eq}} - \mu_h\right) N_l + \sigma A_s. \tag{7.30}$$

Of course, both $p_v^{\mathrm{eq}} - p_h$ and $\mu_v^{\mathrm{eq}} - \mu_h$ go to zero at the binodal. Using the characteristics of an ideal gas expressed by equations (1.35) and (1.40), we can rewrite this as

$$\frac{\Delta F}{k_B T} = -\left(n_v^{\mathrm{eq}} - n_h\right) V_l + \ln\left(\frac{n_v^{\mathrm{eq}}}{n_h}\right) N_l + \sigma A_s$$

$$= \left[-\left(\frac{n_v^{\mathrm{eq}} - n_h}{n_h} \right) n_h + \ln \left(1 + \frac{n_v^{\mathrm{eq}} - n_h}{n_h} \right) n_l \right] V_l + \sigma A_s \qquad (7.31)$$

(where in the second stage we have used the fact that $N_l = n_l V_l$). For small x, $\ln(1+x) \approx x$, so near the binodal (7.31) becomes

$$\frac{\Delta F}{k_B T} = \left(\frac{n_v^{\mathrm{eq}} - n_h}{n_h} \right) (-n_h + n_l) V_l + \sigma A_s; \qquad (7.32)$$

since $n_l \gg n_h$, this leads to the disappearance of the term derived from the pV term in (7.30), and

$$\Delta F \approx \left(\mu_v^{\mathrm{eq}} - \mu_h \right) N_l + \sigma A_s. \qquad (7.33)$$

A similar development applied to (7.29) produces an expression for $\Delta\Omega^*$ which looks identical to that for ΔF provided that the vapour is negligibly perturbed by the formation of the critical cluster ($p_v = p_h$).

Expressions of the form (7.33) for the work of formation are often given in the literature [92, 93], which is why it is important to discuss the link between (7.33) and the expression for ΔF derived in the previous section. It is important to remember that (7.33) requires approximations which hold only close to the binodal; thus it can only be justified thermodynamically when the metastable vapour is close to the binodal. Deeper into the coexistence region, it leads to significant, though not catastrophic, errors in calculations for a colloidal system; however, the errors are generally assumed to be insignificant for simple molecular fluids, because pV terms are usually small in such condensed phases.

7.5 Calculation of excess energies from experimental data

In the next chapter, we shall introduce a method for calculating surface tension, and apply it to a colloidal system. First, however, we look at how the thermodynamic properties of the surface can be estimated using experimental results for the nucleation rate. In the absence of data for colloidal systems, we use nucleation data for simple fluids as an example: n-pentanol and dibutylphthalate (DBP). Such data are generally presented in terms of the supersaturation $S = p_h/p_v^{\mathrm{eq}}$, which is the ratio of the pressure of the metastable (supersaturated) vapour to that of the saturated (binodal) vapour.

These results have been published in the Journal of Chemical Physics [94, 95].

7.5.1 Nucleation theorems

The method for extracting details of the critical cluster from experimental data on the nucleation rate makes use of the two nucleation theorems, which relate the derivatives of the nucleation rate, with respect to supersaturation and temperature, to the size and excess energy, respectively, of the critical cluster. The first nucleation theorem [93] was introduced originally by Kashchiev; according to a more recent statistical mechanical derivation by Ford [96], it reads

$$\left(\frac{\partial \ln J}{\partial \ln S}\right)_T = 1 + i^*, \tag{7.34}$$

while the second nucleation theorem, which was derived by Ford [97, 96], is

$$\left(\frac{\partial \ln J}{\partial T}\right)_S = \frac{1}{k_B T^2}\left[L - k_B T + E_x(i^*)\right], \tag{7.35}$$

where L is the latent heat of condensation per molecule, and $E_x(i^*)$ is the excess energy of the critical cluster. The nucleation theorems in this form assume that the vapour can be described as an ideal gas. Corrections for nonideal effects have been derived [94], but their effect appears to be small.

7.5.2 Fitting the data

The two nucleation theorems allow us to calculate the size and excess energy of a critical cluster if we know the dependence of the nucleation rate on temperature and supersaturation. The most effective way to obtain this dependence from the experimental data is to fit a function $J(S,T)$ to the data. Then the derivatives $(\partial \ln J/\partial \ln S)_T$ and $(\partial \ln J/\partial T)_S$ can be used, in conjunction with the nucleation theorems, to produce expressions for i^*, the number of molecules in the critical cluster, and E_x^*, its excess energy; a relation between i^* and E_x^* follows from these expressions. We write E_x^* as shorthand for $E_x(i^*)$, the excess energy evaluated at size i^*.

We chose to fit the data with a function of the form

$$\ln J = a - \frac{b\,(c/T - 1)^3}{(\ln S)^2}, \tag{7.36}$$

where a, b and c are fitting parameters. This fitting function was motivated by the work of Hale [98, 99], who found that a phenomenological expression which took a form similar to this was surprisingly effective in correlating nucleation rates for a

variety of substances. We use it since it permits a better fit to the experimental data than other functions which we tried; in fact, given the scatter in the available data, a fitting function which is definitively better than this one seems unlikely to be identified.

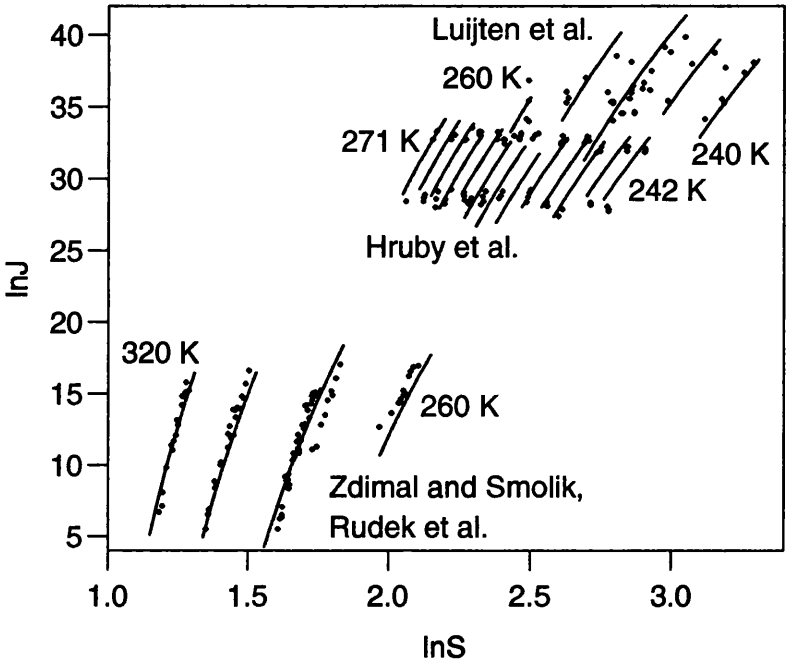

Figure 7.4: Comparison of experimental data for n-pentanol with the functions fitted to them. Dots: experimental data; lines: predictions for the fitting functions for $\ln J$ along isothermal lines corresponding to the experimental data. J has units of $\mathrm{m^{-3}s^{-1}}$.

Three sets of experimental data on the nucleation of n-pentanol were used. The data of Ždímal and Smolík [100] and of Rudek *et al.* [101] (which we regard as one set) were obtained using thermal diffusion cloud chambers, the data of Hrubý *et al.* [102] were collected using an expansion cloud chamber, and the data of Luijten *et al.* [103, 104] were gathered using the pulse expansion method. Collectively the sets of data cover a range of temperatures from 240 K to 320 K, supersaturations from 3.3 to 27, and resultant nucleation rates (in $\mathrm{m^{-3}s^{-1}}$) from 10^2 to 10^{17}. Table 7.1 shows the values of a, b and c for the three sets of data. Figure 7.4 demonstrates that equation (7.36), with the parameters as in table 7.1, provides a good fit to the data; the limitations of the fitting function are revealed by the fact that the fit is not perfect.

The data for DBP are from Mikheev *et al.* [95], and were obtained using a

Reference	a	b	c (K)
Hrubý *et al.* [102]	68.5	101	591
Ždímal and Smolík, Rudek *et al.* [100, 101]	54.4	16.1	830
Luijten *et al.* [103, 104]	76.5	394	485
Mikheev *et al.* (DBP) [95]	67.4	5730	490

Table 7.1: Values of the fitting parameters a, b and c for the sets of data on n-pentanol and DBP.

laminar flow tube reactor. The fitting parameters for this data are also shown in table 7.1; fig. 7.5 demonstrates that the resulting function fits the data well.

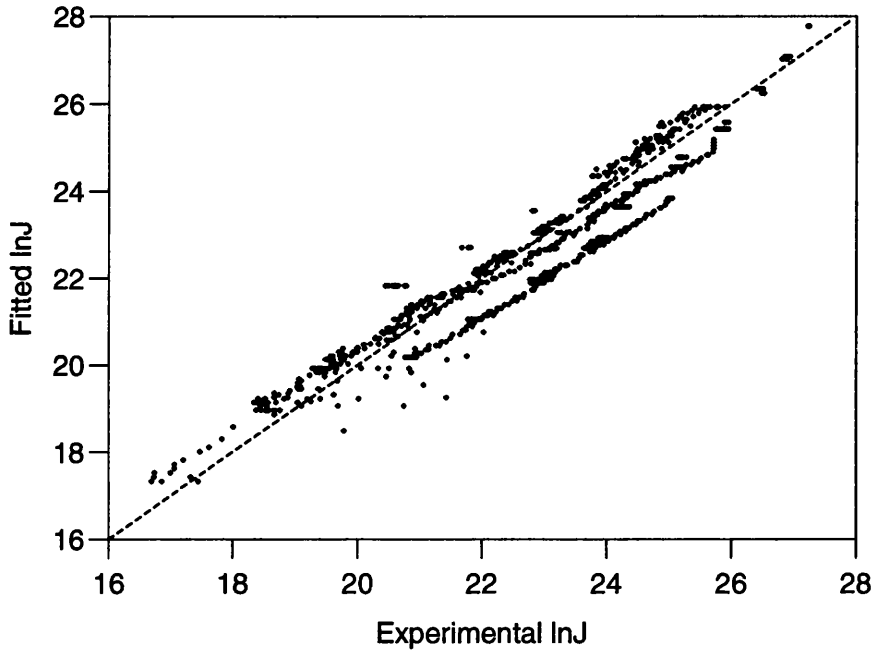

Figure 7.5: Evaluation of the success of the fitting function for DBP. The dots denote the experimental and fitted values of $\ln J$. The dashed line represents a perfect fit to the data. J has units of $\mathrm{m}^{-3}\mathrm{s}^{-1}$.

7.5.3 The energetics of critical clusters in n-pentanol and DBP

By finding the derivatives of equation (7.36) with respect to $\ln S$ and T and applying the two nucleation theorems, one can derive the following expressions for E_x^* and i^* in terms of S and T:

$$i^* = \frac{2b\,(c/T-1)^3}{(\ln S)^3} - 1, \tag{7.37}$$

$$E_x^* = \frac{3bck\,(c/T-1)^2}{(\ln S)^2} - L + k_B T. \tag{7.38}$$

We use these expressions to find a relation between i^* and E_x^*. Since both of these quantities are functions of S and T, there will not be a unique relation between them: we can write

$$E_x^* = f(S,T,\gamma)\,(1+i^*)^\gamma - L + k_B T, \tag{7.39}$$

and the relation between the critical cluster size and excess energy will depend on γ, which can take any value. However, since the excess energy is analogous to the surface energy of a macroscopic system, we expect $E_x^* \propto i^{*2/3}$ in the limit of a large critical cluster. Therefore we set $\gamma = 2/3$, which yields the expression

$$E_x^* = \frac{3b^{1/3}ck}{2^{2/3}}\,(1+i^*)^{2/3} - L + k_B T. \tag{7.40}$$

The latent heat of condensation per molecule, L, can be calculated using the Clausius-Clapeyron equation, together with an empirical expression for the saturation vapour pressure p_s as a function of temperature. For n-pentanol, we use [105]

$$p_s = 133.324 \exp(90.08 - 9788/T - 9.90 \ln T), \tag{7.41}$$

where the pressure is expressed in Pa and the temperature T in K; therefore the latent heat is given by

$$L = 9788 k_B - 9.90 k_B T. \tag{7.42}$$

The equivalent empirical expression for DBP is [95]

$$L = 3836 k_B T + 2522000 k_B / T. \tag{7.43}$$

Figures 7.6 and 7.7 show the curves of E_x^* as a function of i^* (in units of $k_B T_0$, where $T_0 = 273.15$ K) which were produced from each of the sets of data. It should be noted that these $E_x^*(i^*)$ curves are not very sensitive to small changes in the fitting function.

A comparison is also made with the results of classical nucleation theory, for which we use the following formula for the nucleation rate, based on the original classical rate modified [96] by a factor of n_l/n to take account of the positional

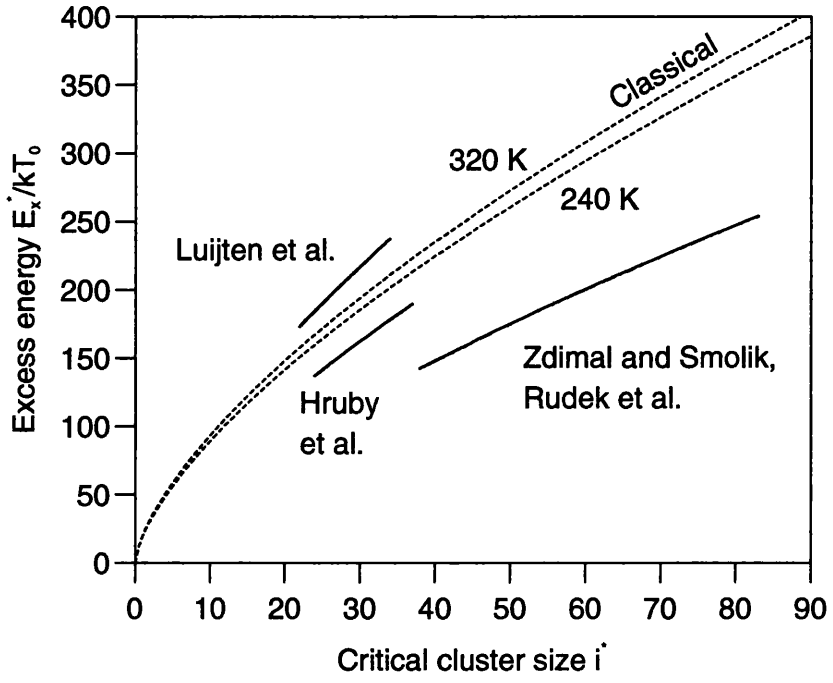

Figure 7.6: The excess energy of critical clusters of n-pentanol as a function of critical cluster size. Solid lines: calculations from the experimental data, each valid within the range of (S, T) values covered by its respective data set. Dashed lines: predictions of classical nucleation theory.

entropy of a cluster,

$$\ln J_{cl} = \ln\left(\sqrt{\frac{2\sigma}{\pi m}}\frac{Sp_s}{k_BT}\right) - \frac{16\pi}{3}\frac{\sigma^3}{n_l^2\left(k_BT\right)^3\left(\ln S\right)^2}, \tag{7.44}$$

where σ is the surface tension, m the mass of a molecule, and p_s the saturated vapour pressure (the vapour pressure at the binodal). Combining this with the two nucleation theorems and the Clausius-Clapeyron equation, we find

$$E_{xcl}^* = k_BT^2\left[\frac{1}{2\sigma}\frac{d\sigma}{dT} - \frac{(36\pi)^{1/3}}{3}\left(\frac{3}{\sigma}\frac{d\sigma}{dT} - \frac{2}{n_l}\frac{dn_l}{dT} - \frac{3}{T}\right)\frac{\sigma}{k_BTn_l^{2/3}}i^{*2/3}\right], \tag{7.45}$$

where E_{xcl}^* represents the classical excess energy evaluated at the classical critical size i_{cl}^*. For the temperature dependence of σ (in Jm^{-2}) and of the liquid molecular density n_l (in m^{-3}), we use the following correlations for n-pentanol [101]:

$$\sigma = 10^{-3}\left[26.85469 - 0.07889\left(T - 273.15\right)\right], \tag{7.46}$$

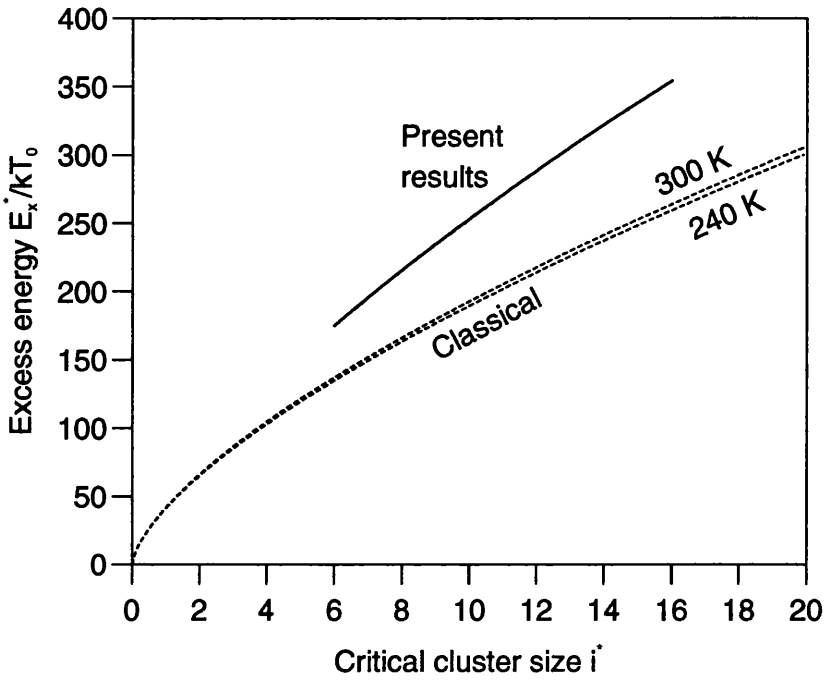

Figure 7.7: The excess energy of critical clusters of DBP as a function of critical cluster size. Solid line: calculations from the experimental data, valid within the range of (S, T) values covered by the data set. Dashed lines: predictions of classical nucleation theory.

$$n_l = 10^3 N_A \left(3.06 + 21.90Z^{1/3} - 95.46Z^{2/3} + 218.1Z - 210.5Z^{4/3} + 74.37Z^{5/3}\right), \tag{7.47}$$

where N_A is Avogadro's number and $Z = 1 - T/T_c$; the critical temperature T_c is taken to be 588.15 K. The equivalent correlations for DBP are [95]:

$$\sigma = 0.03393 - 0.0000894\,(T - 293.15)\,, \tag{7.48}$$

$$n_l = \frac{10^6 N_A}{278}\,[1.0492 - 0.00067\,(T - 293.15)]\,, \tag{7.49}$$

where we have used the fact that the molecular mass number of DBP is 278.

The critical clusters in DBP are remarkably small, containing as few as six molecules, and there is no reason to expect them to be described by classical nucleation theory. It appears that the excess energies of the clusters can be well described by regarding the latent heat L as resulting from bonds between nearest neighbours and estimating how many dangling bonds are present at the surface of the cluster [95].

Figures 7.8 and 7.9 show the critical cluster size and the excess energy as func-

tions of S and T, calculated from the n-pentanol data of Zdimal and Smolik and of Rudek *et al.* and covering the region of the (S,T) plane investigated by them. Similar plots could be produced for the other sets of data.

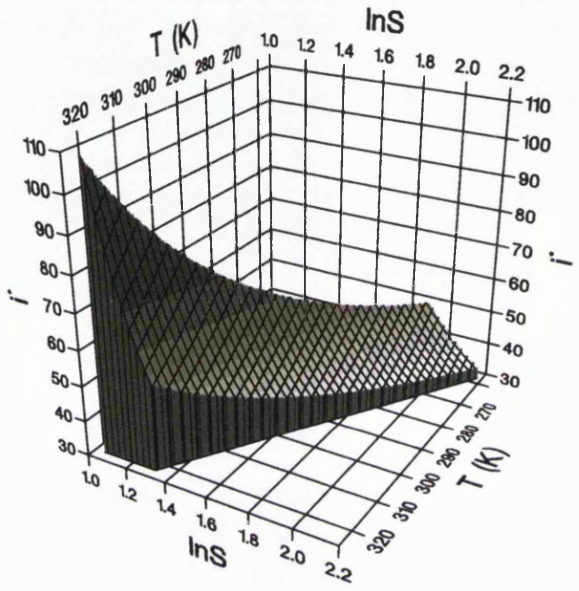

Figure 7.8: The critical cluster size as a function of temperature and supersaturation, calculated from the data of Zdimal and Smolik and of Rudek *et al.* and valid within the (S,T) range covered by those data.

It is notable that equation (7.36), unlike an arbitrary function $J(S,T)$, leads to a situation where, if we set γ equal to $2/3$ on the physical grounds mentioned above, the first and most significant term in equation (7.39) does not depend on the supersaturation or temperature other than through i^*; that is, $f(S,T,2/3)$ is actually independent of S and T. This means that, if the less significant $-L+k_BT$ term is disregarded, there is a one to one correspondence between the number of molecules in a critical cluster and its excess energy. A given i^* will always be associated with the same E_x^*, irrespective of the values of S and T which produced it. If γ were set to a different value, this would still be true, but the point would be obscured by the appearance of explicit T- and S-dependence in E_x^*. (It is useful to bear in mind that we are seeking information on the excess energy $E_x(T,S,i)$ for a general cluster size i, given data on $E_x^*(T,S,i^*(T,S))$ for a T- and S-dependent critical size i^*. The value of γ determines how much of the T- and S-dependence is explicitly present in the expression for E_x^*, and how much is locked up in i^*.)

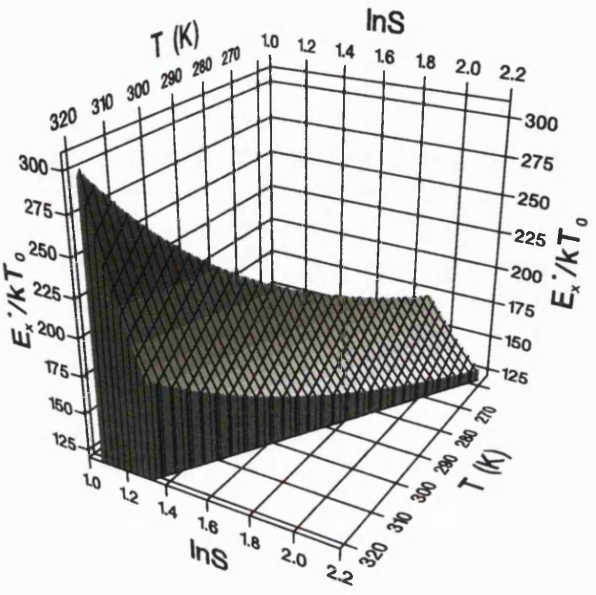

Figure 7.9: The excess energy as a function of temperature and supersaturation, calculated from the data of Zdimal and Smolik and of Rudek *et al.* and valid within the (S,T) range covered by those data.

The fact that the Hale function can be made to fit the experimental data shows that, over the small region of the (S,T) plane which is covered by a single set of experimental measurements, this one to one correspondence between i^* and E_x^* is approximately correct. From a physical point of view, too, we would expect this to be the case, since the excess energy is closely related to the number of dangling bonds on the surface of a cluster. This depends on the number of molecules in the cluster, but not strongly on the temperature or pressure (provided the cluster is compact, which it is at temperatures well below the critical temperature).

In general, however, the correspondence does not hold. This is demonstrated by the inconsistency between the three different $E_x^*(i^*)$ curves in figure 7.6, which use sets of data from different regions of the (S,T) plane.

These excess energy curves, then, should be regarded as approximations which are valid on restricted regions of the (S,T) plane. Without such an approximation, it would be hard to produce a graph such as figure 7.5. Introducing the approximation enables us to gain insight into the energetics of the critical cluster.

Chapter 8

Interfaces and nucleation in charged colloidal suspensions

8.1 Introduction

In this chapter, we apply the principles of nucleation which were detailed in chapter 7 to phase transitions in the type of colloidal system that was introduced in earlier chapters. There are a number of reasons for doing this. Experiments by Yoshida *et al.* [4] have investigated the evolution of a suspension from an initial homogeneous state to a phase separated final state. It should be possible to explain the resulting 'Swiss Cheese' structure in terms of surface free energies and nucleation; it is clear, then, that the thermodynamic effects of phase boundaries in these systems can be observed and are therefore worthy of theoretical investigation. There is also the possibility that insights gained from the consideration of nucleation events in colloidal systems could benefit the study of nucleation processes in general, and of nucleation processes in molecular systems in particular. It has often been pointed out that colloidal crystals provide a good model system for atomic matter, as similar processes take place at larger length scales and longer time scales. Nucleation in colloidal systems happens more slowly and on a larger length scale than in molecular systems, where the fast rate of the phase transition and the unobservable size of the critical cluster make the phenomenon very difficult to investigate accurately, either by experiment or by theory. Another problem with the study of homogeneous nucleation in molecular systems is that it may be preempted by heterogeneous nucleation, the process by which the new phase nucleates around foreign bodies or on the walls of the container. The larger length scales in colloidal systems should make heterogeneous nucleation less of a problem: sufficiently large impurities are unlikely to be present in the bulk of a suspension, while the container walls may or may not

act as sites for heterogeneous nucleation (depending on whether the free energy of the interface between the metastable phase and the wall is smaller or larger than that of the interface between the metastable phase and the nucleating phase).

The next section of the current chapter will introduce a simple approximate method by which the free energy of an interface can be calculated. Then we shall set out the results of applying the method to calculate the surface tension in a charged colloidal suspension under conditions of zero added salt, and the nucleation rate of a liquid cluster from a metastable vapour in the same system. The final part of the chapter discusses the 'Swiss Cheese effect' in the context of nucleation theory.

8.2 The square gradient approximation

We shall now outline a method by which the free energy cost of forming a surface between two phases of a fluid can be calculated, if we know the characteristics of the fluid and the phases, using the ideas of density functional theory. Known as the square gradient approximation [106], the method originated with van der Waals and was rederived by Cahn and Hilliard [107]. Along with more sophisticated density functional theories [108], it has often been applied to molecular systems, and recently it has been applied by Brader and Evans [109] to a colloid-polymer mixture.

Consider a system containing two phases α and β, separated by an interface. The system has total Helmholtz free energy F; the volumes of the phases are expressed as V^α and V^β and the free energy densities as ρ_F^α and ρ_F^β. The excess free energy F^x is defined as the difference between the free energy of a system and the value which the free energy would take if the system contained the two homogeneous phases and an idealised, infinitesimally thin boundary with no free energy of its own:

$$F^x = F - \rho_F^\alpha V^\alpha - \rho_F^\beta V^\beta. \tag{8.1}$$

If we use the Gibbs dividing surface, $F^x = \sigma A_s$, where A_s is the area of the surface. The surface tension σ can be found by

$$\sigma = \int_{-\infty}^{\infty} \rho_F^x(z) dz, \tag{8.2}$$

where $\rho_F^x(z)$ is the density in space of the excess Helmholtz free energy and z is the distance measured perpendicular to the surface, which is considered here to be planar and to be homogeneous except in the z-direction.

The basic idea of classical density functional theory (DFT), as applied to this problem, is to choose a physically plausible form for the excess free energy density

$\rho_F^x[n(z)]$ as a functional of the particle density profile $n(z)$ and then to minimise the total excess free energy density $F^x = A_s \int_{-\infty}^{\infty} \rho_F^x[n(z)]dz$, for given α and β, with respect to $n(z)$ to find the 'true' physical particle density profile $n_{phys}(z)$ between phases α and β. The 'true' excess free energy density will then be $\rho_F^x[n_{phys}(z)]$. The accuracy of the results depends, of course, on the form of the excess free energy density being well chosen.

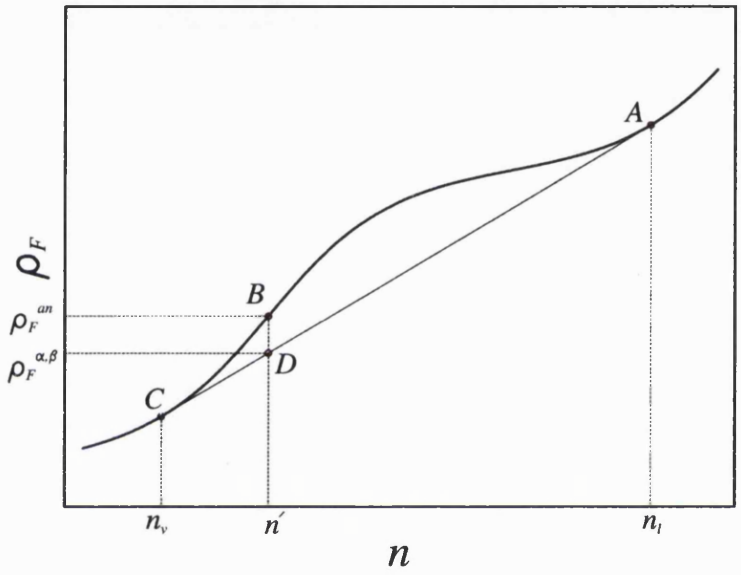

Figure 8.1: Graph of free energy density ρ_F against particle density n, illustrating the components of the free energy density in the point thermodynamic approximation.

Here, the main aim is to calculate the surface tension rather than the details of the interfacial structure. A form for $\rho_F^x(z)$ needs to be chosen. A first approximation might be that the free energy density $\rho_F(z)$ at a point in the interfacial region where the particle density is n' is the same as that in a homogeneous phase of density n'. This is known as the local density or point-thermodynamic approximation, and amounts to assuming that local inhomogeneities have no effect on the free energy, which is therefore a function only of the local density. It leads to

$$\rho_F^x(z) = \rho_F^{an}(z) - \rho_F^{\alpha,\beta}, \tag{8.3}$$

where $\rho_F^{an}(z)$ is the free energy density calculated by analytic extension of the $\rho_F(n)$ curve into the metastable region and $\rho_F^{\alpha,\beta}$ is the free energy density resulting from

the mixture of homogeneous states α and β, ignoring the effects of the interface. Figure 8.1 illustrates the situation on the $\rho_F(n)$ diagram: ρ_F^{an} is on the upward bulge, while $\rho_F^{\alpha,\beta}$ is on the tie line. Unfortunately, if the two phases are separated by a step function interface the local density approximation gives zero excess free energy (since the width of the interface can be taken to zero while ρ_F^x remains finite despite the fact that $|\partial n/\partial z| \to \infty$, as ρ_F^x does not depend on the gradient), and this is the result which will be produced by the minimisation procedure. Equation (8.3) is clearly an unphysical form for $\rho_F^x(z)$: a term needs to be added to take account of the effects of the local inhomogeneity.

Van der Waals added a term proportional to the square of the density gradient:

$$\rho_F^x(z) = \rho_F^{an}(z) - \rho_F^{\alpha,\beta} + C(n)\left(\frac{\partial n}{\partial z}\right)^2. \tag{8.4}$$

The extra term is to be regarded as the next in an expansion in terms of the derivatives of the density; (8.4) is thus strictly valid only for small gradients. The parameter C should be independent of $\partial n/\partial z$ and higher derivatives.

In this square gradient approximation, the total free energy density $\rho_F(z) = \rho_F^x(z) + \rho_F^{\alpha,\beta}$ is given by

$$\rho_F(z) = \rho_F^{an}(z) + C(n)\left(\frac{\partial n}{\partial z}\right)^2. \tag{8.5}$$

Consequently, if $\rho_F(z)$ and $\rho_F^{an}(z)$ can be calculated, we can find $C(n)$ using

$$C(n) = \frac{\rho_F(n) - \rho_F^{an}(n)}{(\partial n/\partial z)^2}. \tag{8.6}$$

The Euler-Lagrange equation which minimises the integral in equation (8.2), where $\rho_F^x(z)$ is given by (8.4), is

$$2C(n)\frac{d^2n}{dz^2} + \frac{dC}{dn}\left(\frac{dn}{dz}\right)^2 - \frac{d}{dn}\left(\rho_F^{an}(z) - \rho_F^{\alpha,\beta}\right) = 0, \tag{8.7}$$

of which a first integral is

$$\rho_F^{an}(z) - \rho_F^{\alpha,\beta} = C(n)\left(\frac{\partial n}{\partial z}\right)^2. \tag{8.8}$$

Substituting (8.8) and (8.4) into equation (8.2) for σ gives

$$\sigma = 2\int_{-\infty}^{\infty} C(n)\left(\frac{\partial n}{\partial z}\right)^2 dz$$

$$= 2\int_{n^\alpha}^{n^\beta} C(n)\frac{\partial n}{\partial z} dn$$

$$= 2\int_{n^\alpha}^{n^\beta} \left[(C(n))^2\left(\frac{\partial n}{\partial z}\right)^2\right]^{1/2} dn. \tag{8.9}$$

Further application of equation (8.8) to (8.9) results in

$$\sigma = 2\int_{n^\alpha}^{n^\beta} \left[C(n)\left(\rho_F^{an} - \rho_F^{\alpha,\beta}\right)\right]^{1/2} dn. \tag{8.10}$$

The value of equation (8.10) is that it permits calculation of the surface tension without explicit calculation or consideration of the particle density profile, or even of the density gradient, in the interface [106]. All we need is the coefficient $C(n)$ in the gradient expansion (8.4).

8.3 Application to colloidal suspensions

In order to calculate the surface tension in a colloidal suspension, we first calculate $C(n)$ at different densities, using equation (8.6). At each density n', this requires the calculation of $\rho_F(n')$ and of $\rho_F^{an}(n')$. The analytic free energy density ρ_F^{an} is simply the free energy density in a homogeneous phase of particle density n'; therefore it can be evaluated with equations (3.74) and (3.78). The procedure for the evaluation of the total free energy ρ_F is more complicated: equations (3.74) and (3.78) must be applied in a modified way.

The results produced by these equations depend both on the microion density through the parameter κa (and hence on the macroion density by the charge neutrality principle) and on the macroion separations S_{mn}. In the homogeneous system, we approximate the macroion distribution by a crystalline structure (simple cubic for the calculations in the current chapter), and the separations between nearest neighbours, next nearest neighbours, and so on, can easily be related to κa. All macroions are regarded as equivalent, in the sense that the macroion density is a constant throughout the region; figure 8.2 illustrates this situation schematically. The procedure for calculating the electrostatic free energy per macroion is to choose one macroion (marked m) and sum over the contributions from its neighbours. Every

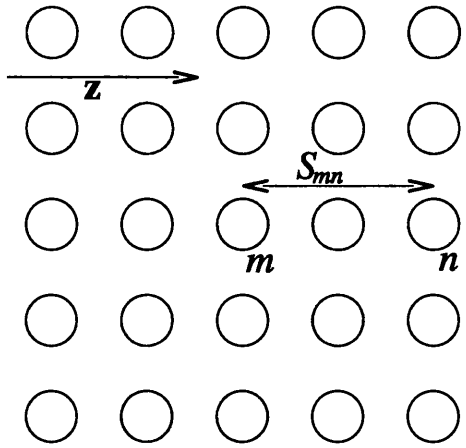

Figure 8.2: Schematic of the macroion configuration used in this chapter in the calculation of the electrostatic free energy of the homogeneous system.

macroion in the phase can then be regarded as equivalent to this 'test' macroion.

For the inhomogeneous system, we consider a lattice as in figure 8.3, with the particle separation varying in one direction notated as **z**, where **z** is to be interpreted as perpendicular to the surface. This is not intended to be a realistic representation of the interface: it is simply a device to enable us to evaluate the effect of a density gradient on the free energy of the test macroion m. The macroion separations are determined by considering each macroion n to lie at the centre of a cuboidal cell, and to associate a density $n_n = 1/V_n$ with the macroion, where V_n is the volume of the cell. Let the length of those sides of cell n that lie parallel to **z** be equal to s_n. Other sides of the cell have length s_m, where s_m is the side length of the cubic cell around the test macroion m. The density at n can then be expressed as

$$n_n = \frac{1}{s_m^2 s_n}. \tag{8.11}$$

The density gradient enters the model as a constant K. This does not mean that the density gradient is constant throughout the interface, only that it is possible to define a density gradient which is valid in the vicinity of macroion m. The density as a function of distance z perpendicular to the interface is thus given by

$$n(z) = n_n + K\,(z - z_n)\,, \tag{8.12}$$

where z_n is the value of z at some macroion n. This density has physical meaning only at the points occupied by the macroions, and we write

$$n_q = n_n + K\,(z_q - z_n)\,, \tag{8.13}$$

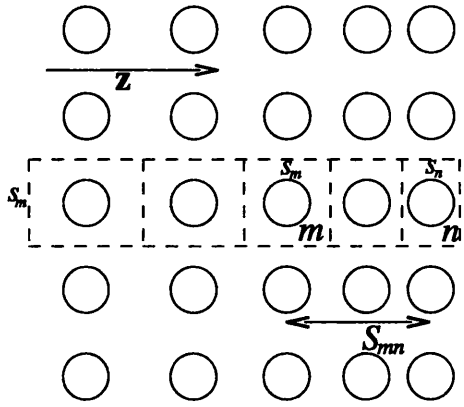

Figure 8.3: Schematic of the macroion configuration used in the calculation of the electrostatic free energy of the inhomogeneous system.

where z_q is the z-coordinate of macroion q. Recalling that $n_q = 1/(s_m^2 s_q)$, we rewrite (8.13) to give

$$n_n + K(z_q - z_n) - \frac{1}{s_m^2 s_q} = 0. \tag{8.14}$$

If q and n are next door neighbours in the z-direction, their separation can be found using (8.14). There are two possible cases here. If $q = n+1$, that is $z_q > z_n$, corresponding to $n_q > n_n$ for $K > 0$, we have $z_{n+1} - z_n = (s_n + s_{n+1})/2$, which leads to $s_{n+1} = 2(z_{n+1} - z_n) - s_n$. Then (8.14) is transformed into

$$n_n + K z_{n,n+1} - \frac{1}{s_m^2 (2z_{n,n+1} - s_n)} = 0, \tag{8.15}$$

where $z_{n,n+1} = z_{n+1} - z_n$. This leads on to a quadratic for $z_{n,n+1}$ in terms of the densities and the gradient:

$$z_{n,n+1}^2 + \left(\frac{n_n}{K} - \frac{n_m^{2/3}}{2n_n}\right) z_{n,n+1} - \frac{n_m^{2/3}}{K} = 0. \tag{8.16}$$

Here, we have used equation (8.11) to find $s_m = 1/n_m^{1/3}$ and $s_n = n_m^{2/3}/n_n$. The physically significant solution of (8.16) is

$$z_{n,n+1} = \frac{1}{2}\left\{\frac{n_m^{2/3}}{2n_n} - \frac{n_n}{K} + \sqrt{\left(\frac{n_m^{2/3}}{2n_n} - \frac{n_n}{K}\right)^2 + \frac{4n_m^{2/3}}{K}}\right\}. \tag{8.17}$$

The second case is $q = n - 1$, that is $z_q < z_n$, which corresponds to $n_q < n_n$ for $K > 0$. Then $z_{n,n-1} = -(s_n + s_{n-1})/2$ and $s_{n-1} = -2z_{n,n-1} - s_n$. The quadratic

equation in $z_{n,n-1}$ is

$$z_{n,n-1}^2 + \left(\frac{n_n}{K} + \frac{n_m^{2/3}}{2n_n} \right) z_{n,n-1} + \frac{n_m^{2/3}}{K} = 0, \tag{8.18}$$

the physically significant solution of which is

$$z_{n,n-1} = -\frac{1}{2} \left\{ \frac{n_m^{2/3}}{2n_n} + \frac{n_n}{K} - \sqrt{\left(\frac{n_m^{2/3}}{2n_n} + \frac{n_n}{K} \right)^2 - \frac{4n_m^{2/3}}{K}} \right\}. \tag{8.19}$$

We can calculate the macroion separations which satisfy equations (8.11) and (8.13) by starting from the 'test' macroion m and moving outward, repeatedly applying (8.17) or (8.19) depending on the direction in which we are travelling. This allows us to find macroion separations S_{mn} for the inhomogeneous system, and these separations can be used in equations (3.74) and (3.78), which involve sums over macroions n, to estimate the electrostatic free energy per macroion in an inhomogeneous system. The local microion density, which is required for the calculation of κa, is assumed to take the same value as it would in a homogeneous system of the same macroion density. One consequence of this assumption is that the only change which the inhomogeneous system requires in the calculation of f_{el} is in the macroion separations S_{mn}. As the density gradients are required to be small for the square gradient approximation to be valid, we take the ideal gas contribution f_0 to the free energy, as given by equation (4.5) to have the same value in the inhomogeneous system as in a homogeneous system.

An alternative choice for the local microion density, in those parts of the free energy which depend on the separation S_{mn} of pairs of macroions, would be the mean of the densities at m and n. It is not clear, in the context of this simple model, whether this alternative choice would be better or worse. However, it would be slightly more complicated: it would require two different values for κa, because contributions to the free energy which do not depend on S_{mn} would still require κa to be defined as described above. Therefore, we do not choose this alternative.

The difference which appears in the numerator of equation (8.6) for C can be expressed as a difference in electrostatic free energy contributions:

$$\rho_F(n) - \rho_F^{an}(n) = n \left(f_{el}(n, K) - f_{el}^{an}(n) \right), \tag{8.20}$$

where f_{el} is the electrostatic free energy per macroion in the inhomogeneous system, calculated using equations (3.74) and (3.78) as detailed above, and f_{el}^{an} is the elec-

trostatic free energy per macroion in a homogeneous system at the same density. According to the square gradient approximation, the calculated value of C should be a function of the density n, but should not depend on the density gradient $\partial n/\partial z$ at a given value of n. Of course, this is only true for small $\partial n/\partial z$, as the square gradient approximation is not expected to be valid in a system with a large density gradient.

Having calculated C numerically as a function of density, we can insert it into equation (8.10); the integral can then be performed numerically in order to evaluate the surface tension. This procedure also requires the calculation of $\rho_F^{\alpha,\beta}$, which can be found using the geometry of figure 8.1. Since the state on the bulge and the state on the tie line have the same macroion density, the ideal gas contributions to the free energy of the two states can be regarded as equal. Therefore,

$$\rho_F^{an} - \rho_F^{\alpha,\beta} = n\left[f_{el}^{an}(n) - \left(\frac{n^\beta - n}{n^\beta - n^\alpha}\right) f_{el}^\alpha - \left(\frac{n - n^\alpha}{n^\beta - n^\alpha}\right) f_{el}^\beta\right], \tag{8.21}$$

where f_{el}^α and f_{el}^β are the electrostatic free energies per macroion in homogeneous systems of densities n^α and n^β.

8.4 The surface tension

We find that the following relation holds for the surface tensions calculated under conditions of zero added salt:

$$\sigma(C\,|Z|\,, Ca) = \frac{1}{C}\sigma(|Z|\,, a), \tag{8.22}$$

where C is an arbitrary constant. This means that σ, if expressed in units proportional to $|Z|\,/a^2$, depends only on the ratio $\zeta = |Z|\,/a$ (we use a expressed in nm for the purpose of the definition of ζ) and not on $|Z|$ or a individually. Figure 8.4 shows the calculated surface tension σ, as a function of volume fraction η, for an interface around a liquid drop whose density is equal to that of the equilibrium liquid and which is surrounded by metastable vapour. The surface tension is expressed in units of $|Z|\,k_BT/1000a^2$. The domain of the calculations spans the metastable region between the binodal (low η) and the spinodal (high η); the surface tension of the interface between the liquid and the equilibrium vapour is at the binodal end of the lines. Because of equation (4.7), the end points of the lines depend only on ζ.

The dependence of σ on η is weak; the vapour is always much less dense than the liquid, so that small changes in the vapour density have little effect on the difference

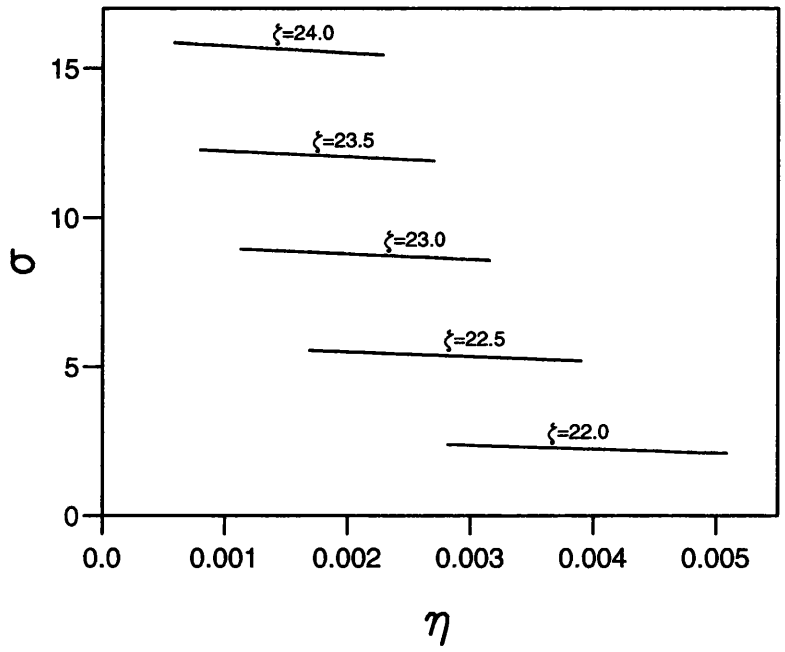

Figure 8.4: Surface tension σ, expressed in units of $|Z|\, k_B T/1000a^2$, as a function of the volume fraction η of the metastable vapour, for various values of ζ under conditions of zero added salt. The range of values of η spans the binodal-spinodal range.

in density between the two phases, and therefore little effect on the nature of the interface. Figure 8.4 makes it clear that, at fixed colloid radius, the surface tension increases with charge Z, and therefore diminishes as the critical point is approached, and that σ increases with decreasing macroion radius at fixed charge.

If the macroions have a radius of 50 nm, the actual values of the surface tension are of the order of 10^{-5} Jm^{-2}, which is several orders of magnitude smaller than the surface tensions encountered in molecular fluids ($\sim 10^{-2}$ Jm^{-2}), but closer to, although somewhat larger than, the figures calculated for colloid-polymer mixtures by Brader and Evans [109] ($\sim 10^{-6} - 10^{-5}$ Jm^{-2}). Experimental and theoretical results [110] for solid-liquid interfaces in hard sphere systems suggest a figure of around 10^{-7} Jm^{-2} for hard spheres of diameter 100 nm. Larsen and Grier [27] used their observations of metastable colloidal crystallites to estimate a lower limit of $\sim 10^{-8}$ Jm^{-2} for charged colloidal particles of radius 326 nm. Our results for $\zeta = 22.0$ suggest a figure of around 5×10^{-7} Jm^{-2} for macroions of this radius, so the Larsen and Grier experiments may have been undertaken very close to the critical point ($\zeta < 22$).

8.5 Modification of classical nucleation theory

Examination of the classical expressions for i^* and ΔF^* given in equation (7.24) reveals a problem: since both Δf_b and i^* are nonzero at the spinodal, ΔF^* will also be nonzero here, which disagrees with results from density functional theory [111, 112]. Intuitively, also, ΔF^* should go to zero at the spinodal, since the vapour at this point should be unstable against arbitrarily small density fluctuations. It is not surprising that classical nucleation theory is unreliable, since a liquid cluster containing only a small number of particles does not really resemble a macroscopic droplet with a well-defined surface. We shall apply a simple phenomenological correction which is due to McGraw and Laaksonen [113] and to Talanquer [?]. This assumes that, while i^* continues to be expressed by equation (7.23), ΔF^* contains a correction term which depends only on the temperature:

$$\Delta F^* = -\frac{1}{2}\Delta f_b i^* + D(T). \tag{8.23}$$

The correction term $D(T)$ is evaluated by requiring that ΔF^* vanishes at the spinodal, which gives

$$D(T) = \frac{1}{2}\Delta f_b^{sp} i^{*sp}, \tag{8.24}$$

where Δf_b^{sp} and i^{*sp} are equal to Δf_b and the critical cluster size, respectively, evaluated at the spinodal. Thus, the corrected expression for the critical work of formation is

$$\Delta F^* = -\frac{1}{2}\left(\Delta f_b i^* - \Delta f_b^{sp} i^{*sp}\right). \tag{8.25}$$

In the next section we shall use (8.25) to calculate some nucleation rates in colloidal systems.

8.6 Nucleation in colloidal systems

When the dependence of the surface tension on the densities of the phases is known, we can calculate the critical size of a liquidlike cluster using equation (7.23) and the work of formation of the critical cluster using (8.25). Figures 8.5 and 8.6 show the variation of the critical size as a function of colloid volume fraction (and therefore of 'distance' into the metastable region) for macroions of radius $a = 50$ nm and various surface charges. Figure 8.6 is a magnification of figure 8.5. The critical size is infinite at the binodal, and falls rapidly as we move further into the metastable region. The critical size also increases as the macroion charge decreases towards the

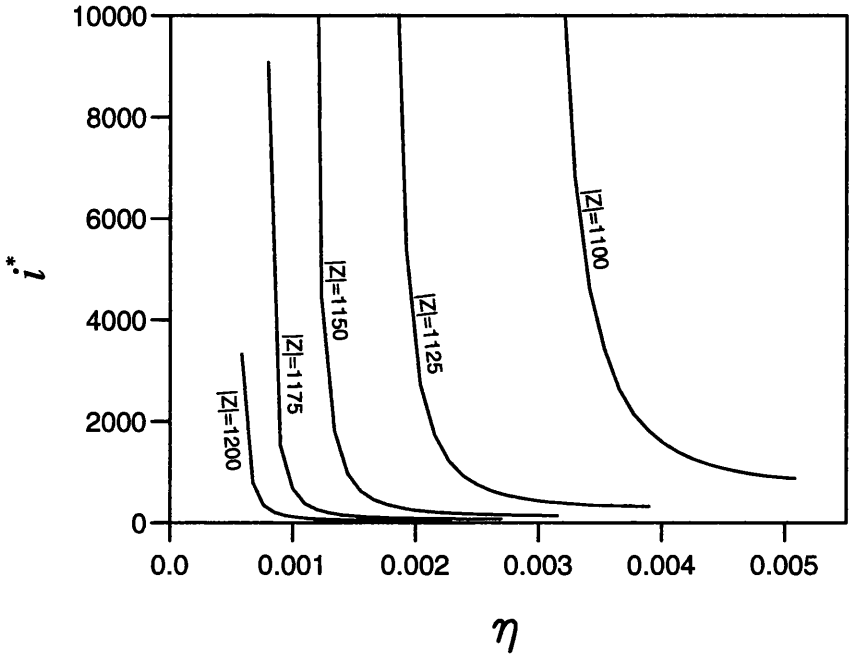

Figure 8.5: Critical cluster size i^* as a function of the volume fraction of the metastable vapour, for colloidal particles of radius $a = 50$ nm under conditions of zero added salt.

critical point ($|Z| = 1070$). This is in line with the results of a recent investigation of the critical size at the approach to the spinodal in molecular systems by Anisimov *et al.* [115].

Figures 8.7 and 8.8 show the barrier to nucleation of the critical cluster (figure 8.8 is a magnification of figure 8.7). The barrier is infinite at the binodal, and falls steeply as we move further into the metastable region, reaching zero at the spinodal. Of course, we have modified classical nucleation theory to ensure that the barrier is zero at the spinodal; otherwise, it could easily be of the order $10^2 - 10^3\ k_BT$.

The calculated nucleation rate (number of critical clusters formed per second) is illustrated in figure 8.9. This uses the nucleation rate from equation (7.2), where ΔF^* is given by equation (8.25) and the prefactor J_0 comes from classical nucleation theory [116]:

$$J_0 = \sqrt{\frac{2\sigma}{\pi m}} \frac{n_h^2}{n_l}, \tag{8.26}$$

where n_h and n_l are the number densities of particles in the homogeneous metastable vapour and the liquid state, respectively, and the mass m of a particle is calculated by assuming the colloidal particles to have the same density as water. Like the

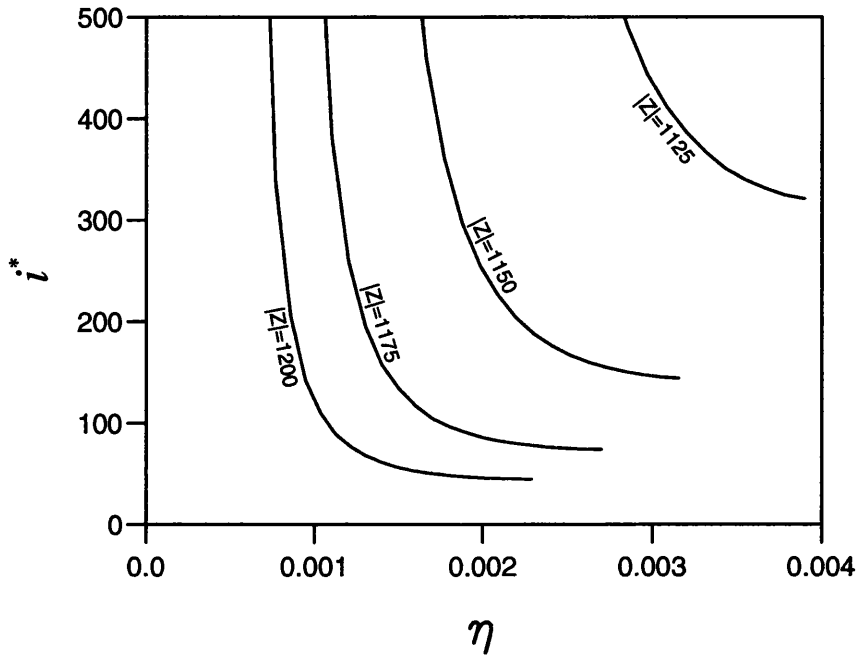

Figure 8.6: Critical cluster size i^* as a function of the volume fraction of the metastable vapour, for colloidal particles of radius $a = 50$ nm under conditions of zero added salt.

work of formation, the homogeneous nucleation rate depends very steeply on the location within the metastable region of the homogeneous system prior to phase separation. In most of the metastable region, the nucleation rate is so small that the process would not occur on an observable timescale. It is only in a small region that nucleation rates are in the vicinity of $\ln J = 0$, allowing the progress of the nucleation process to be observed as it was (for crystals nucleating from a metastable fluid and voids nucleating from a metastable crystal) by Yoshida *et al.* For $|Z| = 1100$ the critical cluster size when $\ln J \approx 0$ is of the order of 10^3, which is large enough for the assumptions underlying classical nucleation theory to be reasonable. For $|Z| = 1200$, this critical cluster size is of the order of 50, and classical nucleation theory begins to appear implausible. If the macroion surface charge were larger than this, there would be no reason to think that an observed homogeneous nucleation process could be described using the classical theory, since it would involve critical clusters too small to be regarded as liquidlike droplets with surfaces.

The upper limit of the nucleation rate would be limited by the rate at which colloidal particles can diffuse, and would not be well described by classical nucleation theory.

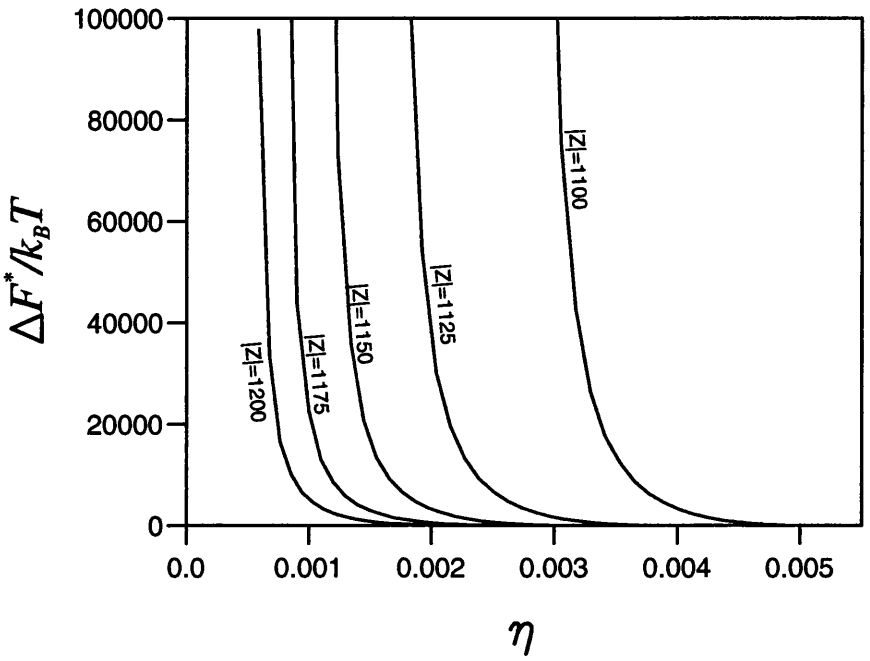

Figure 8.7: Nucleation barrier ΔF^* of the critical cluster as a function of the volume fraction η of the metastable vapour, for colloidal particles of radius $a = 50$ nm and various charges, under conditions of zero added salt. The range of values of η spans the binodal-spinodal range.

8.7 The Swiss Cheese effect

Finally, we shall discuss the 'Swiss cheese effect' (see figure 2.2) with reference to nucleation theory. The initial disordered state is metastable with respect to a solidlike state, which is itself metastable with respect to the final phase separated state comprising a solidlike state of slightly higher density together with voids or a gaslike state. The initial state lies in a region of the phase diagram where the most thermodynamically favourable single phase is solidlike, and this solidlike phase can nucleate fairly quickly (on a timescale of seconds to minutes): the initial liquidlike phase and the nucleating solidlike phase have similar densities and therefore the surface tension of their interface is small. The fact that the metastable crystallites appear to grow from clusters in the bulk of the suspension demonstrates that the process of homogeneous nucleation is taking place.

The nucleation of the voids or gaslike regions within the metastable solidlike phase is a much slower process, because the large difference in the densities of the two phases leads to a relatively large surface tension, and therefore to a large

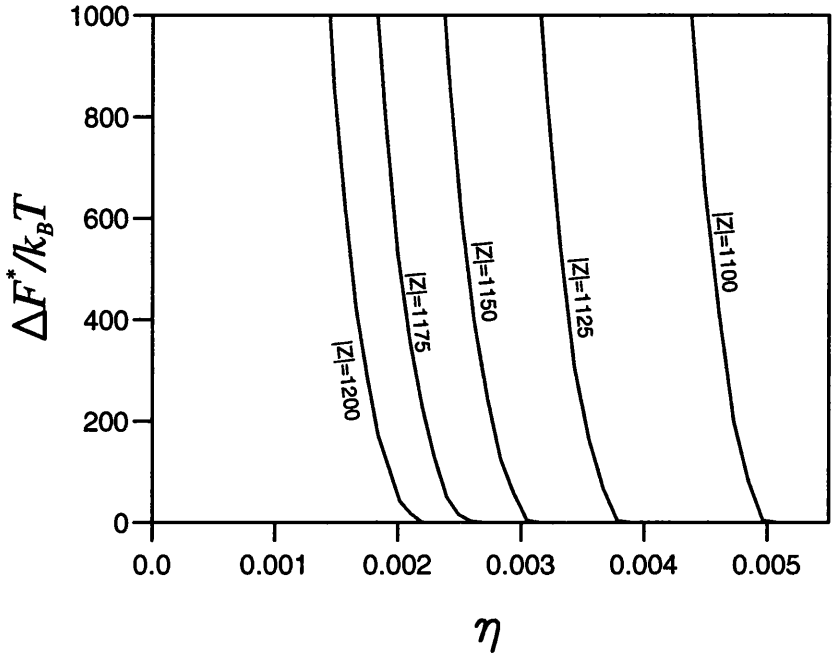

Figure 8.8: Nucleation barrier ΔF^* of the critical cluster as a function of the volume fraction of the metastable vapour, for colloidal particles of radius $a = 50$ nm under conditions of zero added salt.

barrier to nucleation. There is evidence of both homogeneous (in the interiors of the crystals) and heterogeneous nucleation here: the heterogeneous nucleation takes place at the interfaces between crystals and is the cause of the gaps which form between them. This process happens because particles at the interface are already thermodynamically 'disadvantaged' by the presence of the interface, and so the additional free energy required to form the surface of a void is smaller than it is in the bulk. However, the heterogeneous nucleation is not so much more favoured that it preempts homogeneous nucleation and prevents it from being observed; if this were the case, the 'cheese' would have no holes in it.

There is another mechanism that could contribute to the appearance of the gaslike regions at the interfaces of the crystals: small 'bubbles' of gaslike phase, formed by homogeneous nucleation, could diffuse to an interface from the body of a crystal. This process is thermodynamically favourable since it reduces the surface area of the crystal. However, we cannot attribute the formation of the gaslike regions at the interfaces entirely to this mechanism; if homogeneous nucleation occurs in the interior of the crystals, heterogeneous nucleation at the interfaces seems inevitable, since it is by definition a faster process than homogeneous nucleation.

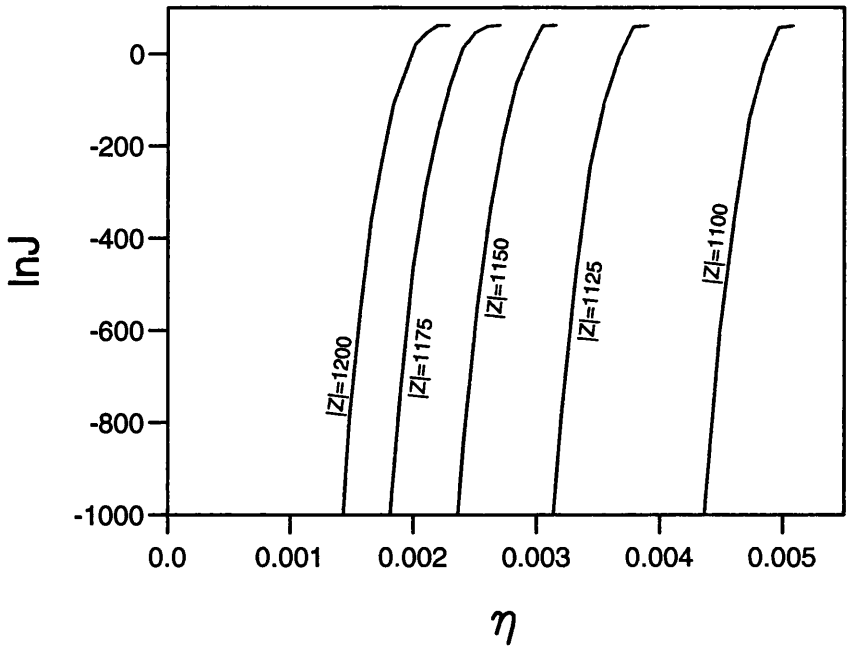

Figure 8.9: Natural logarithm $\ln J$ of the nucleation rate, as a function of volume fraction, for colloidal particles of radius $a = 50$ nm under conditions of zero added salt. J has units of $\mathrm{m}^{-3}\mathrm{s}^{-1}$.

It can be seen from figure 8.9 that the rate of homogeneous nucleation is vanishingly small in most of the metastable region, so that in practice the process would only be observed in a small part of the region. This is not just a feature of colloidal systems: it results from the exponential dependence of the nucleation rate on the work of formation of the critical cluster, and applies also to simple fluids. However, in simple fluids the process of homogeneous nucleation is usually preempted by heterogeneous nucleation (because the roughness on the molecular scale of the surfaces of impurities and of the walls of the container provides highly advantageous sites for heterogeneous nucleation), so that a metastable state is unlikely to endure for long. It was argued, in the introduction to this chapter, that this should not be the case for colloidal systems, and the experimental results of Yoshida *et al.* support this conclusion.

Unless heterogeneous nucleation were much faster than homogeneous nucleation in a particular colloidal suspension, metastable states in most of the metastable region would, to all intents and purposes, be stable: phase separation would not be seen to occur on any experimentally accessible timescale. Thus, consideration of surfaces and non-equilibrium processes would be essential to the study of these

systems. Even an exact calculation of the equilibrium phase diagram would be an incomplete description of the phase behaviour: only a calculation of the nucleation rates could tell us which phase separated states would be observed in practice. These conclusions suggest that the simulations of Linse and Lobaskin [68, 69], who failed to find phase separation in a charged colloidal system, are not conclusive. In most parts of the metastable region, simulations would have to run for an extremely long time before evidence of phase separation was detected.

However, the Yoshida experiments suggest a mechanism by which phase separation could occur even if direct homogeneous nucleation were too slow a process to be observable, even if there were no possibility of heterogeneous nucleation at the walls of the container. If the system is in a region of the phase diagram where the most stable state of homogeneous density is solidlike rather than disordered, an initially disordered state will tend to change to the solidlike state, and this will happen much more easily than the phase separation into a dense and a rarefied phase. The competing crystals which result from this first nucleation process will leave interfaces at which heterogeneous nucleation might take place, although in this particular system the process is not significantly faster than homogeneous nucleation.

Chapter 9

Conclusions

9.1 Colloidal stability

It has been shown in this thesis that an expression for the Helmholtz free energy, calculated by direct solution of the linearised Poisson-Boltzmann equation for a system containing a large number of macroions, leads to a prediction of phase separation into a dense and a rarefied phase for certain values of the macroion charge and radius. It has become clear from the work presented in this thesis and from the work of other authors [53, 62] that the theory of the stability of charged colloids needs revision, and that the DLVO picture of this phenomenon is no longer tenable. The picture that is emerging involves cohesive electrostatic effects and repulsive counterion entropy effects: the electrostatic contribution to the free energy pushes the system towards coagulation, while the counterion entropy is responsible for its stability. This permits an interpretation equivalent to that applied to the same phenomenon in simple fluids. The situation is complicated, however, since the dependence of the counterion density, and hence entropy, on the macroion density is a result of requiring that each part of the system be charge neutral - in other words, a result of electrostatic effects.

While the prediction of electrostatic cohesion and phase coexistence on the basis of the mean field Poisson-Boltzmann theory does not actually prove that the phenomena are genuine and are not merely a result of the effect of impurities, it strengthens the case for phase coexistence. The theoretical predictions are in qualitative agreement with experiment, notably in the fact that coexistence between dense and rarefied phases appears only at low salt concentrations and at high macroion charges. Disagreement with theory (that is, with the DLVO theory) is probably the strongest factor in any reluctance to accept these experimental results at face value. But the present work and other recent theoretical treatments suggest that, if such

phenomena had not been observed, they should be predicted and sought after on the basis of theory.

Indeed, in some ways it is unnecessary to do these calculations in order to make this prediction. Physical insight should tell us that the lowest energy configuration for the electrostatic fields will occur when the particles are aggregated. Of course, the existence of an electrostatic attraction does not automatically imply phase coexistence. Theories that apply the linearised model do so in the belief that the qualitative behaviour they predict would carry through to the nonlinear model. But it is at least conceivable that the repulsive effect of counterion entropy would always outweigh the electrostatic attraction in the nonlinear system, as it does below a certain macroion charge in the linear system. Therefore, the development of nonlinear approaches to these systems will be essential in the future.

A number of new predictions have been introduced by the present theoretical treatment. The occurrence or non-occurrence of phase coexistence is shown to depend approximately on the ratio of the macroion charge to the macroion radius, with coexistence appearing above a critical value of this ratio. This conclusion is similar, although not identical, to that of Ise *et al.* [2], who suggested that the macroion surface charge density was the important parameter. The liquid-gas phase coexistence is predicted to persist at zero salt, and a 'reverse Donnan effect' is predicted, with the added salt being denser in the macroion-rich phase under some conditions. All of these predictions could be tested experimentally. We have also shown that the predicted phase coexistence is not simply an artefact of assuming constant macroion charge, as it persists when a simple model for the dissociation at the macroion surfaces is introduced.

Where does this leave DLVO theory? These conclusions were reached within linearised Poisson-Boltzmann theory, which is a mean field theory and makes the same physical assumptions as the DLVO theory. We conclude that, when applied to colloidal stability, the DLVO theory is incorrect: its failure to take into account the link between the macroion and counterion densities leads to the neglect of important contributions to the free energy and the misinterpretation of the pair term as a repulsive potential. Any agreement with experimental results on colloidal stability must be ascribed to coincidence: DLVO theory was derived theoretically [3] on the basis of electrostatics and thermodynamics, and it is now clear that this derivation cannot be justified.

However, it is important to realise that, although it should not be applied to stability against coagulation, DLVO theory is correct for a wide variety of phenomena in colloidal systems. It is theoretically justifiable, and supported by experimental

[16, 15] and simulation [48] results, for the interaction between an isolated pair of colloidal particles or surfaces. In dispersions containing a large number of particles, it predicts the existence of solid and liquid phases of similar density [22], and simulation results have shown that a colloidal particle surrounded by fixed particles in a suspension will experience forces that are described well by DLVO theory [50]. In fact, the theory fails only in the description of phenomena that involve density changes in the whole of a dispersion: that is, in the description of stability against coagulation or solid- or liquid-gas phase coexistence. This is clearly a significant failure, as DLVO theory was originally created to explain colloidal stability (which is also the main subject of this thesis). However, DLVO theory can still safely and profitably be applied to many other phenomena.

Similarly, the Sogami-Ise theory is in error due to its failure to allow the counterion density to vary with the macroion density. But the expressions derived for the Helmholtz free energy are valuable, as is the insight that the electrostatic interactions are attractive rather than repulsive.

9.2 Interfaces and nucleation

This thesis includes the first theoretical estimates of surface tension in charged colloidal suspensions, calculated using density functional theory in the square gradient approximation. The calculated values are of a reasonable order of magnitude, and approach zero, as expected, as the critical macroion surface charge is approached. Knowledge of the surface tension allows the characteristics of the critical cluster, and therefore also the rate of homogeneous nucleation, to be calculated, at least within classical nucleation theory. The results emphasise the fact that the homogeneous nucleation rate depends very steeply on the conditions, so that, in large parts of the metastable region, homogeneous nucleation would not be observed on any practical timescale. Physical arguments and experimental evidence suggest that heterogeneous nucleation is not significantly faster than homogeneous nucleation in many colloidal systems; in this case, phase separation might never occur in large parts of the metastable region, and the calculation of nucleation rates would then be as important as equilibrium calculations in the theoretical prediction of phase coexistence. Therefore, simulations which fail to find evidence of phase separation are inconclusive.

The 'Swiss Cheese effect' observed by Yoshida *et al.* [4] can be explained qualitatively in the context of nucleation theory. The initial formation of competing metastable crystals from a metastable liquidlike phase is evidence of homogeneous

nucleation, while the subsequent formation of gaslike regions shows signs of both homogeneous and heterogeneous nucleation. The possibility of heterogeneous nucleation at the boundaries of metastable crystals suggests a mechanism by which phase separated states which are inaccessible by homogeneous nucleation might nonetheless be observed, even in the absence of other heterogeneous nucleation sites.

Bibliography

[1] R. J. Hunter, *Foundations of Colloid Science*, 2nd ed. (Oxford University Press, Oxford, 2001).

[2] N. Ise, T. Konishi and B. V. R. Tata, Langmuir **15**, 4176 (1999).

[3] E. J. W. Verwey and J. Th. G. Overbeek, *Theory of the Stability of Lyophobic Colloids* (Elsevier, New York, 1948).

[4] H. Yoshida, J. Yamanaka, T. Koga, T. Koga, N. Ise and T. Hashimoto, Langmuir **15**, 2684 (1999).

[5] D. Kondepudi and I. Prigogine, *Modern Thermodynamics: From Heat Engines to Dissipative Structures* (Wiley, Chichester, 1998).

[6] D. Frenkel and B. Smit, *Understanding Molecular Simulation: From Algorithms to Applications* (Academic, San Diego, 1996).

[7] C. Domb, *The Critical Point* (Taylor and Francis, London, 1996).

[8] D. H. Everett, *Basic Principles of Colloid Science* (Royal Society of Chemistry, London, 1988).

[9] H. R. Kruyt, in *Colloid Science*, Volume 1 (H. R. Kruyt, ed., Elsevier, New York, 1952).

[10] B. Deryagin and L. Landau, Acta Physicochim. USSR **14**, 633 (1941).

[11] P. W. Debye and E. Hückel, Phys. Z. **24**, 185 (1923).

[12] D. A. McQuarrie, *Statistical Mechanics* (University Science Books, Sausalito, CA, 2000).

[13] P. W. Atkins, *Physical Chemistry*, 6th ed. (Oxford University Press, Oxford, 1998).

[14] R. G. Horn, D. R. Clarke and M. T. Clarkson, J. Materials Res. **3**, 413 (1988).

[15] K. Vondermassen, J. Bongers, A. Mueller and H. Versmold, Langmuir **10**, 1351 (1994).

[16] J. C. Crocker and D. G. Grier, Phys. Rev. Lett. **73**, 352 (1994).

[17] T. Alfrey, Jr., E. B. Bradford, J. W. Vanderhoff and G. Oster, J. Opt. Soc. Am. **44**, 603 (1954).

[18] A. Kose, M. Ozaki, K. Takano, Y. Kobayashi and S. Hachisu, J. Colloid Interface Sci. **44**, 330 (1973).

[19] S. Hachisu and Y. Kobayashi, J. Colloid Interface Sci. **46**, 470 (1974).

[20] Y. Monovoukas and A. P. Gast, J. Colloid Interface Sci. **128**, 533 (1989).

[21] K. Kremer, M. O. Robbins and G. S. Grest, Phys. Rev. Lett. **57**, 2694 (1986).

[22] M. O. Robbins, K. Kremer and G. S. Grest, J. Chem. Phys. **88**, 3286 (1988).

[23] E. Velasco, L. Mederos, G. Navascués, P. C. Hemmer and G. Stell, Phys. Rev. Lett. **85**, 122 (2000).

[24] N. Ise, T. Okubo, Y. Hiragi, H. Kawai, T. Hashimoto, M. Fujimura, A. Nakajima and H. Hayashi, J. Am. Chem. Soc. **101**, 5836 (1979).

[25] N. Ise, T. Okubo, K. Yamamoto, H. Kawai, T. Hashimoto, M. Fujimura and Y. Hiragi, J. Am. Chem. Soc. **102**, 7901 (1980).

[26] N. Ise, T. Okubo, M. Sugimura, K. Ito and H. J. Nolte, J. Chem. Phys. **78**, 536 (1983).

[27] A. E. Larsen and D. G. Grier, Nature **385**, 230 (1997).

[28] S. Dosho, N. Ise, K. Ito, S. Iwai, H. Kitano, H. Matsuoka, H. Nakamura, H. Okumura, T. Ono, I. S. Sogami, Y. Ueno, H. Yoshida and T. Yoshiyama, Langmuir **9**, 394 (1993).

[29] K. Ito, H. Yoshida and N. Ise, Science **263**, 66 (1994).

[30] B. V. R. Tata, E. Yamahara, P. V. Rajamani and N. Ise, Phys. Rev. Lett. **78**, 2660 (1997).

[31] A. K. Arora, B. V. R. Tata, A. K. Sood and R. Kesavamoorthy, Phys. Rev. Lett. **60**, 2438 (1988).

[32] B. V. R. Tata, M. Rajalakshmi and A. K. Arora, Phys. Rev. Lett. **69**, 3778 (1992).

[33] T. Palberg and M. Würth, Phys. Rev. Lett. **72**, 786 (1994); B. V. R. Tata and A. K. Arora, Phys. Rev. Lett. **72**, 787 (1994).

[34] V. Reus, L. Belloni, T. Zemb, N. Lutterbach and H. Versmold, J. Phys. II France **7**, 603 (1997).

[35] L. Belloni, J. Phys.: Condens. Matter **12**, R549 (2000).

[36] H. Yoshida, N. Ise and T. Hashimoto, J. Chem. Phys. **103**, 10146 (1995).

[37] H. Yoshida, J. Yamanaka, T. Koga, N. Ise and T. Hashimoto, Langmuir **14**, 569 (1998).

[38] H. Matsuoka, T. Harada and H. Yamaoka, Langmuir **10**, 4423 (1994).

[39] H. Matsuoka, T. Harada, K. Kago and H. Yamoka, Langmuir **12**, 5588 (1996).

[40] J. Yamanaka, H. Yoshida, T. Koga, N. Ise and T. Hashimoto, Phys. Rev. Lett. **80**, 5806 (1998).

[41] J. Yamanaka, H. Yoshida, T. Koga, N. Ise and T. Hashimoto, Langmuir **15**, 4198 (1999).

[42] I. Sogami, Phys. Lett. **96A**, 199 (1983).

[43] I. Sogami and N. Ise, J. Chem. Phys. **81**, 6320 (1984).

[44] M. V. Smalley, Mol. Phys. **71**, 1251 (1990).

[45] J. Th. G. Overbeek, J. Chem. Phys. **87**, 4406 (1987).'

[46] C. E. Woodward, J. Chem. Phys. **89**, 5140 (1988).

[47] M. Tokuyama, Phys. Rev. E **59**, R2550 (1999).

[48] H. Löwen, J.-P. Hansen and P. A. Madden, J. Chem. Phys. **98**, 3275 (1993).

[49] I. D'Amico and H. Löwen, Physica A **237**, 25 (1997).

[50] H. H. von Grünberg and L. Belloni, Phys. Rev. E **62**, 2493 (2000).

[51] R. van Roij and J.-P. Hansen, Phys. Rev. Lett. **79**, 3082 (1997).

[52] M. Dijkstra and R. van Roij, J.Phys.: Condens. Matter **10**, 1219 (1998).

[53] R. van Roij, M. Dijkstra and J.-P. Hansen, Phys. Rev. E **59**, 2010 (1999).

[54] R. van Roij and R. Evans, J. Phys.: Condens. Matter **11**, 10047 (1999).

[55] E. Canessa, M. J. Grimson and M. Silbert, Mol. Phys. **64**, 1195 (1988).

[56] M. J. Grimson and M. Silbert, Mol. Phys. **74**, 397 (1991).

[57] H. Graf and H. Löwen, Phys. Rev. E **57**, 5744 (1998).

[58] A. R. Denton, J. Phys.: Condens. Matter **11**, 10061 (1999).

[59] A. R. Denton, Phys. Rev. E **62**, 3855 (2000).

[60] K. S. Schmitz and L. B. Bhuiyan, Phys. Rev. E **63**, 011503 (2000).

[61] B. Beresford-Smith, D. Y. C. Chan and D. J. Mitchell, J. Colloid Interface Sci. **105**, 216 (1985).

[62] P. B. Warren, J. Chem. Phys. **112**, 4683 (2000).

[63] M. Knott and I. J. Ford, Phys. Rev. E **63**, 031403 (2001).

[64] D. Y. C. Chan, P. Linse and S. N. Petris, Langmuir **17**, 4202 (2001).

[65] L. Belloni, J. Chem. Phys. **85**, 519 (1985).

[66] H. Löwen and E. Allahyarov, J. Phys.: Condens. Matter **10**, 4147 (1998).

[67] G. W. Kwon, Y. S. Won and B. J. Yoon, J. Colloid Interface Sci. **205**, 423 (1998).

[68] P. Linse and V. Lobaskin, Phys. Rev. Lett. **83**, 4208 (1999).

[69] P. Linse and V. Lobaskin, J. Chem. Phys. **112**, 3917 (2000).

[70] I. S. Sogami, T. Shinohara and M. V. Smalley, Mol. Phys. **74**, 599 (1991).

[71] I. S. Sogami, T. Shinohara and M. V. Smalley, Mol. Phys. **76**, 1 (1992).

[72] J. Th. G. Overbeek, Mol. Phys. **80**, 685 (1993).

[73] R. Ettelaie, Langmuir **9**, 1888 (1993).

[74] T. Palberg, W. Mönch, F. Bitzer, R. Piazza and T. Bellini, Phys. Rev. Lett. **74**, 4555 (1995).

[75] M. J. Stevens, M. L. Falk and M. O. Robbins, J. Chem. Phys. **104**, 5209 (1996).

[76] M. Quesada-Pérez, J. Callejas-Fernández and R. Hidalgo-Álvarez, Phys. Rev. E **61**, 574 (2000).

[77] A. Fernández-Nieves, A. Fernández-Barbero and F. J. de las Nieves, Phys. Rev. E **64**, 032401 (2001).

[78] S. Alexander, P. M. Chaikin, P. Grant, G. J. Morales, P. Pincus and D. Hone, J. Chem. Phys. **80**, 5776 (1984).

[79] T. Gisler, S. F. Schulz, M. Borkovec, H. Sticher, P. Schurtenberger, B. D'Aguanno and R. Klein, J. Chem. Phys. **101**, 9924 (1994).

[80] M. N. Tamashiro, Y. Levin and M. C. Barbosa, Physica A **258**, 341 (1998).

[81] A. Diehl, M. C. Barbosa and Y. Levin, Europhys. Lett. **53**, 86 (2001).

[82] P. Attard, Adv. Chem. Phys. **92**, 1 (1996).

[83] R. R. Netz and H. Orland, Eur. Phys. J. E **1**, 203 (2000).

[84] R. Messina, C. Holm and K. Kremer, Phys. Rev. E **64**, 021405 (2001).

[85] N. F. Carnahan and K. E. Starling, J. Chem. Phys. **53**, 600 (1970).

[86] P. Tarazona, Phys. Rev. A **31**, 2672 (1985).

[87] I. J. R. Aitchison and A. J. G. Hey, *Gauge Theories in Particle Physics* (Adam Hilger, Bristol, 1982).

[88] W. H. Press, B. P. Flannery, S. A. Teukolsky and W. T. Vetterling, *Numerical Recipes: The Art of Scientific Computing* (Cambridge University Press, Cambridge, 1989).

[89] B. W. Ninham and V. A. Parsegian, J. Theor. Biol. **31**, 405 (1971).

[90] L. D. Landau and E. M. Lifshitz, *Statistical Physics*, 3rd edn., Part 1 (Butterworth-Heinemann, Oxford, 1980).

[91] F. F. Abraham, *Homogeneous Nucleation Theory* (Academic Press, New York, 1974).

[92] D. W. Oxtoby, J. Phys.: Condens. Matter **4**, 7627 (1992).

[93] D. Kashchiev, *Nucleation: Basic Theory with Applications* (Butterworth-Heinemann, Oxford, 2000).

[94] M. Knott, H. Vehkamäki and I. J. Ford, J. Chem. Phys. **112**, 5393 (2000).

[95] V. B. Mikheev, N. S. Laulainen, S. E. Barlow, M. Knott and I. J. Ford, J. Chem. Phys. **113**, 3704 (2000).

[96] I. J. Ford, Phys. Rev. E **56**, 5615 (1997).

[97] I. J. Ford, J. Chem. Phys. **105**, 8324 (1996).

[98] B. N. Hale, Phys. Rev. A **33**, 4156 (1986).

[99] B. N. Hale, Metall. Trans. A **23**, 1863 (1992).

[100] V. Ždímal and J. Smolík, Atmos. Res. **46**, 391 (1998).

[101] M. M. Rudek, J. L. Katz, I. V. Vidensky, V. Zdimal and J. Smolik, J. Chem. Phys. **111**, 3623 (1999).

[102] J. Hrubý, Y. Viisanen and R. Strey, J. Chem. Phys. **104**, 5181 (1996).

[103] C. C. M. Luijten, O. D. E. Baas and M. E. H. van Dongen, J. Chem. Phys. **106**, 4152 (1997).

[104] C. C. M. Luijten, *Nucleation and Droplet Growth at High Pressure* (Ph.D. thesis, Technische Universiteit Eindhoven, 1998).

[105] T. Schmeling and R. Strey, Ber. Bunsenges. Phys. Chem. **87**, 871 (1983).

[106] J. S. Rowlinson and B. Widom, *Molecular Theory of Capillarity* (Clarendon Press, Oxford, 1982).

[107] J. W. Cahn and J. E. Hilliard, J. Chem. Phys. **28**, 258 (1958).

[108] R. Evans, in *Fundamentals of Inhomogeneous Fluids* (D. Henderson, ed., Marcel Dekker, New York, 1992).

[109] J. M. Brader and R. Evans, Europhys. Lett. **49**, 678 (2000).

[110] D. W. Marr and A. P. Gast, Langmuir **10**, 1348 (1994).

[111] J. W. Cahn and J. E. Hilliard, J. Chem. Phys. **31**, 688 (1959).

[112] D. W. Oxtoby and R. Evans, J. Chem. Phys. **89**, 7521 (1988).

[113] R. McGraw and A. Laaksonen, Phys. Rev. Lett. **76**, 2754 (1996).

[114] V. Talanquer, J. Chem. Phys. **106**, 9957 (1997).

[115] M. P. Anisimov, I. N. Shaymordanov and P. K. Hopke, J. Aerosol Sci. **32**, S17 (2001).

[116] D. W. Oxtoby, in *Fundamentals of Inhomogeneous Fluids* (D. Henderson, ed., Marcel Dekker, New York, 1992).